

DEVELOPMENT OF METAL NANOPARTICLE- DOPED POLYANILINO-GRAPHENE OXIDE HIGH PERFORMANCE SUPERCAPACITOR CELLS



By

NOMXOLISI RUTH DYWILI

(Magister Scientiae in Nanoscience)

A thesis submitted in fulfilment of the requirements for the degree of

PHILOSOPHIAE DOCTOR

In the

**Department of Chemistry
Faculty of Science
University of the Western Cape, South Africa**

Supervisor: Professor Emmanuel I. Iwuoha

Co-supervisors: Prof. Konstantinos Kordatos and Dr Chinwe O. Ikpo

May 2018

Abstract

Supercapacitors, also known as ultracapacitors or electrochemical capacitors, are considered one of the most important subjects concerning electricity or energy storage which has proven to be problematic for South Africa. In this work, graphene oxide (GO) was supported with platinum, silver and copper nanoparticles anchored with dodecylbenzenesulphonic acid (DBSA) doped polyaniline (PANI) to form nanocomposites. Their properties were investigated with different characterization techniques. The high resolution transmission electron microscopy (HRTEM) revealed GO's nanosheets to be light, flat, transparent and appeared to be larger than 1.5 μm in thickness. This was also confirmed by high resolution scanning electron microscopy (HRSEM) with smooth surfaces and wrinkled edges observed with the energy dispersive X-ray analysis (EDX) confirming the presence of the functional groups such as carbon and oxygen. The HRTEM analysis of decorated GO with platinum, silver and copper nanoparticles (NPs) revealed small and uniformly dispersed NPs on the surface of GO with mean particle sizes of 2.3 ± 0.2 nm, 2.6 ± 0.3 nm and 3.5 ± 0.5 nm respectively and the surface of GO showed increasing roughness as observed in HRSEM micrographs. The X-ray fluorescence microscopy (XRF) and EDX confirmed the presence of the nanoparticles on the surface of GO as platinum, silver and copper which appeared in abundance in each spectra. Anchoring the GO with DBSA doped PANI revealed that single GO sheets were embedded into the polymer latex, which caused the DBSA-PANI particles to become adsorbed on their surfaces. This process then appeared as dark regions in the HRTEM images. Morphological studies by HRSEM also supported that single GO sheets were embedded into the polymer latex as composite formation appeared aggregated and as bounded particles with smooth and toothed edges. Fourier transform infrared spectroscopy (FTIR) of GO shows the respective vibrational bands of O-H stretching vibrations at 3434

cm^{-1} , C–O (carboxylic acid and carbonyl moieties) at 1736 cm^{-1} and the graphitic domains of C–C at 1635 cm^{-1} and C=C–O at 1392 cm^{-1} . The band at $980\text{--}1250 \text{ cm}^{-1}$ contains the C–O (1040 cm^{-1}) and the O–H (1227 cm^{-1}) deformation, respectively, of carboxylic acid groups. Anchoring GO with DBSA doped PANI revealed broad adsorption band at $\sim 3144 \text{ cm}^{-1}$ attributed to polyaniline N–H stretching vibrations and two vibrational peaks centered at 1557 and 1464 cm^{-1} attributed to the stretching frequencies of quinoid and benzenoid rings of polyaniline. The band produced at 1297 cm^{-1} belongs to the C–N stretching of secondary amide group and the band that appear at 1135 cm^{-1} was attributed to the in-plane bending of the C–H bond and bands at, 1044 and 1004 cm^{-1} were due to SO_3^- group (O=S=O and S–O stretching) of DBSA. X-ray powder diffraction (XRD) of GO revealed a very sharp diffraction band (001) appearing at $2\theta = 11.08^\circ$ and this band indicates that AB stacking exists in GO with larger interlayer spacing. The decoration of GO with NPs revealed diffraction peaks at 39.5° , 46.0° and 67° indexed to the (111), (200) and (220) diffraction planes of metallic Pt, Ag and Cu, respectively. These diffraction bands fall in line with the angles found in the Joint Committee on Powder Diffraction Standards (JCPDS). Raman spectroscopy of GO revealed a D band at (1346 cm^{-1}) which is a second-order overtone of a different in-plane vibration and corresponds to defects within the sp^2 network, a G band at (1595 cm^{-1}) and a 2D band at (2689 cm^{-1}) attributed to primary in-plane vibrational mode. However, the GO loaded with nanoparticles displays a decrease in intensity ratio of D/G (0.85) compared to that of GO (0.95) due to the increase in intensity of the G band. This indicates a decrease in average size of sp^2 domain upon the reduction of GO. Meanwhile, the D and G bands of the decorated GO exhibited a shift toward lower frequencies as observed from the nanocomposites. Electrochemical properties of GO were characterized by cyclic voltammetry (CV) which revealed that GO shows an ideally capacitive behavior. Capacitance of GO could also be determined from the CV graphs and was determined to be 180 F g^{-1}

which falls between the ranges of 100–200 F g⁻¹ found in literature. The composites were tested for application as suitable supercapacitor materials and specific capacitances were determined as 227.2, 206.4 and 192.8 F g⁻¹ which correspond to GO/Pt/DBSA-PANI, GO/Ag/DBSA-PANI and GO/Cu/DBSA-PANI, respectively. GO decorated with platinum nanoparticles showed good response and consistent results throughout the work. This is due to platinum being a good conductor and that it can resist high temperatures. Therefore it was highly expected that GO decorated with platinum nanoparticles will exhibit good results.



Keywords

Energy crisis

Supercapacitors

Graphene oxide

Reduced graphene oxide

Platinum nanoparticles

Silver nanoparticles

Copper nanoparticles

DBSA doped PANI

Electrolytes

Galvanostatic charge-discharge

Specific discharge capacitance

Specific charge capacitance

Specific power

Specific energy




Declaration

I declare that “Development of Metal Nanoparticle-Doped Polyanilino-Graphene Oxide High Performance Supercapacitor Cells” is my own work and has not been submitted before for any degree or examination in any other university, and that all the sources I have used or quoted have been indicated or acknowledged as complete references.



Nomxolisi Dywili

May 2018

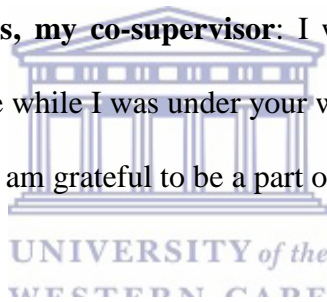
Signed..... 

Acknowledgements

First and foremost, I would like to thank God for giving me strength, courage, patience and for giving me opportunities to finish this work.

To Prof Emmanuel Iwuoha, my supervisor: I would like to thank you for your support, guidance, encouragement and supervision throughout the duration of this work and for being an inspiration to so many students.

To Prof Konstantinos Kordatos, my co-supervisor: I would like to thank you for your supervision, support and guidance while I was under your wing in a foreign country (Greece). You made me feel welcome and I am grateful to be a part of your research group.



To Dr Chinwe Ikpo, my second co-supervisor: I thank you for all your support and guidance, particularly during the writing of the thesis.

To my Family: To my mother and father, **Nosipho Dywili and Bonisile Mankayi**, I would like to thank you for all the support, unconditional love, guidance and sacrifices you had to make to ensure that I was at this place. To **Luxolise Dywili**, all I wanted was to secure a bright future for you and my parents, you deserve only the best life has to give and thank you for being patient and coping without my absence.

To Naledi Raleie and Nomaphelo Ntshongontshi: Thank you for your constant support and encouragement and for being there every step of the way. You have been there when this journey started and you will still be there when it ends. Thank you so much for everything.

To Chemistry Department: Mrs Wilhemina Jackson, thank you very much for your assistance in solving all the academic and technical problems.

SensorLab Researchers: To Dr Tesfaye Waryo, Dr Abd Baleg, Dr Milua Masikini, Dr Natasha Ross, Dr Rachel Fanelwa Ajayi, and Dr Chinwe Ikpo, thank you for sharing your opinions and experience through which I received the required information for my project.

To SensorLab Colleagues: Usisipho Feleni, Unathi Sidwaba, Wonderboy Ntuthuko Hlongwa, Nolukholo Tyombo, Danielle Sass, Laura Pacoste thank you for being such good colleagues.



To my colleagues at the National Technical University of Athens, School of Chemical Engineering, and Analytical Chemistry: Afroditi Ntziouni, Lida Givalou, Katerina Mikedi, Pinelopi Gyftou, Dimitrios Karampatsos, thank you for your warm welcome and assistance during my stay in Athens.

To Sponsors: My sincere gratitude goes to the National Research Foundation (NRF) of South Africa for awarding me a Doctoral Scholarship. I will also like to thank the European Union's Erasmus Mundus programme for granting me an AESOP (A European and South African Partnership on Heritage and Past) Doctoral Scholarship for a research exchange visit to the National Technical University of Athens, Greece from 18 November 2015 to 17 May 2017.

Dedication

This dissertation is dedicated to:

My mother and father

Nosipho Dywili and Bonisile Mankayi

My uncle

Thembile Dywili

My cousins

Nondumiso Siphambo, Singathwa Siphambo, Gcobisa Tyhilana, Fundiswa Tyhilana, Unathi

Khohliso, Nosabelo Mdunana, Thobeka Tikina, Vuyisa Wambi,

My friends

Nomaphelo Ntshongontshi, Naledi Raleie, Audrey Cobus, Ayanda Jack, Zukolwakhe

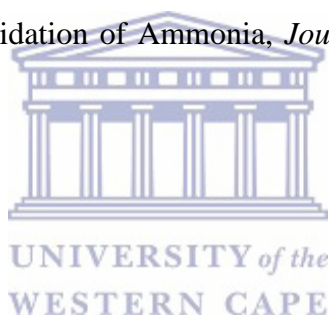


UNIVERSITY of the
WESTERN CAPE
And Finally

Luxolise Dywili

List of publications

1. **Dywili, N. R.**^{1,2}, Njomo, N.¹, Ikpo, C.O.¹, Yonkeu, A. L. D.¹, John, S. V.¹, Hlongwa, N. W.¹, Raleie, N.¹ and Iwuoha, E. I.², Anilino-Functionalized Graphene Oxide Intercalated with Pt Metal Nanoparticles for Application as Supercapacitor Electrode Material, *Journal of Nano Research* 44 (2016) 79-89
2. Matinise, N., Mayedwa, N., Ikpo, O. C., Hlongwa, N. W., Ndipingwi, M., Molefe, L., **Dywili, N.**, Yonkeu, A. L. d. et al. Bimetallic Nanocomposites of Palladium (100) and Ruthenium for Electro-oxidation of Ammonia, *Journal of Nano Research* 44 (2016) 100-113
3. John, S. V., Mayedwa, N., Ikpo, C., Molefe, L., Ndipingwi, M., **Dywili, N.**, van Wyk, J., Mapolie, S. et al., Photoluminescence quenching of poly (octylfluorenylbenzothiadiazole) luminophore by n-type cobalt(II) salicylaldimine metallodendrimer, *Synthetic Metals* 220 (2016) 114-122



List of conference presentations

Title: Anilino-Functionalized Graphene Oxide Intercalated with Pt Metal Nanoparticles for Application as Supercapacitor Electrode Material **Poster presentation** at the 3rd International Symposium on Electrochemistry under on “Materials, Analytical and Physical Electrochemistry Today” (MAPET’15)”, University of the Western Cape, Cape Town, South Africa, **26-28 May 2015**. Authors: Dywili, N., Njomo, N., Ikpo, C.O., Yonkeu, A. L. D., John, S. V., Hlongwa, N. W., Raleie, N. and Iwuoha, E. I.



Title: Polyanilino-graphene oxide intercalated with platinum group metal nanocomposites for application as novel as supercapacitor materials. **Poster presentation** at the 3rd International Symposium on Electrochemistry under “Materials, for Advanced Metallization” (MAM’14)”, University of the Western Cape, Cape Town, South Africa, **23-28 Nov 2014**. Authors: Dywili, N, Ikpo, C, Iwuoha, E.

Title: Supercapacitor characteristics of DBSA doped polyaniline – graphene oxide supported with Ag, Cu and Pt nanoparticles. **Poster presentation** at the 4th International Symposium on Electrochemistry under “Pure and Applied Electrochemistry”, University of Johannesburg (UJ), Johannesburg, South Africa, 3-5 April 2018. Authors: Dywili, N., Iwuoha, E., Kordatos, K.

List of abbreviations and acronyms

AC - Activated carbon

CB - Carbon black

CP - Conducting polymers

CV - Cyclic Voltammetry

DBSA – Dodecylbenzenesulphonic Acid

DL - Double Layer

EC - Electrochemical Capacitors

EDLC - Electrochemical Double Layer Capacitor

EDS – Energy Dispersive Spectroscopy

FTIR – Fourier Transform Infra-red

GO – Graphene Oxide

HRSEM – High Resolution Scanning Electron Microscopy

HRTEM – High Resolution Transmission Electron Microscopy

rGO – Reduced Graphene Oxide

PANI -Polyaniline

XRD – X-ray Diffraction

XRF – X-ray Fluorescence

UV-Vis - Ultraviolet-Visible spectrophotometry



Table of Contents

Abstract.....	i
Keywords	iv
Declaration.....	v
Acknowledgements.....	vi
Dedication	viii
List of publications	ix
List of conference presentations	x
List of abbreviations and acronyms	xi
Table of Contents.....	xii
List of Figures	xvi
Chapter 1	1
Introduction.....	1
Summary.....	1
1.1 Research Background.....	2
1.1.1 <i>What are supercapacitors?</i>	2
1.1.2 <i>Materials for supercapacitor electrodes</i>	10
1.2 Problem statement	12
1.3 Rationale and Motivation	13
1.4 Objectives.....	15
1.5 Thesis Outline	17
References	19
Chapter 2	23
Literature Review.....	23
<i>Summary</i>	23

Abstract	24
2.1 Introduction	25
2.2 Energy storage mechanism.....	26
2.2.1 <i>Electrochemical double layer capacitors (EDLCs)</i>	28
2.2.2 <i>Pseudocapacitors</i>	30
2.2.3 <i>Hybrid capacitors</i>	31
2.2.4 <i>Composite</i>	33
2.3 Electrode materials	34
2.3.1 <i>Graphene oxide/reduced graphene oxide</i>	35
2.3.2 <i>GO/metal nanocomposites</i>	40
2.3.3 <i>DBSA doped Polyaniline</i>	45
2.4 Synthesis of electrode materials	47
2.4.1 <i>Synthesis of Graphene oxide and reduced graphene</i>	47
2.4.2 <i>Metal nanoparticles</i>	49
2.4.3 <i>DBSA doped PANI</i>	50
2.5 Electrolytes for supercapacitors	51
2.5.1 <i>Aqueous electrolytes</i>	51
2.6 Supercapacitors in South Africa.....	52
2.7 Conclusions	54
References	56
Chapter 3	88
Synthesis and Evaluation of the Supercapacitor Properties of Graphene Oxide (GO) and Reduced Graphene Oxide.....	88
Summary	88
Abstract	89
3.1 Introduction	91
3.2 Experimental	92
3.2.1 <i>Chemicals and sample preparation</i>	92
3.2.2 <i>Instrumentation</i>	93

3.2.3	<i>Synthesis of GO</i>	94
3.2.4	<i>Reduction of graphene oxide (GO)</i>	95
3.2.5	<i>Fabrication of the electrode</i>	95
3.3	Results and Discussion.....	97
3.3.1	<i>Particle size properties of GO</i>	97
3.3.2	<i>Morphological properties of GO and rGO</i>	98
3.3.3	<i>Optical properties of GO and rGO</i>	99
3.3.4	<i>Structural properties of GO and rGO</i>	102
3.3.5	<i>Internal Structural properties of GO and rGO</i>	104
3.3.6	<i>Crystal properties of GO and rGO</i>	106
3.4	Electrochemical properties of GO and rGO.....	107
3.4.1	<i>Electrochemistry of GO and rGO</i>	107
3.4.2	<i>Testing GO as a supercapacitor material using Galvanostatic-charge discharge</i>	110
3.4.3	<i>Testing rGO as a supercapacitor material using Galvanostatic-charge discharge</i>	111
3.5	Conclusions.....	113
	References.....	114
	Chapter 4.....	122
	<i>Summary</i>	122
	Abstract.....	123
4.1	Introduction.....	124
4.2	Experimental.....	124
4.2.1	<i>Chemicals and sample preparation</i>	124
4.2.2	<i>Instrumentation</i>	125
4.2.3	<i>Synthesis of graphene oxide loaded with Pt, Ag and Cu NPs</i>	126
4.3	Results and Discussion.....	127

4.3.1	<i>Particle size analysis of GO/Pt NPs, GO/Ag NPs and GO/Cu NPs</i>	127
4.3.2	<i>Morphological properties of GO/Pt NPs, GO/Ag NPs and GO/Cu NPs</i>	129
4.3.3	<i>Optical properties of GO/Ag NPs</i>	130
4.3.4	<i>Structural properties of GO/Pt NPs, GO/Ag NPs and GO/Cu NPs</i>	132
4.3.5	<i>Internal Structural properties of GO/Pt NPs, GO/Ag NPs, GO/Cu NPs</i>	135
4.3.6	<i>Elemental composition studies of GO/Pt NPs, GO/Ag NPs and GO/Cu NPs</i> .	137
4.3.7	<i>Crystallographic properties of GO/Pt NPs, GO/Ag NPs and GO/Cu NPs</i>	140
4.4	Conclusions	142
	References	144
	Chapter 5.....	150
	Abstract	151
5.1	Introduction	152
5.2	Experimental	153
5.2.1	<i>Chemicals and sample preparation</i>	153
5.2.2	<i>Instrumentation</i>	154
5.2.3	<i>Synthesis of GO/NPs, GO/AgNPs and GO/Cu NPs anchored DBSA doped PANI</i>	154
5.2.4	<i>Fabrication of the electrode material</i>	155
5.3	Results and Discussion.....	157
5.3.1	<i>Structural analysis of GO/Pt/DBSA-PANI, GO/Ag/DBSA-PANI and GO/Cu/DBSA-PANI</i>	157
5.3.2	<i>Morphological properties of GO/Pt/DBSA-PANI, GO/Ag/DBSA-PANI and GO/Cu/DBSA-PANI</i>	159
5.3.3	<i>Elemental composition of (a) GO/Pt/DBSA-PANI, (b) GO/Ag/DBSA-PANI and (c) GO/Cu/DBSA-PANI</i>	161
5.3.4	<i>Structural properties of GO/Pt/DBSA-PANI, GO/Ag/DBSA-PANI and GO/Cu/DBSA-PANI.</i>	163

5.4	<i>Electrochemical studies</i>	165
5.4.1	<i>Testing GO/Pt/DBSA-PANI as a supercapacitor material using Galvanostatic-charge discharge</i>	165
5.4.2	<i>Testing GO/Ag/DBSA-PANI as a supercapacitor material using Galvanostatic-charge discharge</i>	167
5.4.3	<i>Testing GO/Cu/DBSA-PANI as a supercapacitor material using Galvanostatic-charge discharge</i>	169
5.5	Conclusions	171
	References	172
Chapter 6	177
	Conclusions and Recommendations.....	177
	Summary	177
6.1	Conclusions	178
	References	182



List of Figures

Figure 1. 1: Ragone plot (Gonzalez <i>et al.</i> , 2016; Layer, 1966).	4
Figure 1. 2: Representation diagram of a conventional dielectric capacitor (Halper & Ellenbogen, 2006)	6
Figure 1. 3: Schematic diagram of a supercapacitor (Halper & Ellenbogen, 2006).....	9
Figure 2. 1: Classification of supercapacitors (Simon & Gogotsi, 2009).....	27
Figure 2. 2: Symmetric supercapacitor schematic diagram (Y. Shao <i>et al.</i> , 2013).....	28
Figure 2. 3: Schematic of an electrical double layer (Pellecchia & Holmes, 2008).	29
Figure 2. 4: Schematic of a pseudocapacitor (Kiamahalleh <i>et al.</i> , 2012)	31
Figure 2. 5: Schematic of a hybrid capacitor (Li <i>et al.</i> , 2017).....	32
Figure 2. 6: The stacking of graphene sheets results in a layered structure (Casero <i>et al.</i> , 2012).	36
Figure 2. 7: Representation of the chemical route from graphite to the reduced graphene oxide (Gao, 2015; Song <i>et al.</i> , 2014).	38
Figure 2. 8: Representation diagram of graphene oxide-based electrodes for electrochemical applications (Gao, 2015).	39
Figure 2. 9: Application fields for conducting polymer nanomaterials (Jangid <i>et al.</i> , 2014; Ravichandran <i>et al.</i> , 2010).	46
Figure 2. 10: Schematic for the synthesis of graphene oxide (Settanni <i>et al.</i> , 2016).....	49
Figure 3. 1: HR-TEM micrograph of (a) GO, (b) EDX spectrum of GO.	98
Figure 3. 2: HR-SEM micrographs of (a) GO at 2 μm (b) rGO at 2 μm	99

Figure 3. 3: UV-Visible spectra of (a) GO from increasingly concentrated aqueous solutions, 20, 40, 60, 80 and 100 μL in the region (200-800 nm) in de-ionized water (b) (i) GO and (ii) rGO at concentration of 20 μL in the region (200-800 nm) in de-ionized water. 101

Figure 3. 4: (a) FTIR spectra of GO (i) and rGO (ii) and (b) table showing the frequencies and their respective bonds found in GO. 103

Figure 3. 5: (a) Raman spectroscopy of (i) GO and (ii) rGO (b) Table showing the bands and their respective Raman shift in cm^{-1} found in GO and rGO. 105

Figure 3. 6: XRD patterns of (i) GO and (ii) rGO. 107

Figure 3. 7: CV behavior of (a) GO, (b) CV behavior of GO at scan rate 50 mV/s (c) calibration curve of rGO (d) CV behavior of rGO (e) Calibration curve of rGO. The electrochemical behavior of GO and rGO was studied in the potential window of +1.0 V to -1.0 V in 0.1 M H_2SO_4 and the calibration curves were drawn from a linear region. 109

Figure 3. 8: Voltage/time cycling plot of GO voltage range (0 to -0.9 V v Ag/AgCl) at 50 A g^{-1} in 1 M H_2SO_4 (aq). Specific charge/discharge current density = 45.7 A g^{-1} . Specific capacitance = $(45.7 \times 3.6)/0.9 = 182.8 \text{ F g}^{-1}$ 111

Figure 4. 1: (a) HRTEM micrograph of GO/Pt NPs, (b) EDS spectrum of GO/Pt NPs, (c) HRTEM micrograph of GO/Ag NPs (d) EDS spectrum of GO/Ag NPs, (e) HRTEM micrograph of GO/Cu NPs (f) EDS spectrum of GO/Cu NPs..... 129

Figure 4. 2: HRSEM micrographs of (a) GO/Pt NPs, (b) GO/Ag NPs, (c) GO/Cu NPs..... 130

Figure 4. 3: UV-Vis spectra of (a) Ag NPs (b) GO/Ag NPs..... 132

Figure 4. 4: FTIR spectra of (a) GO/Pt NPs (b) GO/Ag NPs (c) GO/Cu NPs. For comparison reasons, the FTIR spectra of GO is presented as (i) in all three spectras. 134

Figure 4. 5: Raman spectra of (a) GO/Pt NPs (b) GO/Ag NPs (c) GO/Cu NPs. For comparison reasons, the Raman spectra of GO is presented as (i) in all three spectras. 137

Figure 4. 6: XRF spectra of (a) GO/Pt NPs (b) GO/Ag NPs (c) GO/Cu NPs.	139
4. 7: XRD patterns of (a) GO/Pt NPs, (b) GO/Ag NPs and (c) GO/Cu NPs. For comparison reasons, the XRD pattern of GO is presented.	142
Figure 5. 1: HRTEM images of (a) GO/Pt/DBSA-PANI, (b) GO/Ag/DBSA-PANI and (c) GO/Cu/DBSA-PANI.....	158
Figure 5. 2: HRSEM images of (a) GO/Pt/DBSA-PANI, (b) GO/Ag/DBSA-PANI and (c) GO/Cu/DBSA-PANI.....	160
Figure 5. 3: EDX images of (a) GO/Pt/DBSA-PANI, (b) GO/Ag/DBSA-PANI and (c) GO/Cu/DBSA-PANI.....	162
Figure 5. 4: FTIR spectra of (a) GO/Pt NPs/DBSA-PANI, (b) GO/Ag NPs/DBSA-PANI and (c) GO/Cu NPs/DBSA-PANI.	164
Figure 5. 5: Figure 3. 9: Voltage/time cycling plot of GO/Pt/DBSA-PANI voltage range (0 to -0.9V v Ag/AgCl) at 50 A g ⁻¹ in 1 M H ₂ SO ₄ (aq). Specific charge/discharge current density =56.8 A g ⁻¹ . Specific capacitance = (56.8 x 3.6)/0.9 = 227.2 F g ⁻¹	166
Figure 5. 6: Voltage/time cycling plot of GO/Ag/DBSA-PANI voltage range (0 to -0.9V v Ag/AgCl) at 50 mA g ⁻¹ in 1M H ₂ SO ₄ (aq). Specific charge/discharge current density.....	168
Figure 5. 7: Voltage/time cycling plot of GO/Cu/DBSA-PANI voltage range (0 to -0.9 V v Ag/AgCl) at 50 A g ⁻¹ in 1M H ₂ SO ₄ (aq). Specific charge/discharge current density.....	170

List of tables

Table 1. 1: Comparison table of selected electrochemical energy storage technologies from a conventional capacitor to a battery.	5
Table 1. 2: Table comparing the properties of batteries and supercapacitors.	5
Table 2. 1: Comparison table of specific capacitance of selected electrode materials (L. L. Zhang et al., 2009)	35



Chapter 1

Introduction

Summary

Storage is one of the most important issues recently faced in electrostatic field. Fossil fuels are considered non-renewable due to the fact that they take millions of years to be reproduced even though they are continually being naturally formed. Known reserves are being depleted quicker than the ones being formed and with these fossil fuels reducing to lower levels and the world facing global warming, alternative sources of energy need to be devised. Wind and solar energy are not so effective due to the need to harness their energies when the wind and the sun are on, therefore, other energy storage technologies such as electrochemical capacitors, batteries, fuel cells need to be built and harvested. This work's main focus is on supercapacitors (electrochemical capacitors). This chapter gives the background details on high power density energy storage devices such as supercapacitors, what they are, their significant importance on energy storage, how energy is stored, advantages and their disadvantages over other energy storage devices such as batteries, fuel cells and conventional capacitors. This chapter also covers all the favorable and unfavorable aspects of supercapacitors on the environment and their applications. Other important features of supercapacitors such as materials for supercapacitor electrodes are discussed. Furthermore, the motivation and rationale of this work, the aim and objectives, the research framework and investigation outline are discussed.

1.1 Research Background

1.1.1 What are supercapacitors?

Supercapacitors are electrical energy storage devices that store and discharge energy at the electrochemical interface. This storing and charging of energy occurs between the electrolyte and electrode. They are storage devices with very high capacity and low internal resistance and are able to store and supply energy at relatively higher rates as compared to other energy storage devices such as batteries, fuel cells and conventional dielectric capacitors. This is due to the simple charge separation at the interface between the electrode and the electrolyte which is a mechanism of charge storage and to the chemical processes of energy storage involving a simple charge separation at the electrochemical interface between the electrode and electrolyte (Iro *et al.*, 2016). Supercapacitors have attracted a substantial amount of attention due to their wide potential in electric vehicles, power back-up in mobile phones, laptops, radio tuners, digital cameras, iPhones, tablets etc., power back-up for UPS applications and other high-power apparatuses. According to the mechanism of energy storage, supercapacitors are classified into (i) electrical double-layer capacitors (EDLCs) that utilize carbon based materials, (ii) Faradaic pseudo-capacitors that utilize metal oxides and/or conducting polymers and (iii) hybrid capacitors that utilize both carbon based materials and metal oxides and/or conducting polymers (Simon & Gogotsi, 2009). Each category is characterized by its unique mechanism for storing charges. Energy storage in EDLC's is electrostatic in nature and arises from the separation of electronic and ionic charges at the interface which occurs across the double-layer of supercapacitor electrodes. There is also no charge transfer across the double layer and the charge is transferred mostly at the surface or in the bulk near the surface of the solid electrode material. In pseudocapacitors, Faradaic reactions quickly take place to an extent limited by finite amount of active material or

available surface and the capacitance arises due to innovative redox reactions between several oxidation states. Transition metal oxides and conducting polymers have been revealed to give the best pseudocapacitance. Hybrid capacitors are electrical capacitors that have been made up with one electrode that is of carbon i.e. EDLC, and the other electrode being of a metal oxide or conducting polymer (pseudocapacitance) (Jayalakshmi & Balasubramanian, 2008; Lu *et al.*, 2012; Winter & Brodd, 2004) . The performance of supercapacitors is usually categorized by two parameters of specific capacitance and rate capability. Specific capacitance is defined as the ratio between the capacitance and the weight of the active materials (Snook *et al.*, 2007). Rate capability is defined as the capability to preserve the specific capacitance as the current increases, and is therefore a measure of the capability to either produce or provide a large power. To produce a high and effective supercapacitor, it is wise to decrease the total weight of the supercapacitor but improve the capacitance and rate capability of the supercapacitor (Zhang *et al.*, 2012). Supercapacitors fall in the middle of other energy storage devices i.e. between conventional capacitors, batteries and fuel cells and this can be observed on the Ragone plot presented in Figure 1.1. Supercapacitors with their higher power densities can maintain a greater shelf-life which makes them perfect alternatives to batteries. However, the energy densities of supercapacitors are lower than those of batteries and fuel cells therefore research on supercapacitors concentrated on developing improved classes to make their energy densities more similar or even higher to those of batteries.

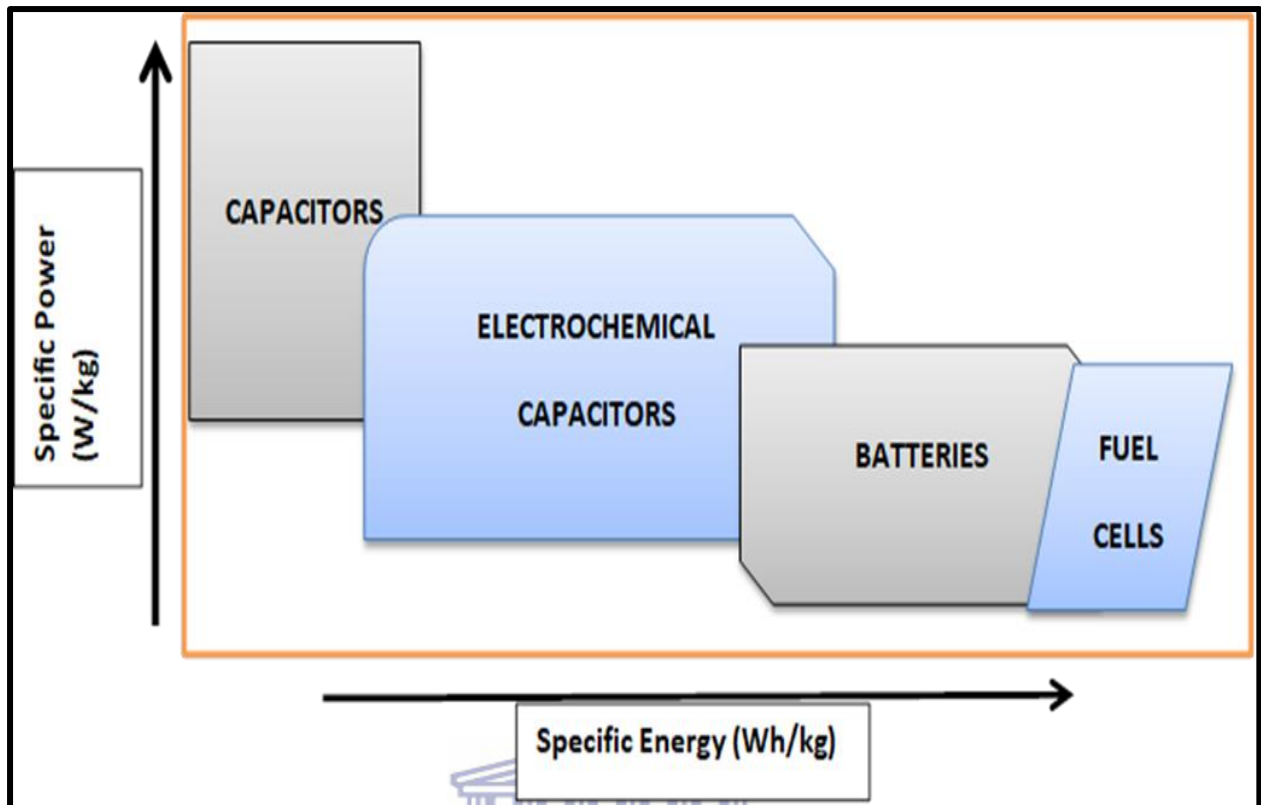


Figure 1. 1: Ragone plot (Gonzalez *et al.*, 2016; Layer, 1966).

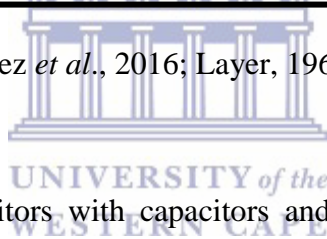


Table 1.1, compares supercapacitors with capacitors and batteries in terms of cycle life, specific power, specific energy etc. and supercapacitors can endure loads of cycles owing to their storage mechanisms which make them beneficial over conventional capacitors and batteries. The highly reversible electrostatic storage produces no changes in the electrode volume hence eliminating the swelling that occurs in typical redox reactions in the majority of a battery's active material during charging and discharging cycles. Table 1.2 compares the key variances in the properties of batteries and supercapacitors (Gonzalez *et al.*, 2016; Halper & Ellenbogen, 2006; Iro *et al.*, 2016). Comparing the properties of batteries and supercapacitors, it can be observed that those of supercapacitors are highly advanced therefore making supercapacitors more ideal for energy storage.

Table 1. 1: Comparison table of selected electrochemical energy storage technologies from a conventional capacitor to a battery.

Characteristics	Capacitor	Supercapacitor	Battery
Specific energy (Whkg ⁻¹)	<0.1	1 - 10	10-100
Specific power(Wkg- 1)	>10 000	500-10 000	<1000
Discharge time	10 ⁻⁶ to 10 ⁻³	s to min	0.3 - 3 h
Charge time	10 ⁻⁶ to 10 ⁻³	s to min	1 - 5 h
Coulombic efficiency (%)	About 100	85 - 98	70 - 85
Cycle life	Almost infinite	>500 000	About 1000

Table 1. 2: Table comparing the properties of batteries and supercapacitors.

Comparison parameter	Battery	Supercapacitor
Storage mechanism	Chemical	Physical
Power limitation	Reaction kinetics mass transport	Electrolyte conductivity
Energy storage	High (bulk)	Limited (surface area)
Charge rate	Kinetically limited	High, same as discharge
Cycle life limitations	Mechanical stability, chemical reversibility	Side reactions

Supercapacitors consist of two electrodes (anodic and cathodic) submerged in an electrolyte with a separator between the electrodes, shown in Figure 1.2. The electrodes are made-up from porous and high surface area materials such as carbon based materials, metal oxides/nanoparticles and conducting polymers. These materials pores are in the nanometer range while the surface area range from 200-500 m² g (Kim *et al.*, 2010).

In a conventional capacitor, there is a separation by an insulating dielectric material between the two conducting electrodes. When there is an application of voltage, opposite charges accumulate on surfaces of each electrode and dielectric keeps the charges separate and therefore produces electricity which then allows a capacitor to store energy. The capacitance of each material is directly proportional to surface area, A , of each electrode and inversely proportional to distance, D , between the electrodes.

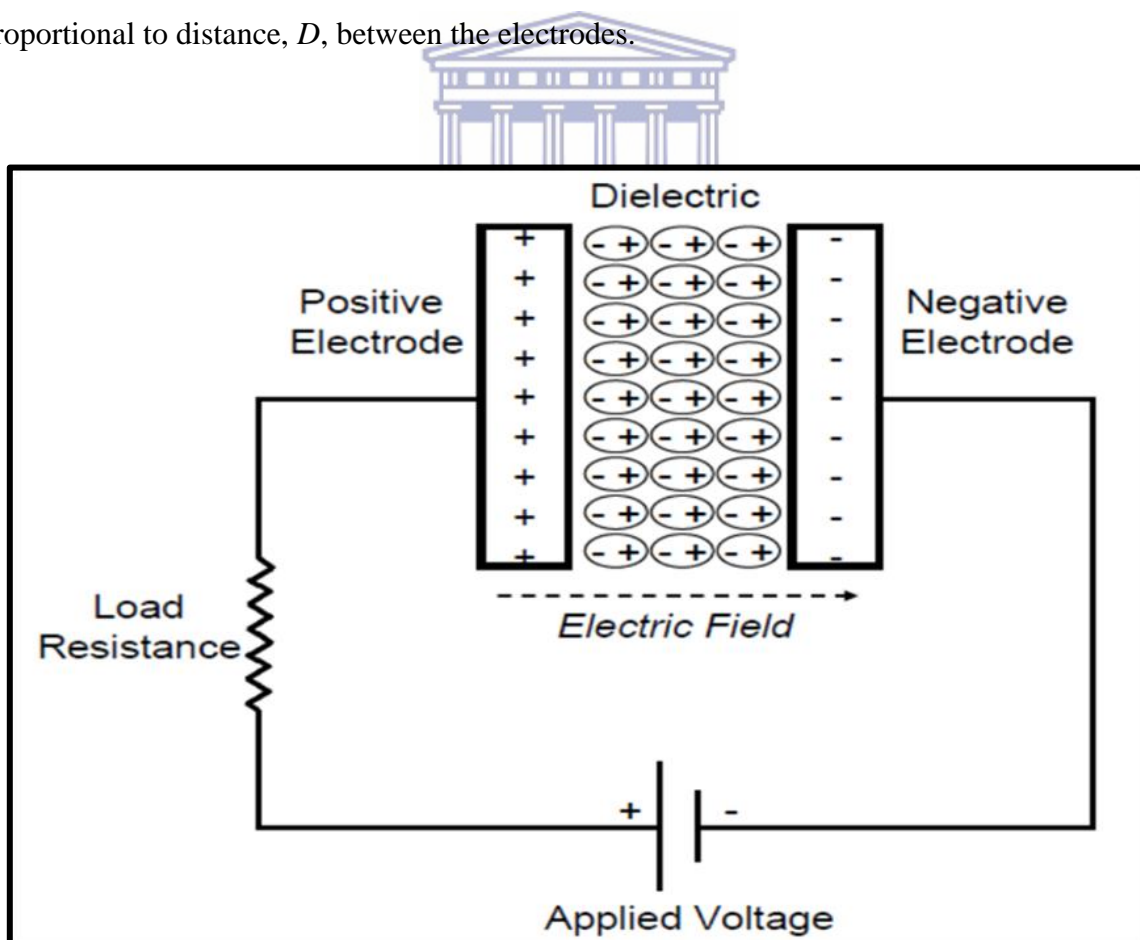


Figure 1. 2: A representation diagram of a conventional dielectric capacitor (Halper & Ellenbogen, 2006).

Charge is basically stored adjacent the interface or at the micropores between the solid electrode material and the electrolyte. When a voltage, V , is applied to a capacitor or supercapacitor, the electrode is accumulated with opposite charges (negative and positive). Conventional dielectric capacitors and supercapacitors are overseen by the same basic principles; however, supercapacitors integrate higher surface area electrodes and thinner dielectrics that decrease the distance, D , between electrodes, shown in Figure 1.3. Therefore, the capacitance and energy stored in a supercapacitor are increased as compared to the capacitance and energy of a conventional capacitor.

Capacitance is defined as the ratio of the variation in an electric charge in a system, positive voltammetric charge Q to the applied voltage V ,

$$C = \frac{Q}{V}$$



(1)

C is directly proportional to the surface area, A , and is inversely proportional to the distance, D , between each electrode.

$$C = \epsilon_0 \epsilon_r \frac{A}{D}$$

(2)

Wherein, ϵ_0 is known as the dielectric constant (or “permittivity”) of free space and, ϵ_r is the dielectric constant of the insulating material between the electrodes.

The two main characteristics of supercapacitors are their energy density and power density and for both of them, the density can be calculated as a quantity per unit volume and/or per unit mass. The energy, E , stored in a capacitor is directly proportional to its capacitance and is given by the following equation:

$$E = \frac{1}{2} CV^2 \quad (3)$$

Power, P , is known as the energy expended per unit time. The power of a supercapacitor is determined by considering that supercapacitors are circuits in series with external resistance, R , in which external components of a supercapacitor e.g. current collector, electrodes and dielectric material, has a high contribution to the resistance and the measured power is as follows (Halper & Ellenbogen, 2006; Kim *et al.*, 2010).

$$\begin{aligned} P_{max} &= \frac{V^2}{4R} \\ &= I^2R \end{aligned} \quad (4)$$



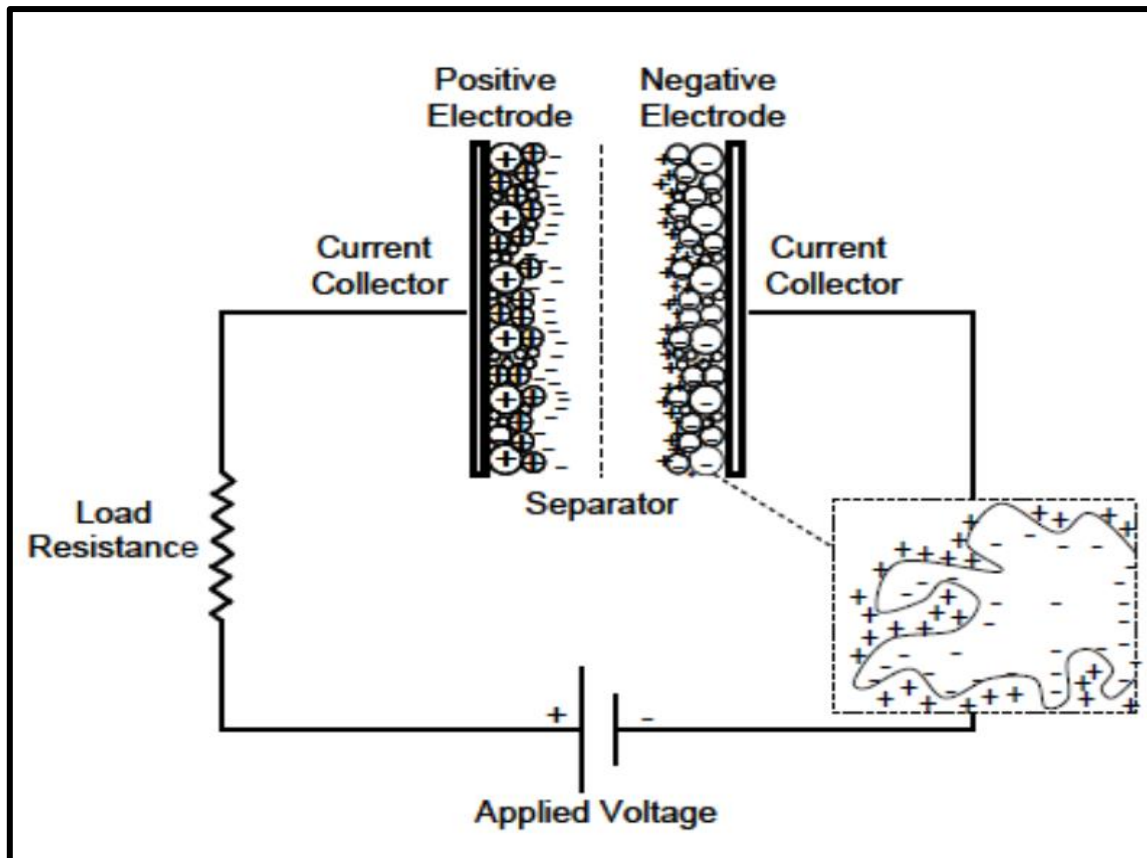


Figure 1. 3: Schematic diagram of a supercapacitor (Halper & Ellenbogen, 2006).

UNIVERSITY of the
WESTERN CAPE

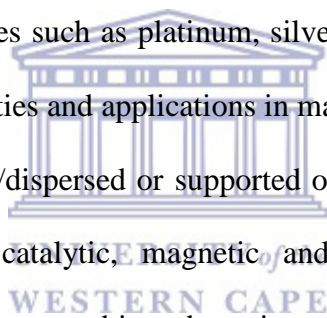
Supercapacitors have several advantages when compared to conventional capacitors, batteries and fuel cells and these include long life-time, low impedance, rapid charging and discharging, simple charge methods, cost effective energy storage, extended operation temperature range, meets environmental standards except when electrolytes that are non-degradable are employed, reduces drop in voltage compared to battery operated device without any supercapacitor, unlimited charging cycles versus secondary battery etc. Supercapacitors also have a low energy density, low voltage, linear discharge and higher self-discharge than that of an electrochemical battery as disadvantages (Conway & Pell, 2003; Kim *et al.*, 2010). Supercapacitors exploit the advantages to provide versatile solutions to a variety of emerging energy applications, especially those that require instant power

applications. These includes (whole/part) applications such as; industrial machinery, transport, storage of wind and solar energy, portable electronics (Burke & Zhao, 2015).

1.1.2 Materials for supercapacitor electrodes

There are three main general classes that make up supercapacitors and each class is categorized by its unique mechanism for storing charge. These are electrochemical double-layer capacitors which utilize only double layer storage and require understanding of surface area, pores structure, and ion size influences on charge storage; pseudo-capacitors in which materials generally exhibit higher specific capacitance and energy density relative to high surface area carbon and hybrid capacitors (Burke & Zhao, 2015; Conway & Pell, 2003; Capacitance, Case, Options, & Compliant, 2002; Endo *et al.*, 2001). Underlying charge-storage mechanism materials are not well understood. Carbon electrode materials such as graphene oxide, reduced graphene oxide, carbon aerogels, carbon black, carbon ink etc. have more established fabrication techniques, have higher surface areas, are synthesized at low cost when compared to other materials (Ganesh *et al.*, 2006; Simon & Gogotsi, 2009; Zhang *et al.*, 2009). The materials used in this study are graphene oxide/reduced graphene oxide (GO/rGO); metal nanoparticles of platinum, silver and copper anchored with dodecylbenzenesulphonic acid (DBSA) doped polyaniline (PANI). Amongst the carbon materials introduced, reduced graphene oxide (rGO) has proven to be a very promising candidate for use in supercapacitors due to its properties, easy exfoliation, easy and cheap synthesis from graphite. The rGO is known as the monolayer of graphite and is a promising material for supercapacitors. It has a large theoretical specific surface area of $2630 \text{ m}^2 \text{ g}^{-1}$, high intrinsic current mobility of $200\,000 \text{ cm}^2 \text{ V}^{-1} \text{ s}^{-1}$, high Young's modulus -1.0 Pa , thermal conductivity of $-5000 \text{ W m}^{-1} \text{ K}^{-1}$, optical transmittance of -97.7% and it has an

excellent electrical conductivity attention for transparent conductive electrode applications (Chen *et al.*, 2011; Rakhi & Alshareef, 2011). The surface area of rGO occurs much lower than the one found theoretically due to the unavoidable aggregation of graphene nanosheets and the capacitance falls in the range of 100 to 200 F g⁻¹ (Chen *et al.*, 2011; Xu *et al.*, 2011). Graphene oxide (GO), a single sheet of graphite oxide and considered to be one of graphenes derivatives, contains a large range of reactive oxygen functional groups, has good electrical, mechanical and thermal properties, high surface area, which then makes it a good candidate in applications such as polymer composites, energy-related resources, medical and biological sensors, field-effect transistors (FET) and biomedical applications (Gao *et al.*, 2015; Xu *et al.*, 2011). With GO/rGO properties being excellent makes it a possible candidate as a new 2D support for metal nanoparticles such as platinum, silver and copper. Metal nanoparticles have attractive and unique properties and applications in many fields. It is expected that metal nanoparticles anchored/deposited/dispersed or supported on graphene oxide/graphene sheets could possibly display novel catalytic, magnetic and optoelectronic properties. The nanoparticles mentioned have been subjected to intensive research for the design of supercapacitor electrodes. Platinum, silver and copper are significant catalysts for many chemical and electrochemical reactions, oxygen reduction, hydrogen oxidation, methanol oxidation and hydrogenations. Well dispersed, small-sized nanoparticles are predicted to exhibit enhanced activity and selectivity for supercapacitor reactions (Das *et al.*, 2011; Grinou *et al.*, 2012; Q. Zhang *et al.*, 2010). PANI is a promising conductive material involved in pseudocapacitance and because of its fundamental electrical conductivity with organic dopants; it has attracted a lot of attention as a possible material for electronic devices, gas sensors, microwave absorption layers and supercapacitors. The electrical properties of PANI can be reversibly controlled and this is achieved by both charge transfer doping and protonation (Ashokan *et al.*, 2015; Kumar *et al.*, 2013). As far as we know and concerned,

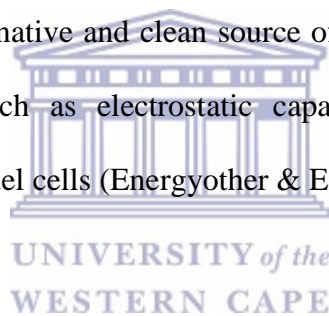


there have been no reports on the synthesis and characterization of GO/Metal nanoparticle/DBSA doped PANI for application in supercapacitors. This work, therefore, combines double layer charging (graphene oxide/reduced graphene oxide) and pseudocapacitance (transition metal nanoparticles) to enhance energy and power densities.

1.2 Problem statement

South Africa in 2008 faced a harsh and unexpected power crisis which was the result of policy and regulatory uncertainty over the previous generations as much as shortcomings in the management of the system (Department of Energy, 2015; Joffe, 2012). In the late 1900's and early 2000's government policy stated that the electricity supply industry should be opened-up to competition and that Eskom (South Africa's main electricity supplier) should not build new power stations. However, the policy and regulatory frameworks were not incorporated for private sector participation nor put in place from the beginning. Critically, nor were electricity tariffs at attractive levels for the private sectors to get the returns they needed to make investment. It was predictable that South Africa was to need massive new investments in producing capacity to meet growth in demand. However, in late 2004 by the time the government withdrew from privatization and gave Eskom the order to build hit was already too late to bring new base and load power classes to prevent a shortfall in generating capacity (Maasdam, 2008). The result was that by 2007, after a period of strong economic growth, the margin between supply and demand had fallen to levels which made the power system extremely susceptible. There were many causes that made it increasingly difficult to meet demand and these included capacity shortage, volatile operating performance, low coal stockpiles and wet weather. Eskom could not meet the demand in energy and had to resort to

national rotational ‘load shedding’ (interruption in power supply at certain times when there is not enough supply capacity available to meet the demand from all customers) from late 2007 to protect the power system from a total shutdown. A national emergency was professed on 25 January 2008 and load shedding continued until the end of March 2008. Eskom was initiating a recovery plan with support from the government and other businesses. South Africa also faced load shedding in the year 2015 for a few months due to the same reason mentioned above (Department of Energy, 2015; Joffe, 2012). To remedy the situation, The Department of Energy has launched to bring in substantial new investment from private renewable energy producers; Eskom has embarked on its own renewable energy projects, in wind and solar power, and aspires to do more. It has become necessary and important to research, invest and find an alternative and clean source of energy. Hence devising efficient energy storage technologies such as electrostatic capacitor, electrochemical capacitors (supercapacitors), batteries and fuel cells (Energyother & Energy, 1950).



1.3 Rationale and Motivation

Global economic development and prosperity over past and present century have been built on cheap and abundant fossil fuels, but there is limited amount of fossil fuels with percentages dropping to low values, with petroleum at 39%, natural gas at 24% and coal at 23%. Recent estimates have shown an average of 2% annual growth in global oil demand with 3% natural decline in production from existing reserves. Wind and solar energy are great alternatives but these renewable energy options are intermittent due to the need to harness their energies when sun or winds are/is on. Hence in electrostatic field, it has become necessary to find an alternative source of energy by devising efficient energy storage

technologies such as electrostatic capacitor, electrochemical capacitors (supercapacitors), batteries and fuel cells (Kvemdokk *et al.*, 1996; Höök & Tang, 2013; Shafiee & Topal, 2009). The fossil fuel energy consumption in South Africa has hit the bottom like the rest of the world. According to the World Energy Outlook fossil fuel energy consumption (% of total) in South Africa was reported to be at 86.91 % in 2014. Comparing the fossil fuel energy consumption of 90.51 % in 1982 with 86.71 % in 2013 while the lowest value was 84.24 % in 2000, we can conclude that fossil fuels in South Africa have also been depleting (Pickard & Makhijani, 2014; WWF, 2008). With South African fossil fuels depleting and the electricity crisis that hits the country now and again, the demand for energy and energy storage devices has greatly increased, to work in different applications such as automobiles and various portable electronic devices. The demand for batteries, fuel cells and supercapacitors has increased, however, the electrode materials and electrolytes employed during the construction of the energy storage devices are very vital and significant. The performance of the automobiles and portable electronic devices strongly depends on these electrode materials and electrolytes that are used during the construction of the energy storage devices (Brumagne *et al.*, 2007). There are several developing materials or nanomaterials that have large surface/interface areas, desired nanostructures which have been developed for applications in energy-related devices, for example, graphene oxide/reduced graphene oxide work well for supercapacitors, lithium-ion works tremendously well for batteries and bimetallic nanoparticles work well for fuel cells. Supercapacitors utilize high surface area electrode materials and thin dielectrics. This allows them to reach higher capacitances comparable to conventional capacitors, higher power density and faster charging comparable to batteries and fuel cells (Miller., 2007). Currently, commercial supercapacitor electrodes are made of carbon which is inexpensive, has high resistance to corrosion and is environmentally friendly. Other commercial supercapacitor electrodes are made of transition

metal oxides/nanoparticles or conducting polymers and these supercapacitors operate under pseudo-capacitance (Liua *et al.*, 2017). This work explores the use of carbon-based materials (graphene oxide/graphene) in combination with metal nanoparticles (platinum, copper and silver) and conducting polymers doped or in combination with dodecylbenzenesulphonic acid. The combination of these prepared materials should enhance capacitance when the materials have been applied for supercapacitors.

1.4 Objectives

The aim of this study is to develop flexible, affordable, high efficient and high performance supercapacitors with electrode materials that will enhance the supercapacitors specific capacitance. The general objective is to develop flexible and high-performance graphene oxide intercalated with metal nanoparticles anchored DBSA doped PANI supercapacitor electrode composite materials. The combination of the properties of these materials will ensure an increase in capacitances, energy and power of the developed supercapacitors. This study would benefit the energy industry of South Africa and many households when there are power shortages. Instead of using batteries which have low specific power and high specific energy, supercapacitors exploit the advantages to provide versatile solutions to a variety of emerging energy applications, especially those that require instant power applications. These includes (whole/part) applications such as; industrial machinery, transport, storage of wind and solar energy, portable electronics etc.

1.4.1 Preparation of graphene oxide and reduced graphene oxide

- To prepare graphene oxide by the modified Hummers method
- To prepare reduced graphene oxide by hydrazine monohydrate under adjusted temperature
- To characterization and electro-analyze of graphene oxide and reduced graphene oxide using different techniques.

1.4.2 Synthesis of graphene oxide loaded with platinum, silver and copper nanoparticles by electrostatic self-assembly

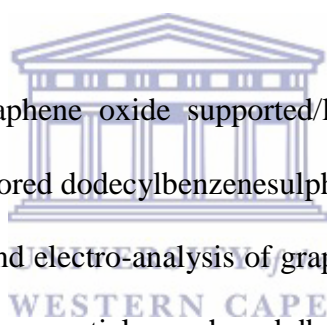
- Characterization and electro-analysis of graphene oxide supported/loaded with platinum, silver and copper nanoparticles

1.4.3 Preparation of graphene oxide supported/loaded with platinum, silver and copper nanoparticles anchored dodecylbenzenesulphonic acid doped PANI

- Characterization and electro-analysis of graphene oxide loaded with platinum, silver and copper nanoparticles anchored dodecylbenzenesulphonic acid doped PANI

1.4.4 Fabrication of the electrode material

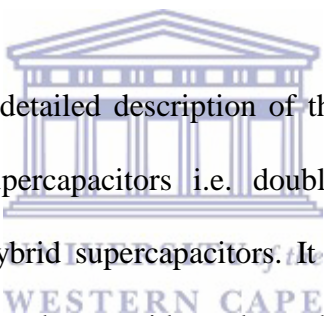
- To prepare the electrode materials
- To construct the supercapacitor cell
- Test materials for supercapacitor application



1.5 Thesis Outline

This study consists of six chapters and the following describes what each chapter entails

Chapter 1: This chapter gives the research background of supercapacitors, what they are, their properties, their applications, the parameters used to calculate the capacitance, specific power and specific energy; and the materials used for supercapacitor electrodes etc. This chapter also gives the problem statement which outlines the reasons for study and the motivational and rationale behind this study. The main aim and objectives of this study have also been outlined.



Chapter 2: The chapter gives a detailed description of the work (literature review) which includes the introduction of supercapacitors i.e. double layer supercapacitors, pseudo capacitive supercapacitors and hybrid supercapacitors. It also includes the main materials used in this work; specifically graphene oxide and graphene, their unique properties and applications as supercapacitor materials. The main important issue is to know which materials i.e. whether graphene oxide or reduced graphene oxide is proper for supercapacitors. Platinum, silver and copper combined with graphene oxide or graphene are also discussed, whether they can be utilized as good supercapacitor materials. Supercapacitors have been applied in many applications and like any other country that wants to improve their energy, South Africa is making use of them. Therefore the chapter also includes how South Africa is making use of supercapacitors in order to improve the energy.

Chapter 3: The chapter gives detailed information on graphene oxide and graphene as good supercapacitor materials. The graphene oxide and reduced graphene oxide are compared to

determine which material is more suitable as a supercapacitor material. Graphene oxide is synthesized by the modified Hummers method in which it was oxidized over a period of five days. The graphene oxide was then reduced to graphene by hydrazine monohydrate. Both materials were then characterized by different instrumental methods of analysis. The results are discussed.

Chapter 4: The chapter discusses graphene oxide decorated with platinum, silver and copper nanoparticles as supercapacitor materials. The materials GO/Pt NPs, GO/Ag NPs and GO/Cu NPs were synthesized and characterized by different characterization techniques. The results are discussed.

Chapter 5: The chapter discusses graphene oxide decorated with platinum, silver and copper nanoparticles anchored with DBSA doped PANI to develop and construct high effective and high performance supercapacitor electrodes. The materials GO/Pt NPs/DBSA doped PANI, GO/Ag NPs/DBSA doped PANI and GO/Cu NPs/DBSA doped PANI were synthesized and characterized by different characterization techniques. The electrode materials are prepared and constructed and then tested by the Galvanostatic charge/discharge for application in supercapacitors.

Chapter 6: The thesis is concluded giving a brief discussion of the objectives achieved in relation to all the chapters involved, the results are briefly discussed and recommendations for future works are given.

References

- Ashokan, S., Ponnuswamy, V., & Jayamurugan, P. (2015). Synthesis and characterization of CuO nanoparticles, DBSA doped PANI and PANI/DBSA/CuO hybrid composites for diode and solar cell device development. *Journal of Alloys and Compounds*, 646, 40–48.
- Brumagne, S., Janssens, L., Claeys, K., & Pijnenburg, M. (2007). *Energy Chapter | 12 |*, 135–144.
- Burke, A., & Zhao, H. (2015). Present and future applications of supercapacitors in electric and hybrid vehicles. *2015 IEEE 82nd Vehicular Technology Conference*, 1–5.
- Capacitance, U. H., Case, S., Options, S., & Compliant, R. (2002). Type EDL electric double layer supercapacitors ultra high capacitance , small case size options RoHS compliant type EDL electric double layer supercapacitors ratings. *Options*.
- Chen, Y., Zhang, X., Zhang, D., Yu, P., & Ma, Y. (2011). High performance supercapacitors based on reduced graphene oxide in aqueous and ionic liquid electrolytes. *Carbon*, 49(2), 573–580.
- Conway, B. E., & Pell, W. G. (2003). Double-layer and pseudocapacitance types of electrochemical capacitors and their applications to the development of hybrid devices. *Journal of Solid State Electrochemistry*, 7(9), 637–644.
- Das, M. R., Sarma, R. K., Saikia, R., Kale, V. S., Shelke, M. V., & Sengupta, P. (2011). Synthesis of silver nanoparticles in an aqueous suspension of graphene oxide sheets and its antimicrobial activity. *Colloids and Surfaces B: Biointerfaces*, 83(1), 16–22.
- Department of Energy. (2015). South Africa's energy situation - Fuel pricing in South Africa. *Energy Advocacy*, (1).

- Endo, M., Takeda, T., Kim, Y. J., Koshiba, K., & Ishii, K. (2001). High power electric double layer capacitor (EDLC's); from operating principle to pore size control in advanced activated carbons. *Carbon Science, 1*(3), 117–128.
- Energyther, R., & Energy, A. (1950). Renewable energy and other alternative energy sources, 149–157.
- Ganesh, V., Pitchumani, S., & Lakshminarayanan, V. (2006). New symmetric and asymmetric supercapacitors based on high surface area porous nickel and activated carbon. *Journal of Power Sources, 158*(2), 1523–1532.
- Gao, W. (2015). The chemistry of graphene oxide. *Graphene Oxide: Reduction Recipes, Spectroscopy, and Applications*, 61–95.
- Gonzalez, A., Goikolea, E., Barrena, J. A., & Mysyk, R. (2016). Review on supercapacitors: Technologies and materials. *Renewable and Sustainable Energy Reviews, 58*, 1189–1206.
- Grinou, A., Yun, Y. S., Cho, S. Y., Park, H. H., & Jin, H. J. (2012). Dispersion of Pt nanoparticle-doped reduced graphene oxide using aniline as a stabilizer. *Materials, 5*(12), 2927–2936.
- Halper, M., & Ellenbogen, J. (2006). Supercapacitors: A brief overview. *Report No. MP 05W0000272*, 1-29.
- Hoel Snorre Kvemdokk, M. (1996). Depletion of fossil fuels and the impacts of global warming. *Resource and Energy Economics, 18*(0928), 115–136.
- Höök, M., & Tang, X. (2013). Depletion of fossil fuels and anthropogenic climate change - A review. *Energy Policy, 52*, 797–809.
- Iro, Z. S., Subramani, C., & Dash, S. S. (2016). A brief review on electrode materials for supercapacitor. *International Journal of Electrochemical Science, 11*(12), 10628–10643.

- Jayalakshmi, M., & Balasubramanian, K. (2008). Simple capacitors to supercapacitors-an overview. *International Journal of Electrochemical Sciences*, 3, 1196–1217.
- Joffe, H. (2012). Challenges for South Africa's Electricity Supply Industry. *Helen Suzman Foundation Focus*, 64, 32–37.
- Kim, T. Y., Lee, H. W., Stoller, M., Dreyer, D. R., Bielawski, C. W., Ruoff, R. S., & Suh, K. S. (2010). High-performance supercapacitors based on polyionic liquid) - modified graphene electrodes. *American Chemical society*, 5(1), 436-442.
- Kumar, R., Ansari, M. O., & Barakat, M. A. (2013). DBSA doped polyaniline/multi-walled carbon nanotubes composite for high efficiency removal of Cr(VI) from aqueous solution. *Chemical Engineering Journal*, 228, 748–755.
- Lu, P., Xue, D., Yang, H., & Liu, Y. (2012). Supercapacitor and nanoscale research towards electrochemical energy storage. *International Journal of Smart and Nano Materials*, 4(1), 2–26.
- Maasdam, R. (2008). Special Report 2008/04: Energy crisis - The case of South Africa. *Rabobank Economic Research Department (1)*.
- Miller. (2007). History of technology A brief history of supercapacitors. *Battey and energy Technologies*, 521452, 61–78.
- Pickard, S., & Makhijani, S. (2014). Fossil fuel exploration subsidies: *Rystad Energy*, 6.
- Rakhi, R. B., & Alshareef, H. N. (2011). Enhancement of the energy storage properties of supercapacitors using graphene nanosheets dispersed with metal oxide-loaded carbon nanotubes. *Journal of Power Sources*, 196(20), 8858–8865.
- Shafiee, S., & Topal, E. (2009). When will fossil fuel reserves be diminished? *Energy Policy*, 37(1), 181–189.
- Simon, P., & Gogotsi, Y. (2009). Materials for electrochemical capacitors. *Nanoscience and Technology: A Collection of Reviews from Nature Journals*, 845–854.

- Snook, G. A., Peng, C., Fray, D. J., & Chen, G. Z. (2007). Achieving high electrode specific capacitance with materials of low mass specific capacitance: Potentiostatically grown thick micro-nanoporous PEDOT films. *Electrochemistry Communications*, 9(1), 83–88.
- Winter, M., & Brodd, R. J. (2004). What are batteries, fuel cells, and supercapacitors? *Chemical Reviews*, 104(10), 4245–4269.
- WWF. (2008). Cheaper electricity with renewable energy in South Africa. *Energy*, 1-28.
- Xu, B., Yue, S., Sui, Z., Zhang, X., Hou, S., Cao, G., & Yang, Y. (2011). What is the choice for supercapacitors: graphene or graphene oxide? *Energy & Environmental Science*, 4(8), 2826.
- Zhang, L. L., Zhou, R., & Zhao, X. S. (2009). Carbon-based materials as supercapacitor electrodes. *Journal of Materials Chemistry*, 38(29), 2520–2531.
- Zhang, Q., Yang, Z., Ding, B., Lan, X., & Guo, Y. (2010). Preparation of copper nanoparticles by chemical reduction method using potassium borohydride. *Transactions of Nonferrous Metals Society of China*, 20(50834003), s240–s244.
- Zhang, X., Zhang, D., Chen, Y., Sun, X., & Ma, Y. (2012). Electrochemical reduction of graphene oxide films: Preparation, characterization and their electrochemical properties. *Chinese Science Bulletin*, 57(23), 3045–3050.

Chapter 2

Literature Review

Summary

Energy storage has proven to be a challenge for the past years. With natural resources and fossil fuels depleting, the need to use alternative sources of energy has been great. Alternative energy storage device are being intensely researched. The focus is to develop cheap, reliable, effective, efficient and environmentally friendly energy storage devices. The chapter gives a detailed description of the three main general classes of supercapacitors, being electrochemical double-layer capacitors, pseudocapacitors and hybrid capacitors and how the charge generation and storage in supercapacitors occur. The materials used for the fabrication of the supercapacitor electrodes have been mentioned including their exceptional properties. A description of the synthesis methods and characterization techniques of these materials has also been included. The chapter also covers the impact that supercapacitors will have on the energy industry of South Africa and how it will improve the energy crisis that South Africa faces.

Abstract

Supercapacitors are distributed into three main general classes, electrochemical double-layer capacitors (EDLCs) which utilize carbon based materials, pseudocapacitors which utilize metal oxides and hybrid capacitors which utilize a combination of both the EDLC and pseudocapacitors. Supercapacitor charges arise from separation of electronic and ionic charges at the interface between electrode materials and the electrolyte solution and there exist no charge transfer between the electrode and electrolytes i.e. across the double-layer and charge storage is highly reversible which enables EDLCs to achieve high cycling stabilities. Carbon materials such as graphene oxide, carbon nanotubes, carbon black etc. give the best EDLC. In pseudo-capacitors Faradaic charge transfer occurs between electrolyte and electrode and the capacitance arises due to progressive surface/bulk redox reactions between oxidation states of transition metal oxides (give the best pseudocapacitance) when applying voltage. Hybrid capacitors exploit the advantages of EDLC's and pseudocapacitors but end to exploit the relative advantages and alleviate the disadvantages to comprehend better performance characteristics. These capacitors make use of Faradaic and non-Faradaic processes to charge storage therefore achieving higher energy and power densities. Most research has been focused on three different types of hybrid capacitors namely composite, asymmetric, and battery-type, respectively, distinguished by their electrode configuration. Applications for supercapacitors in South Africa are reviewed.

2.1 Introduction

It is very important that new, low-cost, flexible and environmentally friendly energy storage systems be developed, to cater for the energy challenges (brought by, by global warming) and needs of modern society and emerging ecological concerns (Wang *et al.*, 2009). Supercapacitors are energy storage devices with very high energy and power capacities and low internal resistance that are able to store and deliver energy at relatively higher capacities when compared to batteries due to the mechanism of energy storage which involves a simple charge separation at the interface between the electrode and electrolyte (Ganesh *et al.*, 2006a; Zheng *et al.*, 2017). A supercapacitor consists of an electrolyte, two electrodes and a separator that electrically separating the electrodes. The active material for the electrode is considered one of the most important components of supercapacitors. Some of the most important advantages of supercapacitors when compared with other energy storage devices are long life, high power, flexible packaging, wide thermal range (-40 °C to 70 °C), low maintenance and low weight (Iro *et al.*, 2016). Supercapacitors also have their shortcomings with challenges such as low energy density, low production cost, low voltage per cell and high self-discharge. Developing new electrode materials overcomes the obstacle of low energy (Portet *et al.*, 2005). The most promising materials for supercapacitors today are carbon materials (carbon nanotubes, carbon black, graphene, carbon aerogels, and activated carbon and carbon ink), metal oxides, conducting polymers and a combination of each which gives a composite (Jampani *et al.*, 2010; Shao *et al.*, 2013). Carbon materials are used due to high specific areas, lower cost, and more established fabrication techniques than other materials (Zhang *et al.*, 2009). Metal oxides are used due to their high specific capacitance and low resistance making it easier to construct high energy and power supercapacitors. In conducting polymers reduction-oxidation process is used to store and release charge (Ganesh

et al., 2006b; Halper & Ellenbogen, 2006; Mahmood *et al.*, 2014; Gcilitshana, 2003; Iro *et al.*, 2016). Currently, researchers focused on supercapacitors are concentrating on how to improve their energy density while maintaining high power density and fast charge/discharge (Joon *et al.*, 2017). The work focuses on graphene oxide (GO) and reduced graphene oxide (rGO) decorated with platinum, silver and copper anchored dodecylbenzenesulphonic acid (DBSA) doped polyaniline (PANI) for the development of high and effective performance supercapacitors. The main aim is to combine the properties of GO/rGO with those of the metal nanoparticles and DBSA doped PANI to enhance the capacitance of the developed supercapacitor electrodes.

2.2 Energy storage mechanism



The mode of operation of supercapacitors is based on energy storage and distribution of ions that are coming from the electrolyte to the surface area of the electrodes. Based on the energy storage mechanism supercapacitors are classified as electrochemical double-layer capacitors, pseudocapacitors, and hybrid supercapacitors as shown in Figure 2.1 (Endo *et al.*, 2001; Lu *et al.*, 2012)

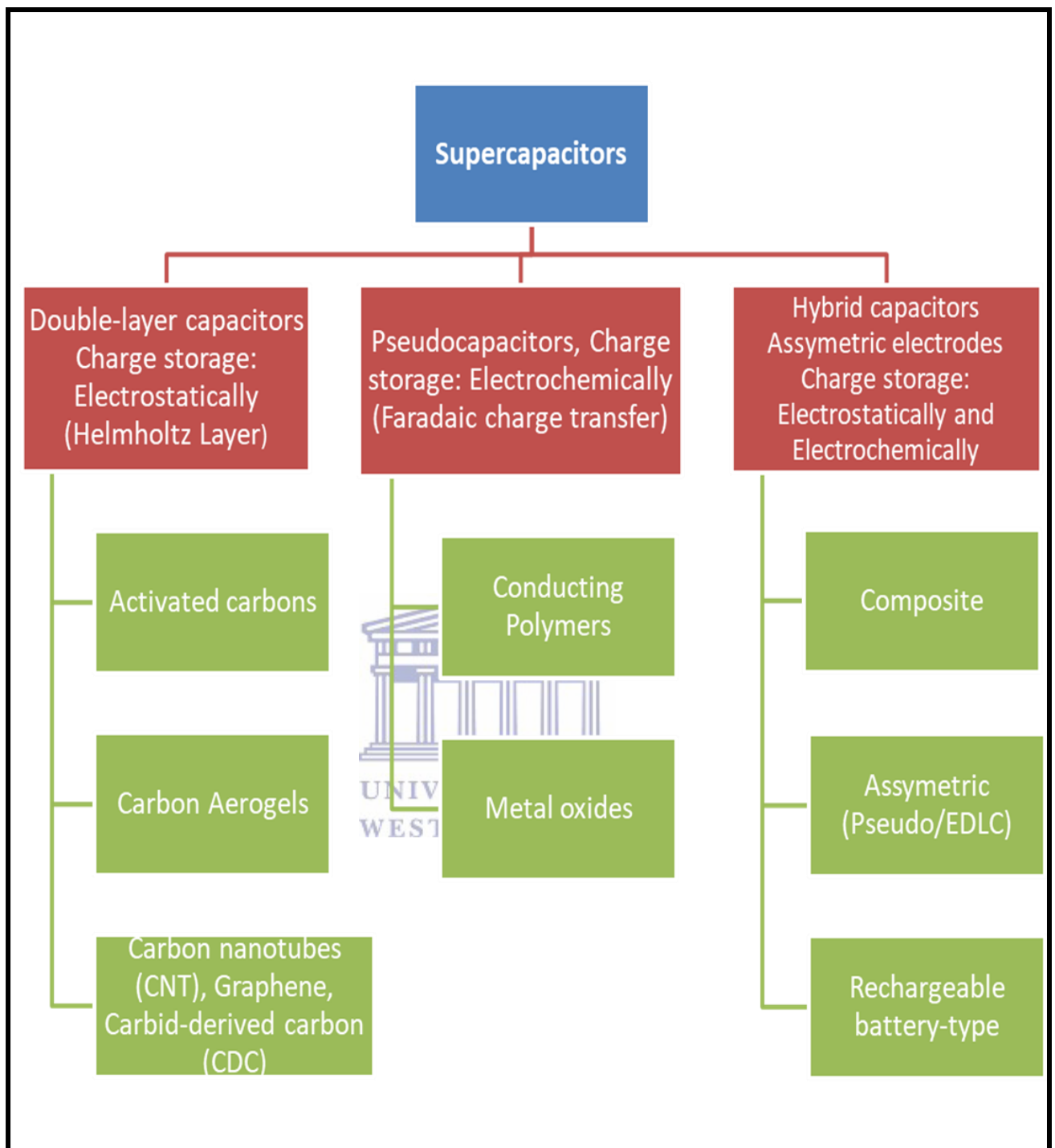


Figure 2. 1: Classification of supercapacitors (Simon & Gogotsi, 2009).

2.2.1 Electrochemical double layer capacitors (EDLCs)

EDLCs are constructed using two carbon substrates as electrodes, an electrolyte and a separator as shown in Figure 2.2.

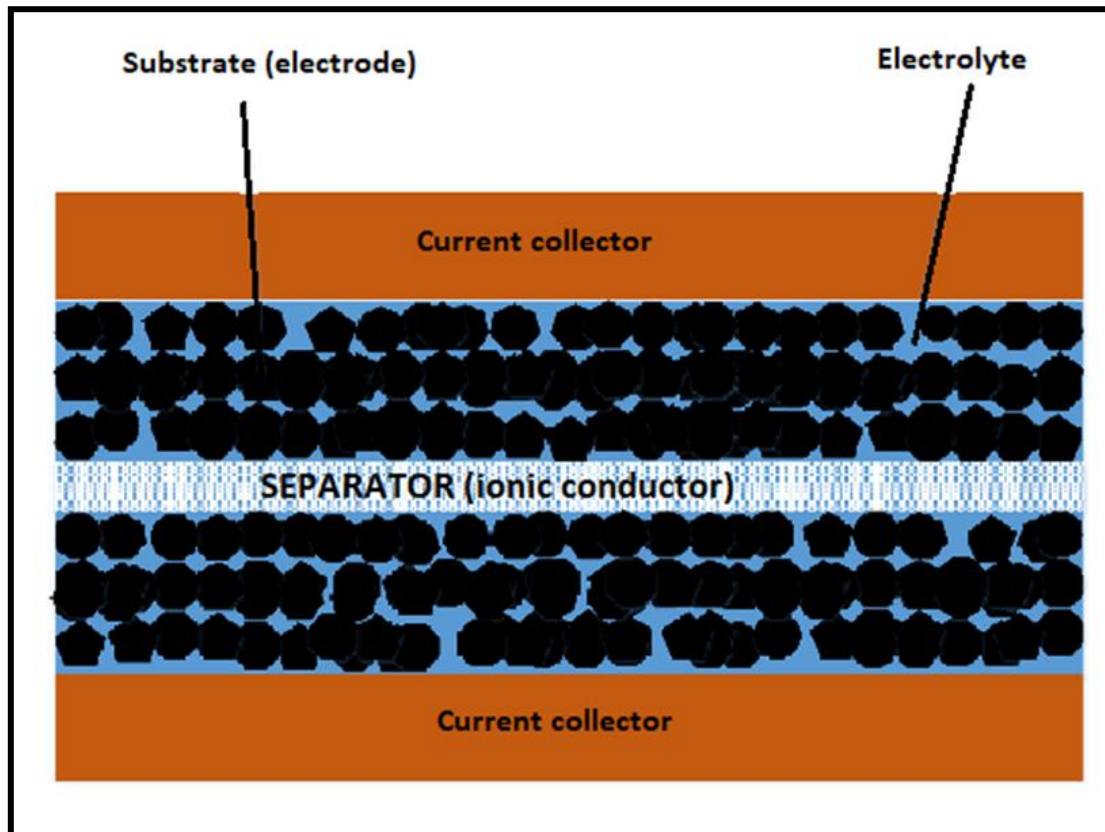


Figure 2. 2: Symmetric supercapacitor schematic diagram (Shao *et al.*, 2013).

EDLCs can either store charge electrostatically or via non faradic process, which involves no transfer of charge between electrode and the electrolyte (Lekakou *et al.*, 2011). Charging a supercapacitor forces electrons to move from the positive electrode to the negative electrode through an external circuit (Endo *et al.*, 2001; P. Sharma & Bhatti, 2010). As a result, there is an imbalance of ions that are formed in the EDL positive electrode that compensates the external charge unbalance and the cations within the electrolyte concentrate in the negative

electrode. Electrons travel from the negative electrode to the positive electrode through an external circuit during discharge and there exists a mix of ions in the pores until the cell is charged (Endo *et al.*, 2001; Jayalakshmi & Balasubramanian, 2008; Lei & Lekakou, 2010). The flexibility of ions into the pores of an electrode material is influenced by pore size therefore the ions in the bulk electrode do not move similarly. However, if the pore size is small makes the pores inaccessible and therefore not contribute anything to double layer capacitance, as shown in Figure 2.3

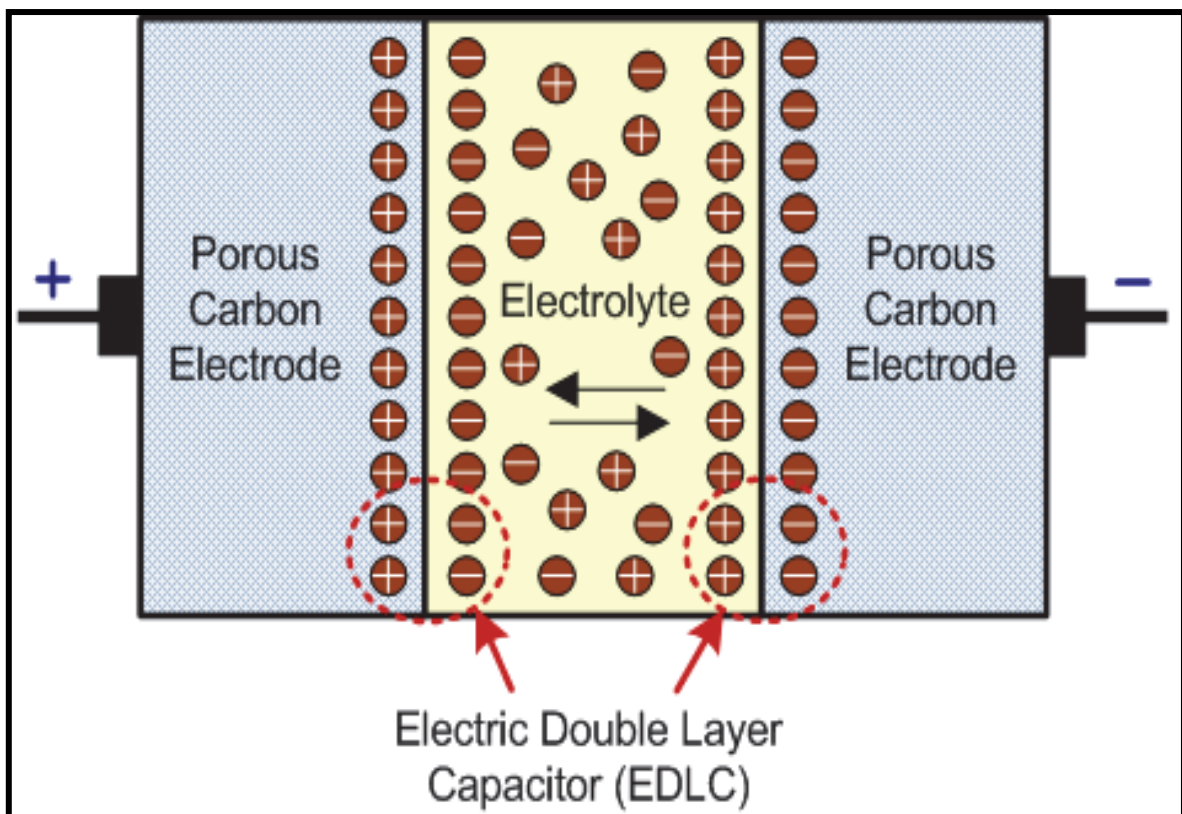
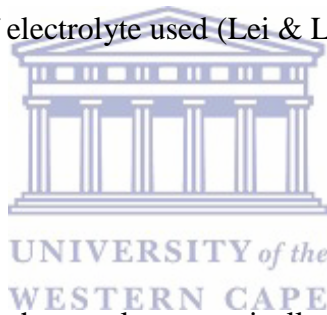


Figure 2. 3: Schematic of an electrical double layer (Pellecchia & Holmes, 2008).

To evade recombination of ions at electrodes a double layer of charge is formed. The double layer, combined with the increase in specific surface area and distances between electrodes decreased, allows EDLCs to attain higher energy density (Bhujun *et al.*, 2017; Hu *et al.*, 2004; Kim *et al.*, 2010). Furthermore, the storage mechanism for EDLCs allows for very fast

energy uptake, better power performance and delivery but due to non-faradaic processes this is therefore, no chemical reaction. It eliminates swelling observed in active material which batteries demonstrate during charging and discharging (Stoller *et al.*, 2008). A few differences between EDLCs and batteries can be observed as (i) EDLCs can endure loads of cycles unlike batteries that can only endure a few thousand at their best. (ii) charge storage mechanism does not involve solvent of the electrolyte (Conway & Pell, 2003; Schneuwly & Gallay, 2000; Stević *et al.*, 2010). However, EDLCs devices experience a limited energy density due to the electrostatic surface charging mechanism (Portet *et al.*, 2005), which is why today's EDLCs research is mainly focused on increasing energy performance and improving temperature range where batteries cannot operate. Performance of EDLC can be adjusted depending on the type of electrolyte used (Lei & Lekakou, 2010).

2.2.2 Pseudocapacitors



Compared to EDLCs, that store charge electro-statically in pseudocapacitors fast faradaic reactions take place to an extent limited by finite amount of active material or available surface and capacitance arises due to progressive redox reactions between several oxidation states (Venkataraman, 2015). Pseudocapacitors store charge via Faradic process which involves the transfer of charge between electrode and electrolyte (Conway & Pell, 2003; Iro *et al.*, 2016; Lota *et al.*, 2007). When applying a potential to a pseudocapacitor, reduction and oxidation take place on the electrode material. The process involves the route of charge transfer across the double layer which then results in Faradaic current passing through the supercapacitor cell (Conway & Pell, 2003; Gonzalez *et al.*, 2016; Venkataraman, 2015). It has been shown that transition metal oxides and conducting polymers are of interest to pseudocapacitors (Yan *et al.*, 2016) but due to the faradic nature, which involves reduction-

oxidation like in the case of batteries; they therefore suffer lack of stability during cycling and low power density (Kim *et al.*, 2010; Mastragostino *et al.*, 2001; Sharma & Bhatti, 2010).

Figure 2.4 shows a schematic of a pseudocapacitor:

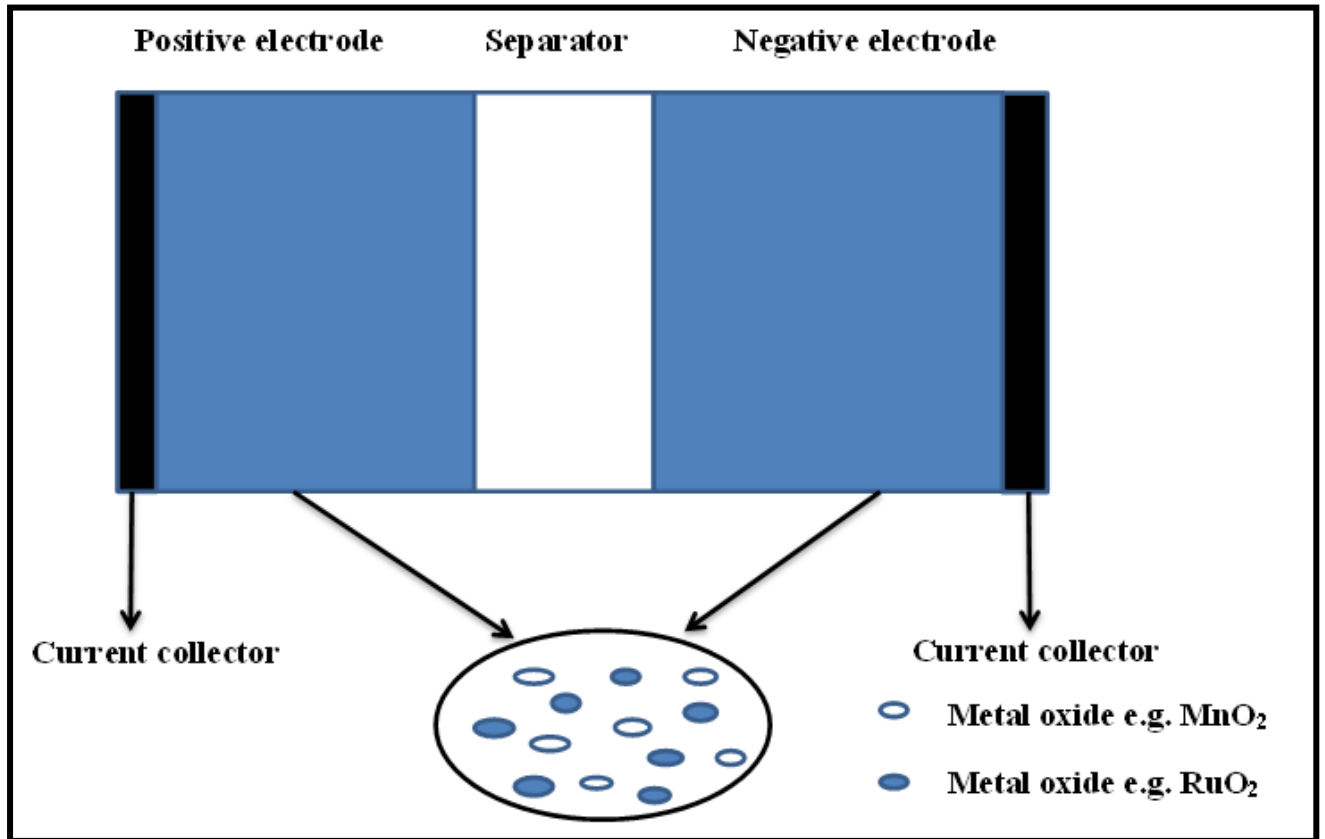


Figure 2. 4: Schematic of a pseudocapacitor (Kiamahalleh *et al.*, 2012).

2.2.3 Hybrid capacitors

As observed EDLCs give good cyclic stability and good power performance while pseudocapacitors give good specific capacitance. In hybrid capacitors it offers or gives a combination of both. That is by combining the energy source of battery-like electrode with a power source of capacitor-like electrode in the same cell (Ehsani *et al.*, 2017; Lota *et al.*, 2007; Reynolds, 2009). When there is a correct electrode combination, a possibility to

increase the cell voltage can be observed which in turn can lead to an improvement in energy and power densities. In the past several combinations have been tested, with both positive and negative electrodes in aqueous and inorganic electrolytes (Jung *et al.*, 2014). Generally, the Faradic electrode results in an increase of energy density but at the cost of cyclic stability. This is the main drawback of hybrid devices when compared to EDLCs, therefore it is more important to avoid turning a good supercapacitor into ordinary battery. Currently, researchers are focused on the three different types of hybrid supercapacitors, which can be distinguished by their electrode configurations: Composite, Asymmetric and Battery-type (Bello *et al.*, 2013; Salas *et al.*, 2014; Ganesh *et al.*, 2006). Figure 2.5 shows a schematic diagram of a hybrid capacitor:

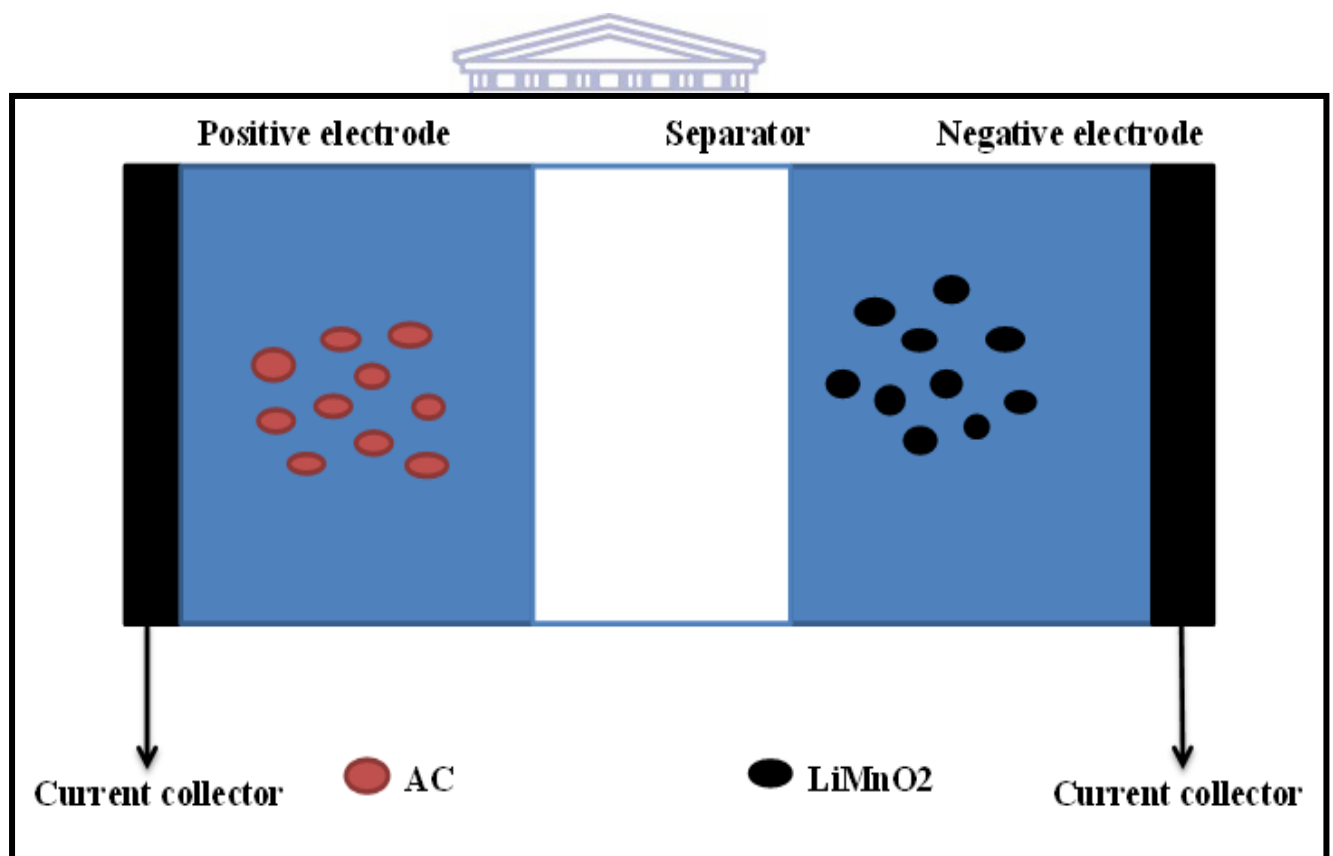


Figure 2. 5: Schematic of a hybrid capacitor (Li *et al.*, 2017).

2.2.4 Composite

Composite electrodes are a combination of carbon based materials such as carbon nanotubes, graphene, carbon black etc. with either a metal oxide such as copper oxide, ruthenium oxide etc. or conducting polymer such as polyaniline, polypyrrole etc. in a single electrode, meaning that the single electrode will consist of both physical and chemical charge storage mechanisms (Cygan *et al.*, 2017; Tang *et al.*, 2014). Carbon based materials permits a capacitive double-layer of charge and high specific surface area support (Zhang *et al.*, 2009) which results in the increase in the contact between the deposited pseudocapacitive materials and electrolyte. The pseudocapacitive material increases capacitance of the composite electrode through Faradaic reaction (Prusty *et al.*, 2017). Composite electrodes constructed from all three classes of supercapacitors i.e. carbon based material, conducting polymer and a metal oxide gives higher capacitances than either pure form of the carbon material, conducting polymer and metal oxide. These combinations have been tested and were observed to give higher capacitances (Endo *et al.*, 2001; Segal *et al.*, 2003). Currently, two types of composites exist, binary and ternary composites. Binary composites use two different electrode materials while ternary composites use three different electrode materials to form a single electrode (Monasterio *et al.*, 2017).

2.2.4.1 Asymmetric-hybrid capacitors

Asymmetric hybrid capacitors use a combination of non-faradaic and faradaic processes by joining an EDLC electrode with a pseudocapacitor electrode. They are setup in a way that the carbon material e.g. carbon nanotubes, graphene acts as a negative electrode while a metal

oxide or conducting polymer e.g. polyaniline, polypyrrole acts as a positive electrode (Ganesh *et al.*, 2006).

2.2.4.2 Battery-type

Battery type hybrid combines two different electrodes i.e. a combination of a supercapacitor electrode with battery electrode. This is like in the case of asymmetric hybrids but instead it's a combination of supercapacitor electrode with a battery electrode. This configuration was set up so as to exploit both properties of supercapacitors and batteries in one cell (Conway & Pell, 2003).

2.3 Electrode materials



Among the parameters that rely on the type of electrode materials used in supercapacitors are capacitance and charge storage. The supercapacitor electrode materials for the work are discussed here and a brief explanation of their properties and applications is given. Table 2.1 shows the specific capacitance of selected electrode materials. The section is divided in three sections, graphene oxide and graphene, metal nanoparticles and DBSA doped polyaniline.

Table 2. 1: Comparison table of specific capacitance of selected electrode materials (Zhang et al., 2009)

Material	Density g cm ³	Electrolyte	F g ⁻¹	F cm ³
Carbon cloth	0.35	KOH	200	70
		organic	100	35
Carbon black	1.0	KOH	95	95
Aerogel carbon	0.6	KOH	140	84
Particulate from SiC	0.7	KOH	175	126
		Organic	100	72
Particulate from TiC	0.5	KOH	220	110
		Organic	120	60
Anhydrous RuO ₂	2.7	H ₂ SO ₄	150	405
Hydrous RuO ₂	2.0	H ₂ SO ₄	650	1300
Doped conducting polymers	0.7	Organic	450	315

2.3.1 Graphene oxide/reduced graphene oxide

Graphene and graphene oxide have recently received rapidly growing attention in supercapacitor applications due to their exceptional properties. Graphene is a single layer of graphite and promises to be a good supercapacitor material due to its properties. It has a large

theoretical specific surface area of $2630 \text{ m}^2 \text{ g}^{-1}$, high intrinsic mobility of $200\,000 \text{ cm}^2 \text{ V}^{-1} \text{ s}^{-1}$, high Young's modulus $\sim 1.0 \text{ Pa}$, thermal conductivity of $\sim 5000 \text{ W m}^{-1} \text{ K}^{-1}$, optical transmittance of $\sim 97.7\%$ and it has an excellent electrical conductivity. These properties deserve attention for transparent conductive electrode applications (Zhu *et al.*, 2010). Due to the agglomeration of graphene nanosheets, the surface area of graphene is usually much lower than the theoretical one and its capacitance is generally in the range $100\text{--}200 \text{ F g}^{-1}$. Graphene oxide (GO), a single sheet of graphite oxide is considered to be one of graphene's derivatives. It contains a large range of reactive oxygen functional groups (Veerapandian *et al.*, 2012).

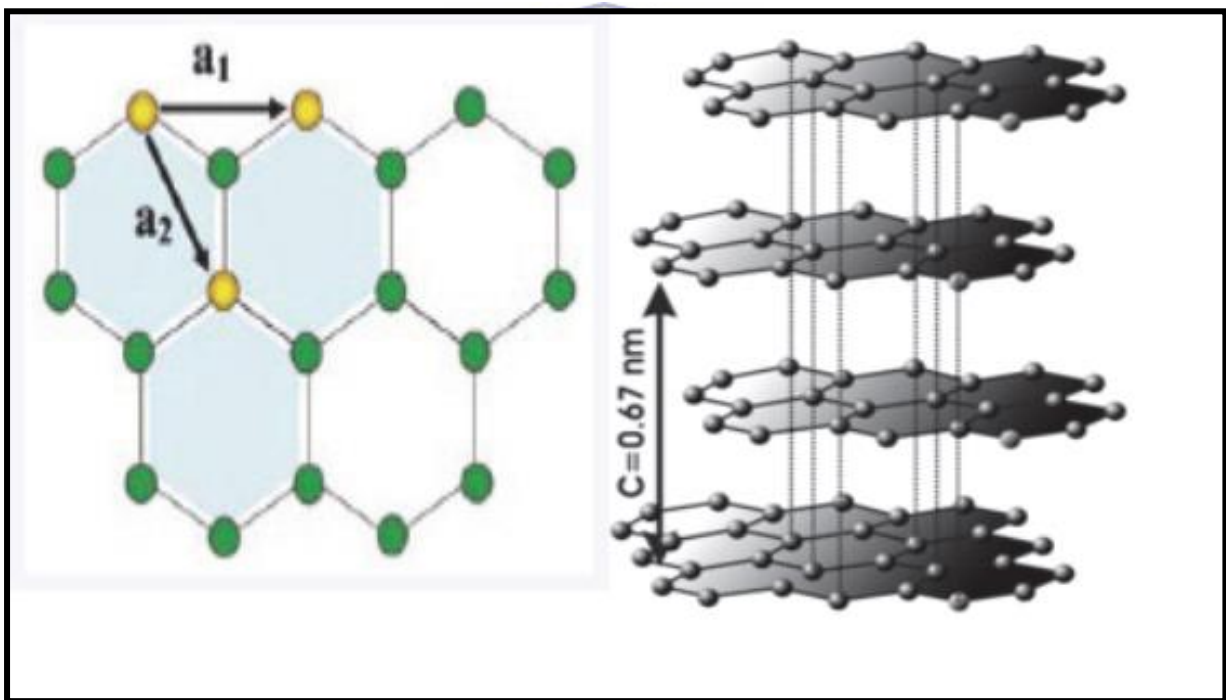


Figure 2. 6: The stacking of graphene sheets results in a layered structure (Casero *et al.*, 2012).

It has good electrical, mechanical, thermal properties and high surface area which then makes it a good candidate in applications such as polymer composites, energy-related materials,

sensors, 'paper'-like materials, field-effect transistors (FET) and biomedical applications (Huang *et al.*, 2012). GO is advantageous due to its easy dispersibility in water and other organic solvents, and as well as in other matrixes (Giudice & Shen, 2017). This advantage derives from the presence of the oxygen functionalities. Functionalization of GO can basically change GO's properties (Kou *et al.*, 2009). The resulting chemically modified graphenes could then potentially become much more adaptable for a lot of applications (Kim *et al.*, 2010; Stoller *et al.*, 2008). GO is usually prepared by the modified Hummers method, which consists of graphite powder mixed with sulphuric acid, sodium nitrate and potassium permanganate with continuous checking of temperature by thermometer. The procedure is performed under an ice bath as a safety measure to avoid the possibility of explosion by reaction of very strong oxidants, H₂SO₄ and KMnO₄ (Shahriary & Athawale, 2014). GO produced from this method has also been used as precursor for the subsequent oxidation to GO (Marcano *et al.*, 2010). GO is hydrophilic due to its polar functional groups. It is well dispersible in water and can be exfoliated in many solvents. Dispersions of GO flakes can be obtained by stirring and more typically by sonication of GO in solvents (Alam *et al.*, 2017; Vadahanambi *et al.*, 2011). The colloidal dispersions are chemically reduced by various reducing agents such as hydrazine, hydroquinone, sodium borohydride and ascorbic acid (Darabdhara *et al.*, 2017). There exist other methods of reduction that are considered to be very effective such as reduction via thermal treatment and electrochemical reduction. Reduction via thermal treatment has not only been reported to be efficient but low cost as well, producing material with a BET surface area of 600-900 m² g⁻¹ (Lima *et al.*, 2017). Electrochemical reduction has been reported as an effective method to remove the oxygen functional groups of GO (Yang & Gunasekaran, 2013; Vadahanambi, 2011). The atomic layers of GO generally involves phenol epoxy and epoxide groups on the basal plane and ionizable carboxylic acid groups around the edges.

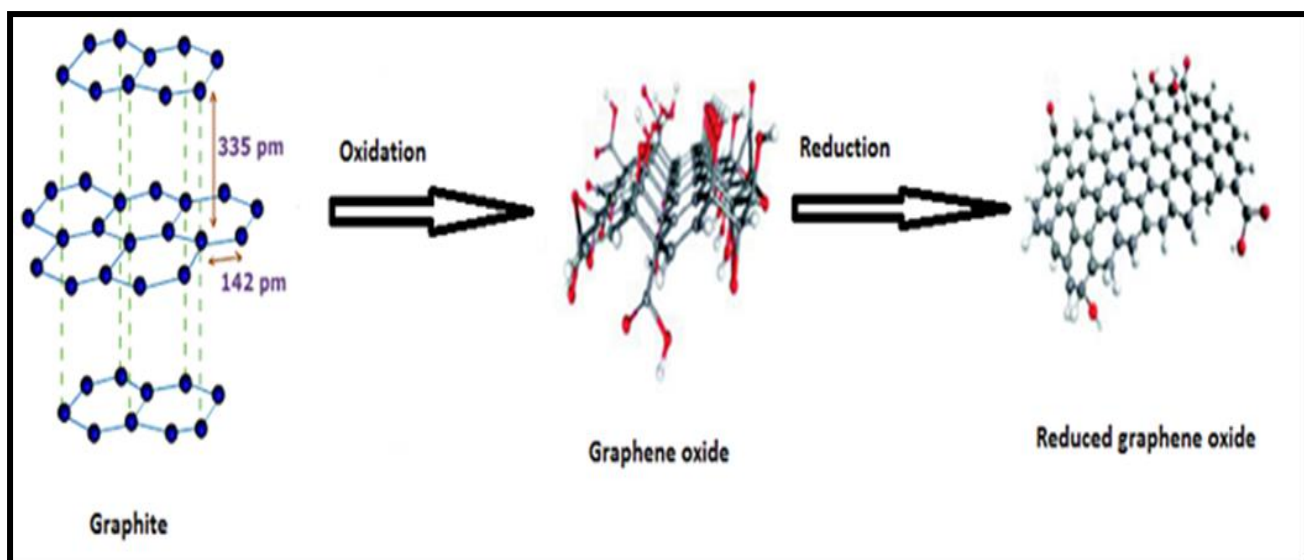


Figure 2. 7: Representation of the chemical route from graphite to the reduced graphene oxide (Gao, 2015; J. Song *et al.*, 2014).

The production of high quality and high yields graphene at low costs has been taken into account in recent years. Generally, the chemical exfoliation of graphite into GO, followed by controllable reduction of GO (with reduction agent such as hydrazine hydrate) into graphene is considered and believed to be the most efficient and low-cost method (Georgakilas *et al.*, 2012; Karthika, 2012). Though individual rGO sheets are often partially agglomerated into particles of approximately 15–25 μm in diameter during the reduction process, the products with high specific surface areas of a few hundred $\text{m}^2 \text{g}^{-1}$ can be obtained, offering potential electrode material for efficient energy storage device applications (Shao *et al.*, 2013).

GO based materials have been extensively studied over the last years with more interest based on the electrochemical behavior (Casero *et al.*, 2012). The use of GO based materials has also provided major control over microenvironment due to the materials being able to be deposited through solution processing with precise surfaces. Therefore, GO gains an advantage when profound and electro-active species are incorporated into electrochemical types (Bello *et al.*, 2013; Mahmood *et al.*, 2014). For the production of GO based devices,

costs can be immensely reduced compared to that of conventional electrodes. This is due to only a fraction of the amount of GO based materials obligatory for solution processed thin film deposition (Chen *et al.*, 2011; Chung & Choi, 2017). Furthermore, thin conductive films of GO deposited on a base material that is cheap can lead to a larger surface area-to-volume ratio, which then further lowers the electrode cost, however, the large surface area can provide a large number of active sites and a higher signal-to-noise ratio. Due to these properties GO based electrodes have been used in many applications in electrochemical sensors and biological electroanalysis as shown in Figure 2.8 (Jiang *et al.*, 2017; Wang *et al.*, 2017).

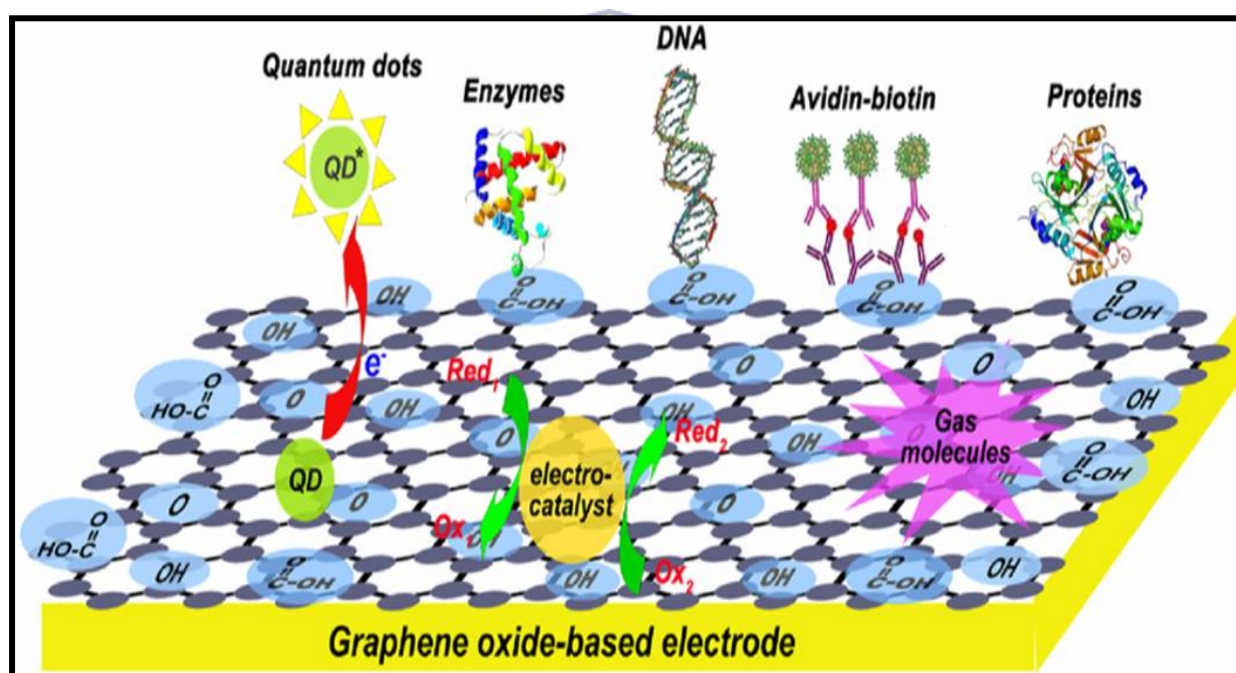
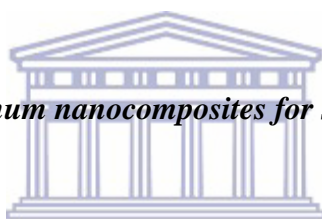


Figure 2. 8: Representation diagram of graphene oxide-based electrodes for electrochemical applications (Gao, 2015).

2.3.2 GO/metal nanocomposites

Metal nanoparticles (NPs) are important due to their unique performance in electronic, magnetic, optical and catalytic applications (Köhler *et al.*, 2008). It is highly anticipated that metal NPs supported/loaded on GO/rGO sheets could possibly display new catalytic, magnetic and optoelectronic properties (Xu *et al.*, 2008). The loading of metal oxides or metal nanoparticles on the surface of GO can potentially allow a novel way to develop new catalytic materials (Deng *et al.*, 2011). A brief review of graphene-metal nanoparticle composites that have been investigated for possible application in supercapacitors is discussed.



2.3.2.1 Graphene oxide/platinum nanocomposites for supercapacitor

Platinum nanoparticles (Pt NPs) have been subjected to intensive research for the design of electrodes for energy storage devices (Hiramatsu & Hori, 2010), and Pt is an important catalyst for many chemical and electrochemical reactions, including oxygen reduction, hydrogen oxidation, methanol oxidation and hydrogenations (Long *et al.*, 2010). Well-dispersed, small-sized Pt NPs are expected to exhibit enhanced activity and selectivity for catalytic reactions (Chen *et al.*, 2004). Lately, graphene oxide supported/loaded by platinum nanoparticles has been considered as a promising as a possible application in catalysis for fuel cell reactions, sensors and gas storage. GO, being easily exfoliated and having excellent intercalation properties, has been successfully used as a host layered material to prepare hybrids of reduced GO and metal NPs (Wang *et al.*, 2016). Researchers have made substantial determinations and developed measures of size-controlled spherical metal NPs along with their assemblies (Li *et al.*, 2010). Different synthesis methods have been detailed

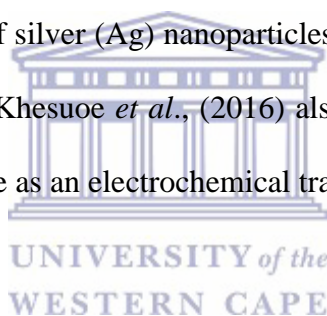
whereby researchers attempted to attach small-sized nanoparticles uniformly on the surface of graphene oxide. There is the one pot hydrothermal method where ethylene glycol is used as the reducing agent for both graphene oxide and hexachloroplatinic acid under synthetic conditions (Grinou *et al.*, 2012). Other methods include the chemical reduction of hexachloroplatinic acid in an ethylene glycol-water solution. Recently, researchers are making use of the electrostatic self-assembly whereby nanoparticles are loaded onto the surface of GO (Cao & Wang, 2018; Fang *et al.*, 2010). GO can also be functionalized in order to ensure successful attachment of the nanoparticles on the surface of graphene oxide (Grinou *et al.*, 2012; Guo *et al.*, 2010; Li *et al.*, 2010). Grinou *et al.*, (2012) developed a simple one step method to load small sized nanoparticles of average sizes (3.1 ± 0.3 nm) in large quantities on the surface of aniline-functionalized and rGO. During the process aniline was used as a stabilizer while ethylene glycol solution was used as a reducing agent without damaging the graphite structures of the functionalized rGO. Platinum nanoparticles uniformly loaded on the surface of aniline-functionalized rGO have a great consequence on electrical conductivity (Grinou *et al.*, 2012; Konio *et al.*, 2014). Dong *et al.*, (2010) worked and reported on the synthesis of Pt and Pt-Ru nanoparticles supported on rGO sheets and investigation on their electro-catalytic activity for methanol and ethanol oxidation. The experimental results revealed that rGO supported Pt and Pt-Ru nanoparticles showed that the efficiency increased for both methanol and ethanol electro-oxidation. The findings therefore favor the use of rGO sheets as a catalyst supports for both methanol and ethanol fuel cells (Iro *et al.*, 2016). Li *et al.*, (2010), worked and investigated an approach that was simple for the deposition of Pt nanoparticles onto surfaces of GO nanosheets with particle size in the range of 1–5 nm by reduction of ethylene glycol and during the process; a majority of oxygenated functional groups on GO were removed. Due to these exceptional properties,

platinum loaded uniformly on the surface of GO will be investigated for application in supercapacitors.

2.3.2.2 Graphene oxide/silver nanocomposites for supercapacitors

Silver nanoparticles have been widely used to prepare graphene oxide-silver nanoparticles nanocomposite to add improved functionalities to its optical and electrochemical properties and catalytic activities. Various methods for synthesizing stable monodispersed silver nanoparticles have been exploited and these include methods such as Brust-Schiffrin method, sonolysis, micro-emulsion method, and electrochemical synthesis with typical advantages and disadvantages in each case (Budhiraja *et al.*, 2013; Huang *et al.*, 2009; Mafuné *et al.*, 2000; Njagi *et al.*, 2011; Yin *et al.*, 2003). However, a common disadvantage is that some of these methods utilize hazardous reducing agents which in turn destroy the layered structure of graphene oxide while some methods apply the top-down strategy which also destroy the layered structure (Khan *et al.*, 2017). In-situ methods for preparation of nanocomposite synthesis also have their disadvantages as they require precarious reducing agents like hydrazine, borohydride and formaldehydes and these complicate the synthesis process. Therefore, proper reducing agents and surfactants should be used for loading silver nanoparticles on the surface of graphene oxide (Wang *et al.*, 2005; Xu *et al.*, 2015). Sarkar *et al.*, (2015) has reported on the growth of silver nanoparticles on the surface of graphene oxide. The report describes various approaches for photo-reduction of different metal nanoparticles, investigations of the formation of nanosized silver nanoparticles and silver nanowires by a spatially controlled radical mediated photo-reduction reaction, studies of the formation of silver nanoparticles in ethanol/toluene medium by using thionine as a sensitizing dye, reports on the growth of size controlled silver nanoparticles by the laser ablation method,

investigations on the formation mechanism of silver nanoparticles through the direct excitation of AgClO_4 in aqueous and alcoholic solutions (Slistan-Grijalva *et al.*, 2008; Yang *et al.*, 2011; Zainy *et al.*, 2012). All proposed a formation mechanism but all these methods use either a photosensitizer or direct photo-reduction of silver salt or photo physical reactions (Das *et al.*, 2011; Sarkar *et al.*, 2015). Electrostatic self-assembly is investigated for the attachment of silver nanoparticles on the surface of graphene oxide. Sarkar *et al.*, (2015), has reported a convenient method for synthesizing GO-silver nanoparticle (SNP) composite and its application as a channel material in thin film (TFT). The SNPs were prepared through photochemical reduction of silver nitrate and they were loaded on the surface of GO in different concentrations to prepare the nanocomposite. Das *et al.*, (2011) worked and reported on an approach to the synthesis of silver (Ag) nanoparticles by chemical reduction of AgNO_3 in a graphene oxide suspension. Khesuoe *et al.*, (2016) also reported on functionalization of silver nanoparticles by polyaniline as an electrochemical transducer.



2.3.2.3 Graphene oxide/copper nanocomposites for supercapacitors

Copper nanoparticles are receiving much attention due to their high electrical conductivity, high melting point, simple preparation, low cost and low electrochemical migration behavior (Devasenathipathy *et al.*, 2016). Copper nanoparticles have been synthesized by the bottom up and top down approach and they have been used in many applications (Chen *et al.*, 2012). Copper nanoparticles have been supported on rGO as a highly active and recyclable catalyst for the synthesis of formamides and primary amine (Moozarm *et al.*, 2017; Suramwar *et al.*, 2016). Gong *et al.*, (2018) has worked and reported on the chemical reduction preparation of a novel graphene-copper nanoparticle composite using graphene oxide and copper (II) ions, potassium borohydride as a reducing agent for electrochemical sensing of carbohydrate. The

GO was mixed with a portion of copper sulphate and EDTA.2Na.2H₂O and sonicated for some time. Potassium was then used as a reducing agent for the mixture. The results indicated that copper nanoparticles with an average diameter of 20.8 nm were successfully deposited on rGO nanosheets forming an interconnected hybrid network (Hu *et al.*, 2012). Fakhri *et al.*, (2014) has worked and reported on the studies for synthesis and characterization of copper nanoparticles supported on rGO as a catalyst for the synthesis of formamides and primary amine. GO was reduced by hydrazine monohydrate in an oil bath and copper nanoparticles were then synthesized by the chemical reduction of copper (II) sulfate pentahydrate with sodium borohydride via wet method. The prepared rGO was suspended in deionized water and the prepared nanoparticles were added to this suspended solution. Sarkar *et al.* (2015), established a method of preparing CuO₂-rGO nanocomposites and investigated their catalytic activity towards reduction of 4-nitrophenol (4-NP). The nanocomposites showed exceptional and steady catalytic activity towards reduction of 4-NP to 4-aminophenol (4-AP) in the presence of NaBH₄ (Madhav *et al.*, 2017; Sarkar & Dolui, 2015). Yang *et al.*, synthesized a GO/Cu/SWCNT hybrid material by a facile electro-deposition method. The materials were deposited on GCE and electro-deposition and electrochemical studies were carried out. Electrochemical results indicated that CuNP/GO/SWCNT electrode exhibited a higher electro-catalytic activity towards the oxidation of glucose than Cu NP, Cu NP/GO and Cu NP/SWCNT electrode, respectively. Due to their impressive results, the intense investigations are ongoing for application of these nanocomposites for high capacitance electrodes.

2.3.3 DBSA doped Polyaniline

Conducting polymers are important polymer materials with a conjugated double bonded backbone that provides the electronic conductivity after doping with suitable dopants (Janata & Josowicz, 2003). Figure 2.9 shows the application fields of conducting polymer nanomaterials. Carbon materials have been considered for supercapacitors but due to the fact that carbon materials only possess double-layer capacitance while metal oxides and conducting polymers possess Faradaic capacitance, conducting polymers have attracted a lot of attention (Álvarez-Torrellas *et al.*, 2016). Faradaic capacitance is around 100 times higher than double-layer capacitance and the likely application of conducting polymers in electrochemical capacitors is dictated by their significant values (Arshak *et al.*, 2009; Janata & Josowicz, 2003; Zhang & Zhao, 2012).



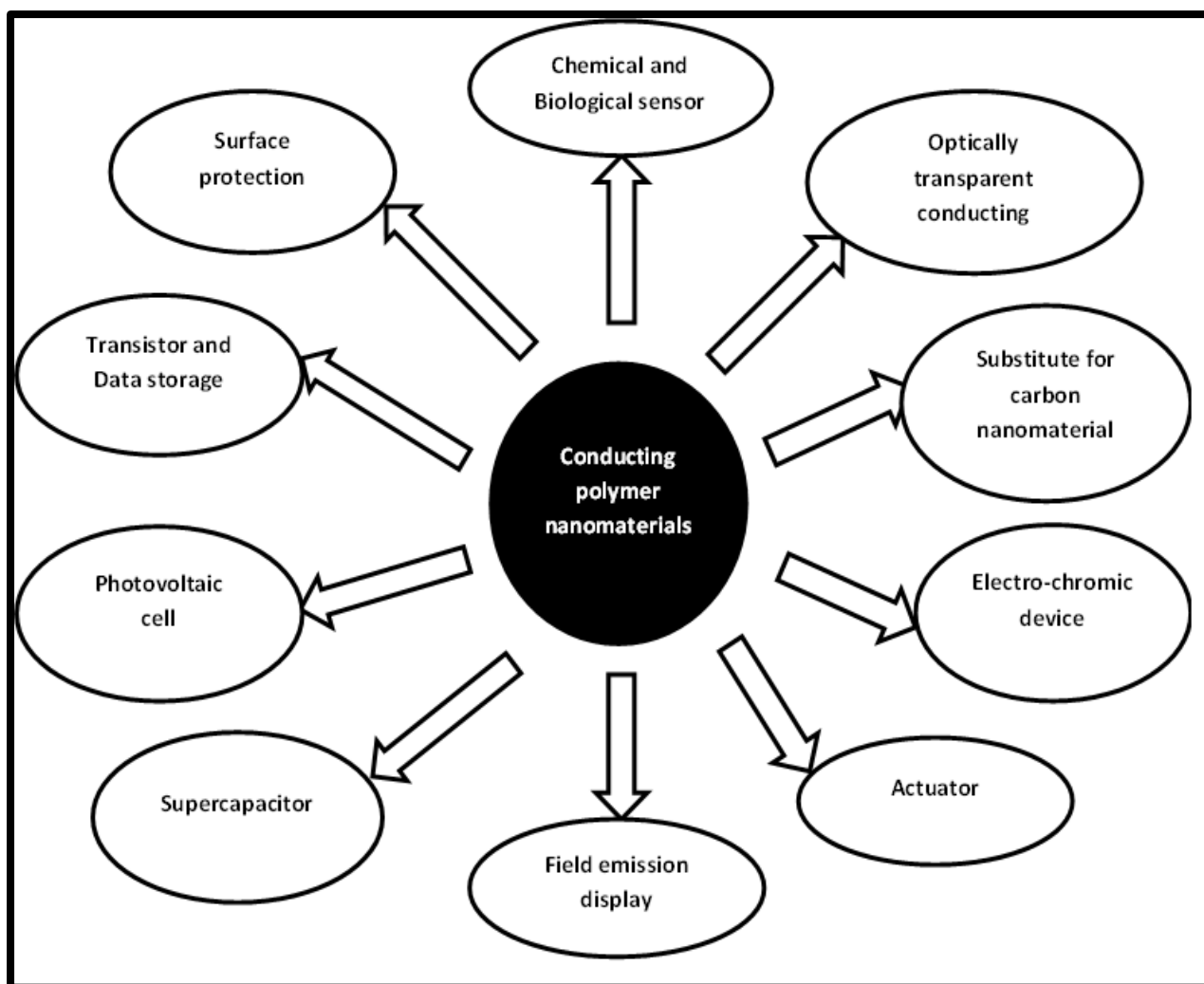


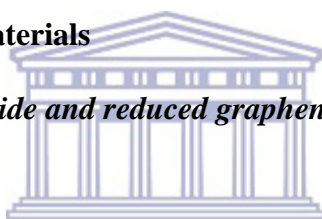
Figure 2. 9: Application fields for conducting polymer nanomaterials (Jangid *et al.*, 2010).

PANI is an electro-conductive polymer that has impressive technological applications that include electronic devices, chemical and biological sensors, energy storage devices, selective membranes, microwave absorption layers etc. (Das & Sarkar, 2017; Kumar *et al.*, 2012). PANI has great possible potential for devices such as light emitting diodes, electro-chemical cells, magnetic device storage, field emitters and humidity sensors. However, due to the shortfalls of PANI which include its insolubility, poor mechanical properties and low processability have lessened its use in industrial applications (Castillo-Castro *et al.*, 2007). Recently, carbon material/conducting polymer/metal oxide nanoparticle composites or carbon material/conducting polymer/metal nanoparticle composites, a new class of materials has

improved properties when compared to conducting polymer or metal oxide/metal nanoparticle alone. The addition of metal oxides or metal nanoparticles improve the size, morphology and conducting properties of the polymer (Ashokan *et al.*, 2015; Li *et al.*, 2004). Lately, PANI was used for the preparation of its composites with inorganic particles to improve their processability. Dodecylbenzenesulphonic acid (DBSA) is in this process used as a dopant to enable the polymer-organic solvent interaction in the process. The DBSA doped PANI has been reported to show higher solubility and enhancement in properties (Calheiros *et al.*, 2017; Li *et al.*, 2004).

2.4 Synthesis of electrode materials

2.4.1 Synthesis of Graphene oxide and reduced graphene



Reduced graphene oxide (rGO) has been prepared by many synthesis techniques in which the first synthesis was prepared by the micromechanical cleavage from extremely ordered graphite. This method includes peeling a layer off from the graphite using scotch tape and then transferring it on to a silicon substrate (Marcano *et al.*, 2010). These routes might be the most favorable and might be preferred for precise device assembly but they can be less effective for manufacturing at a larger scale. Chemical means have been proven to be practical for approach to large scale graphene materials. Currently, chemical paths and efforts at graphite exfoliation have been concentrated more on intercalation, chemical derivatization, thermal expansion, oxidation-reduction, the use of some surfactants and or some combination thereof (Gao, 2015; Govindaraj *et al.*, 2013). Currently, the Hummers method is the mostly used for the synthesis of GO and involves the use of strong oxidizing agents i.e. a combination of potassium permanganate with sulphuric acid (Zaaba *et al.*, 2017). This

method uses H_2SO_4 to intercalate graphite with the assistance of NaNO_3 and KMnO_4 to oxidize the intercalated graphite. Hummers' method has several advantages when compared to the approaches of Brodie and Staudenmaier (Shahriary & Athawale, 2014). Firstly, the use of KMnO_4 as a strong oxidant ensures a quick completion of the reaction. Secondly, since there is an absence of chlorate there is no explosive ClO_2 formed. Thirdly, the replacement of HNO_3 with NaNO_3 prevents and eliminates the acid fog. Hence, this method is regarded more favorable towards the large scale production of GO. However, it also has its drawbacks which include the formation of $\text{NO}_2/\text{N}_2\text{O}_4$ toxic gases due to the introduction of NaNO_3 , the near difficulty of removing the Na^+ and NO_3 from the waste water formed during GO synthesis and purification processes and the incomplete oxidation that results in forming a graphite/GO mixture (Alam *et al.*, 2017; Chen *et al.*, 2015; Chen *et al.*, 2013) . Recently, Tour *et al.* improved Hummers method by withholding the use of NaNO_3 , meanwhile increasing the amount of KMnO_4 and performing the reaction in a 9:1 mixture of $\text{H}_2\text{SO}_4/\text{H}_3\text{PO}_4$ (Marcano *et al.*, 2010). They claimed significant advantages of no evolution of toxic gases $\text{NO}_2/\text{N}_2\text{O}_4$, higher yield of heavily oxidized hydrophilic GO. However, the need of 23 times longer time for oxidation, the use of twice as much KMnO_4 , 5.2 times as much H_2SO_4 , and a new component H_3PO_4 increased both the cost and environmental duties of this method. Moreover, the formation of cyclic phosphate groups via the reaction of vicinal diols with phosphoric acid is an issue that has not yet been addressed (Silwana *et al.*, 2015).

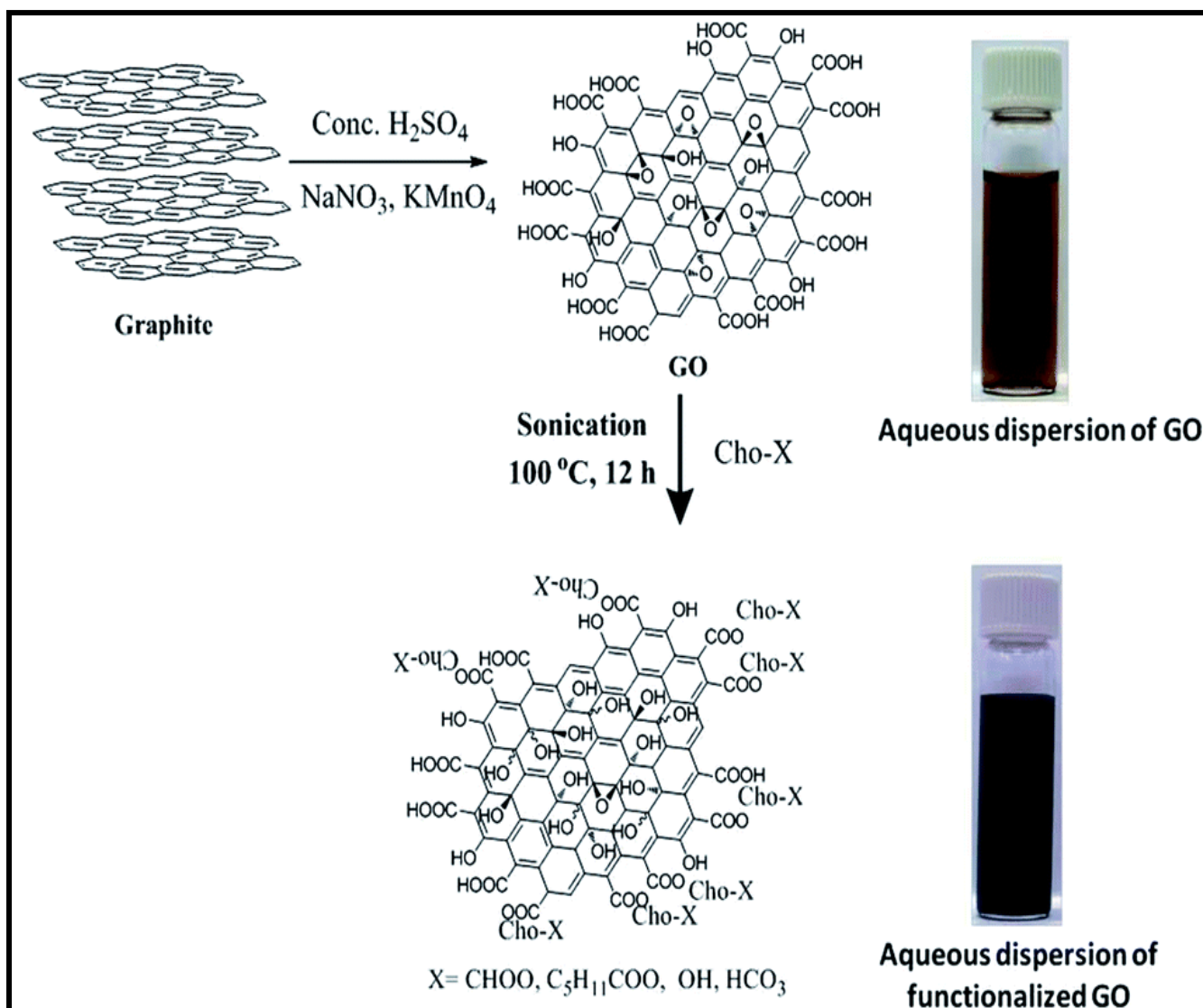
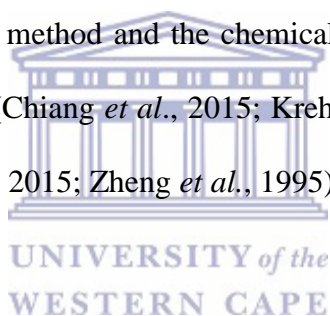


Figure 2. 10: Schematic for the synthesis of graphene oxide (Settanni *et al.*, 2016)

2.4.2 Metal nanoparticles

Metal nanoparticles are important for modern technology due to their catalytic properties and unique performance in many applications and across other fields (Chiang *et al.*, 2015; Grinou *et al.*, 2012). They have application in magnetic, electronic, optical, hydrogenations, oxidations, decomposition reactions etc. (Chiang *et al.*, 2015). These metal nanoparticles can be synthesized using various synthesis techniques such as chemical reduction in solution using hydrogen gas, ethylene glycol, hydrides, alcohols and other known reducing agents

(Köhler *et al.*, 2008; Zielińska *et al.*, 2009). Other synthesis techniques include electrochemical reduction, laser ablation, micro-emulsion, assisted deposition and partial dissolution (Capek, 2004). Presently, the polyol method has been employed to investigate the drawbacks and issues that concern the control of size and shape of metal nanoparticles. The polyol method has been used to fabricate platinum, palladium, silver, gold, etc. nanoparticles with their well-controlled thin size distribution and shape in ethylene glycol (Berger *et al.*, 2010; Byeon & Kim, 2012; Chen *et al.*, 2004; Ha *et al.*, 2011; Herricks *et al.*, 2004). In all cases, the average particle size was found to be smaller than 10 nm. Particle size is highly controlled by changing the initial total metal concentration, the reaction temperature, and the concentration of PVP. Therefore, platinum group metal nanoparticles are synthesized by the hydrothermal process, the polyol method and the chemical reduction of their corresponding metal species in ethylene glycol (Chiang *et al.*, 2015; Krehula & Musi, 2011; Kurbanoglu *et al.*, 2017; Yang *et al.*, 2015; Zeki, 2015; Zheng *et al.*, 1995).



2.4.3 DBSA doped PANI

Conducting polymers can be synthesized using three methods, the soft template method, hard template method and template free method. The soft template method uses micelles formed by surfactants to confine the polymerization of conducting polymer into low dimensional nanomaterials (Zhu *et al.*, 2007). Template free method involves various methods such as electrochemical synthesis, chemical polymerization, aqueous/organic interfacial polymerization, radiolytic synthesis and dispersion polymerization (Wan, 2008). Hard template method includes a number of different templates that have been used for 1D nanostructure analysis and these include anodic alumina, nanochannel glass, ion track-etched polymers and mica films (Wan, 2008; Yin & Yang, 2011). Chemical polymerization of

aniline has been carried out in an acidic solution. This acidic condition provides the solubilization of the monomers as well as the formation of emeraldine salt as a conducting PANI (Huang *et al.*, 2003).

2.5 Electrolytes for supercapacitors

The electrolyte involves one or more solvents containing one or more dissolved ionic species. The physical, power and electrochemical properties of an electrolyte determine the internal resistance of a supercapacitor in numerous instances.

2.5.1 Aqueous electrolytes

Aqueous electrolytes have found application in supercapacitors due to the following properties:

- high conductivity,
- low resistance inside the capacitor,
- easily wetting with the surface of electrode,
- cost effectiveness.

In general, the aqueous electrolyte solutions include acidic (e.g. HNO_3), neutral (Na_2SO_4) and basic solution (e.g. KOH). Due to these remarkable properties, H_2SO_4 , Na_2SO_4 and KOH electrolytes were used in this study (Dvořák, 2010; Pandey *et al.*, 2010; Simon, 2012).

The factors influence these aqueous electrolytes properties

(a) Salt solubility



- b) Degree of dissociation into free ions and factors such as extent of cation-anion association or pairing of ions of the dissolved salt and this is influenced by the salt concentration, temperature and the dielectric constant of the solvent (Madria *et al.*, 2013)
- c) Viscosity of the solvent, which is a temperature dependent property. As temperature increases, there is a corresponding decrease in viscosity. There is also the necessity for the solvent to be chemically stable.

2.6 Supercapacitors in South Africa

South Africa has been experiencing power and energy crisis for the past few years, resulting in electricity or power being turned off for two hours a day. Therefore, it has been making use of supercapacitors coupling them with photo-voltaic PV cells for photo-voltaic street lighting which is used in places where electricity is not available. Street lighting in South Africa accounts for about 24% of the total energy expended by municipalities and supports about 28% of the carbon emitted in the delivery services by municipalities. It was discovered that PV systems need batteries with long cycle life but they use deep cycle batteries for storage that have low efficiencies and have a life expectancy of 2-3 years and can only produce hundreds/thousands of cycles. When compared to supercapacitors which have a life expectancy of 7-10 years and can produce millions of cycles, it was then decided that the PV street lighting would make use of supercapacitors instead of standard batteries (Zhou & Narendran, 2005) and companies such as Mouser electronics produce these supercapacitors and manufacture them for many supercapacitor manufactures such as AVX (Bello *et al.*, 2013; Oyedotun *et al.*, 2017).

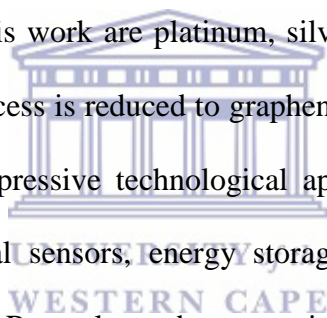
AVX released a new series of cylindrical and EDL supercapacitors. Rated for 2.7 V and delivering high capacitance values (1 F – 3000 F), low ESR (0.16–200 mΩ at 1000 kHz), low leakage (6–5800 μA), high energy density (1.2 to 5.6 Wh kg⁻¹), and long lifetime performance (50 000+ cycles), the new series exhibits excellent pulse power handling characteristics, can be used alone or in conjunction with primary or secondary batteries. The supercapacitors are rated for use in operating temperatures spanning -40 °C to +65 °C (or, with voltage de-rated to 2,3 V per cell, -40 °C to +85 °C) are compatible with hand, reflow and wave soldering so long as appropriate precautions are enacted, and are both lead-free compatible and ROHS compliant (Bello *et al.*, 2013) .

A company named Murata announced an addition of the DMG series to the company's line of low resistance EDLDs and these DMG supercapacitors allow high power back-up, achieve high reliability with a five-year life span at 70 °C and this makes these supercapacitors an ideal choice for enterprise solid state drive (SSD) manufacturers and telecom applications. The DMG series offer high capacitance values due to the carbon used as an electrode in small and low profile design which leads to longer cycle lives. The groundwork behind this technology is due to the partnership of Murata with CAP-XX, with Murata acquiring super cap technology from CAP-XX in 2008, in order to meet demand for consumer for mobile devices with greater functionality and efficiency. Subsequently, Murata's focus on EDLC research and development, coupled with CAP-XX's expertise, has led to the maturity of the enhanced EDLC design due to the carbon which is used as an electrode and leads to a longer cycle life (Murata, 2016).

2.7 Conclusions

Supercapacitors are classified into electrochemical double-layer capacitors (EDLC), pseudocapacitors, and hybrid supercapacitors. In EDLCs the charge storage occurs electrochemically (Helmholtz layer) which involves no transfer of charge between electrode and the electrolyte. It has been shown that carbon materials such as graphene, carbon aerogels, activated carbons, carbon black, carbon nanotubes etc., give the best EDLC. Charge storage in pseudocapacitors occurs electrochemically and via Faradaic process i.e. Faradaic charge transfer, where fast Faradaic reactions take place to such an extent limited by finite amount of available surface area or active material. The process involves the transfer of charge between an electrode and an electrolyte. Capacitance arises due to progressive redox reactions between several oxidation states. Metal oxide and conducting polymers have been shown to give the best pseudocapacitance. In hybrid capacitors, the charge storage occurs both electrostatically and electrochemically i.e. as observed EDLCs give good cyclic stability and good power performance while pseudocapacitors give good specific capacitance. In hybrid capacitors it offers or gives a combination of both i.e. combination of the energy source of battery electrode with a power source of capacitor electrode in the same cell. It has been shown that composites, asymmetric (pseudo/EDLC) and rechargeable battery-type are good for hybrid capacitors. Composite electrodes are a mixture of carbon based materials such as carbon black, carbon ink, graphene, carbon aerogels etc. with metal oxides such as ruthenium oxide, copper oxide, nickel oxide etc. or conducting polymer such as polyaniline, polypyrrole, polythiophene etc. in a single electrode. This means that the single electrode will potentially consist of both physical and chemical charge storage mechanisms. Asymmetric hybrid are setup in a way that the carbon material e.g. carbon nanotubes, reduced graphene oxide etc. (EDLC) acts as a negative electrode while a metal oxide e.g. nickel or manganese

oxide or conducting polymer e.g. polyaniline, polypyrrole acts as a positive electrode (pseudocapacitance), therefore, these capacitors combine non-Faradaic and Faradaic processes by connecting an EDLC electrode with a pseudocapacitor electrode. Battery type hybrid combines two different electrodes i.e. a supercapacitor electrode with battery electrode. This is like in the case of asymmetric hybrids but instead it's a combination of supercapacitor electrode with a battery electrode. Metal nanoparticles have a unique performance in electronic, magnetic, optical and catalytic applications. Metal nanoparticles loaded on graphene sheets are estimated to produce novel catalytic, magnetic and optoelectronic properties and the dispersion of metals and/or metal nanoparticles onto the surface of GO can possibly provide new steps to developing catalytic materials. The nanoparticle materials used in this work are platinum, silver and copper, all combined with graphene oxide, which in the process is reduced to graphene. Polyaniline PANI is an electro-conductive polymer that has impressive technological applications that include electronic devices, chemical and biological sensors, energy storage devices, selective membranes, microwave absorption layers etc. Recently, carbon material/conducting polymer/metal oxide nanocomposites or carbon material/conducting polymer/metal nanoparticle composites were developed as a new class of materials and this is due to their improved properties when compared to conducting polymer or metal oxide/metal nanoparticle alone. The size, morphology and conducting properties of the combination of metal oxide/nanoparticle and PANI are greatly enhanced. South Africa has also been making use of supercapacitors to improve their power and energy crisis.



References

- Alam, S. N., Sharma, N., & Kumar, L. (2017). Synthesis of graphene oxide (GO) by modified Hummers method and its thermal reduction to obtain reduced graphene oxide (rGO). *Graphene*, 06(01), 1–18.
- Álvarez-Torrellas, S., Ribeiro, R. S., Gomes, H. T., Ovejero, G., & García, J. (2016). Removal of antibiotic compounds by adsorption using glycerol-based carbon materials. *Chemical Engineering Journal*, 296, 277–288.
- Arshak, K., Velusamy, V., Korostynska, O., Oliwa-stasiak, K., & Adley, C. (2009). Conducting polymers and their applications to biosensors : emphasizing on foodborne pathogen detection, 9(12), 1942–1951.
- Ashokan, S., Ponnuswamy, V., & Jayamurugan, P. (2015). Synthesis and characterization of CuO nanoparticles, DBSA doped PANI and PANI/DBSA/CuO hybrid composites for diode and solar cell device development. *Journal of Alloys and Compounds*, 646, 40–48.
- Bello, A., Fashedemi, O. O., Lekitima, J. N., Fabiane, M., Dodoo-Arhin, D., Ozoemena, K. I., & Manyala, N. (2013). High-performance symmetric electrochemical capacitor based on graphene foam and nanostructured manganese oxide. *AIP Advances*, 3(8), 1–19.
- Berger, D., Trăistaru, G. A., Vasile, B. S., Jitaru, I., & Matei, C. (2010). Palladium nanoparticles synthesis with controlled morphology obtained by polyol method. *UPB Scientific Bulletin, Series B: Chemistry and Materials Science*, 72(1), 113–120.
- Bhujun, B., Tan, M. T. T., & Shanmugam, A. S. (2017). Results in physics study of mixed ternary transition metal ferrites as potential electrodes for supercapacitor applications. *Results in Physics*, 7, 345–353.
- Budhiraja, N., Sharma, A., Dahiya, S., & Parmar, R. (2013). Synthesis and optical characteristics of silver nanoparticles on different substrates, 19, 80–88.

- Byeon, J. H., & Kim, Y. W. (2012). A novel polyol method to synthesize colloidal silver nanoparticles by ultrasonic irradiation. *Ultrasonics Sonochemistry*, *19*(1), 209–215.
- Calheiros, L. F., Soares, B. G., & Barra, G. M. O. (2017). DBSA-CTAB mixture as the surfactant system for the one step inverse emulsion polymerization of aniline: characterization and blend with epoxy resin. *Synthetic Metals*, *226*, 139–147.
- Cao, J., & Wang, C. (2018). Highly conductive and flexible silk fabric via electrostatic self assemble between reduced graphene oxide and polyaniline. *Organic Electronics: Physics, Materials, Applications*, *55*(September 2017), 26–34.
- Capek, I. (2004). Preparation of metal nanoparticles in water-in-oil (w/o) microemulsions. *Advances in Colloid and Interface Science*, *110*(1–2), 49–74.
- Casero, E., Parra-Alfambra, A. M., Petit-Domínguez, M. D., Pariente, F., Lorenzo, E., & Alonso, C. (2012). Differentiation between graphene oxide and reduced graphene by electrochemical impedance spectroscopy (EIS). *Electrochemistry Communications*, *20*(1), 63–66.
- Chen, J., Li, Y., Huang, L., Li, C., & Shi, G. (2015). High-yield preparation of graphene oxide from small graphite flakes via an improved Hummers method with a simple purification process. *Carbon*, *81*(1), 826–834.
- Chen, J., Yao, B., Li, C., & Shi, G. (2013). An improved Hummers method for eco-friendly synthesis of graphene oxide. *Carbon*, *64*(1), 225–229.
- Chen, Q., Zhang, L., & Chen, G. (2012). Facile preparation of graphene-copper nanoparticle composite by in situ chemical reduction for electrochemical sensing of carbohydrates. *Analytical Chemistry*, *84*(1), 171–178.
- Chen, W. X., Lee, J. Y., & Liu, Z. (2004). Preparation of Pt and PtRu nanoparticles supported on carbon nanotubes by microwave-assisted heating polyol process. *Materials Letters*, *58*(25), 3166–3169.

- Chen, Y., Zhang, X., Zhang, D., Yu, P., & Ma, Y. (2011). High performance supercapacitors based on reduced graphene oxide in aqueous and ionic liquid electrolytes. *Carbon*, 49(2), 573–580.
- Chiang, Y. C., Liang, C. C., & Chung, C. P. (2015). Characterization of platinum nanoparticles deposited on functionalized graphene sheets. *Materials*, 8(9), 6484–6497.
- Chung, M. W., & Choi, C. H. (2017). Carbon nanofibers as parent materials for a graphene-based Fe-N-C catalyst for the oxygen reduction reaction. *Catalysis Today*, 295(April), 125–131.
- Conway, B. E., & Pell, W. G. (2003). Double-layer and pseudocapacitance types of electrochemical capacitors and their applications to the development of hybrid devices. *Journal of Solid State Electrochemistry*, 7(9), 637–644.
- Cygan, T., Wozniak, J., Kostecki, M., Petrus, M., & Jastrz, A. (2017). Mechanical properties of graphene oxide reinforced alumina matrix composites, 43(8), 6180–6186.
- Darabdhara, G., Sharma, B., Das, M. R., Boukherroub, R., & Szunerits, S. (2017). Sensors and Actuators B : Chemical Cu-Ag bimetallic nanoparticles on reduced graphene oxide nanosheets as peroxidase mimic for glucose and ascorbic acid detection. *Sensors & Actuators: B. Chemical*, 238, 842–851.
- Das, M. R., Sarma, R. K., Saikia, R., Kale, V. S., Shelke, M. V., & Sengupta, P. (2011). Synthesis of silver nanoparticles in an aqueous suspension of graphene oxide sheets and its antimicrobial activity. *Colloids and Surfaces B: Biointerfaces*, 83(1), 16–22.
- Das, M., & Sarkar, D. (2017). One-pot synthesis of zinc oxide - polyaniline nanocomposite for fabrication of efficient room temperature ammonia gas sensor. *Ceramics International*, 43(14), 11123–11131.

- De La Fuente Salas, I. M., Sudhakar, Y. N., & Selvakumar, M. (2014). High performance of symmetrical supercapacitor based on multilayer films of graphene oxide/polypyrrole electrodes. *Applied Surface Science*, 296, 195–203.
- Del Castillo-Castro, T., Castillo-Ortega, M. M., Villarreal, I., Brown, F., Grijalva, H., Perez-Tello, M., & Puig, J. E. (2007). Synthesis and characterization of composites of DBSA-doped polyaniline and polystyrene-based ionomers. *Composites Part A: Applied Science and Manufacturing*, 38(2), 639–645.
- Deng, L., Zhu, G., Wang, J., Kang, L., Liu, Z. H., Yang, Z., & Wang, Z. (2011). Graphene-MnO₂ and graphene asymmetrical electrochemical capacitor with a high energy density in aqueous electrolyte. *Journal of Power Sources*, 196(24), 10782–10787.
- Devasenathipathy, R., Kohilarani, K., Chen, S., Wang, S., Wang, S., & Chen, C. (2016). Electrochimica Acta Electrochemical preparation of biomolecule stabilized copper nanoparticles decorated reduced graphene oxide for the sensitive and selective determination of hydrogen peroxide. *Electrochimica Acta*, 191, 55–61.
- Dong, L., Gari, R. R. S., Li, Z., Craig, M. M., & Hou, S. (2010). Graphene-supported platinum and platinum-ruthenium nanoparticles with high electrocatalytic activity for methanol and ethanol oxidation. *Carbon*, 48(3), 781–787.
- Dvořák, P. (2010). Overview of Non-Aqueous Electrolytes for Supercapacitors. *Energy*, 4(3), 2–6.
- Ehsani, A., Kowsari, E., Ajdari, F. B., Safari, R., & Shiri, H. M. (2017). Journal of Colloid and Interface Science Sulfonated graphene oxide and its nanocomposites with electroactive conjugated polymer as effective pseudocapacitor electrode materials. *Journal of Colloid And Interface Science*, 497, 258–265.

- Endo, M., Takeda, T., Kim, Y. J., Koshiba, K., & Ishii, K. (2001). High Power Electric Double Layer Capacitor (EDLC ' s); from Operating Principle to Pore Size Control in Advanced Activated Carbons. *Carbon Science*, 1(3), 117–128.
- Fakhri, P., Jaleh, B., & Nasrollahzadeh, M. (2014). Synthesis and characterization of copper nanoparticles supported on reduced graphene oxide as a highly active and recyclable catalyst for the synthesis of formamides and primary amines. *Journal of Molecular Catalysis A: Chemical*, 383–384, 17–22.
- Fang, Y., Guo, S., Zhu, C., Zhai, Y., & Wang, E. (2010). Self-Assembly of Cationic Polyelectrolyte-Functionalized Graphene Nanosheets and Gold Nanoparticles : A Two-Dimensional Heterostructure for Hydrogen Peroxide Sensing, 26(14), 11277–11282.
- Frackowiak, E., & Béguin, F. (2001). Carbon materials for the electrochemical storage of energy in capacitors. *Carbon*, 39(6), 937–950.
- Ganesh, V., Pitchumani, S., & Lakshminarayanan, V. (2006a). New symmetric and asymmetric supercapacitors based on high surface area porous nickel and activated carbon. *Journal of Power Sources*, 158(2), 1523–1532.
- Ganesh, V., Pitchumani, S., & Lakshminarayanan, V. (2006b). New symmetric and asymmetric supercapacitors based on high surface area porous nickel and activated carbon. *Journal of Power Sources*, 158, 1523–1532.
- Gao, W. (2015). The chemistry of graphene oxide. *Graphene Oxide: Reduction Recipes, Spectroscopy, and Applications*, 61–95.
- Gasgnier, M., & Petit, A. (2003). Syntheses of chromium copper and chromium manganese oxides performed by means of a low power monomode microwave. *Journal of Alloys and Compounds*, 358(1–2), 302–305.

- Georgakilas, V., Otyepka, M., Bourlinos, A. B., Chandra, V., Kim, N., Kemp, K. C., & Kim, K. S. (2012). Functionalization of graphene: Covalent and non-covalent approaches, derivatives and applications. *Chemical Reviews*, *112*(11), 6156–6214.
- Giudice, F. Del, & Shen, A. Q. (2017). Shear rheology of graphene oxide dispersions. *Current Opinion in Chemical Engineering*, *16*, 23–30.
- Gong, S., Chen, J., Wu, X., Han, N., & Chen, Y. (2018). In-situ synthesis of Cu₂O/reduced graphene oxide composite as effective catalyst for ozone decomposition. *Catalysis Communications*, *106*, 25–29.
- Gonzalez, A., Goikolea, E., Barrena, J. A., & Mysyk, R. (2016). Review on supercapacitors: Technologies and materials. *Renewable and Sustainable Energy Reviews*, *58*, 1189–1206.
- Govindaraj, A., Rao, C. N. R., Subrahmanyam, K. S., & Ramakrishna-Matte H. S. S. (2011). Graphene: Synthesis, Functionalization and Properties. *International Journal of Modern Physics B*, *25*(30), 4107-4143.
- Grinou, A., Yun, Y. S., Cho, S. Y., Park, H. H., & Jin, H. J. (2012). Dispersion of Pt nanoparticle-doped reduced graphene oxide using aniline as a stabilizer. *Materials*, *5*(12), 2927–2936.
- Guo, S., Dong, S., & Wang, E. (2010). Three-dimensional Pt-on-Pd bimetallic nanodendrites supported on graphene nanosheet: Facile synthesis and used as an advanced nanoelectrocatalyst for methanol oxidation. *American Chemical Society Nano*, *4*(1), 547–555.
- Ha, H.-W., Kim, I. Y., Hwang, S.-J., & Ruoff, R. S. (2011). One-Pot Synthesis of Platinum Nanoparticles Embedded on Reduced Graphene Oxide for Oxygen Reduction in Methanol Fuel Cells. *Electrochemical and Solid State Letters*, *14*(7), B70-B73.

- Halper, M., & Ellenbogen, J. (2006). Supercapacitors: A brief overview. Supercapacitors: A brief overview. *Report No. MP 05W0000272*, 1-29.
- Herricks, T., Chen, J., & Xia, Y. (2004). Polyol synthesis of platinum nanoparticles: Control of morphology with sodium nitrate. *Nano Letters*, 4(12), 2367–2371.
- Hiramatsu, M., & Hori, M. (2010). Preparation of dispersed platinum nanoparticles on a carbon nanostructured surface using supercritical fluid chemical deposition. *Materials*, 3(3), 1559–1572.
- Hu, C. C., Li, W. Y., & Lin, J. Y. (2004). The capacitive characteristics of supercapacitors consisting of activated carbon fabric-polyaniline composites in NaNO₃. *Journal of Power Sources*, 137(1), 152–157.
- Hu, J., He, B., Lu, J., Hong, L., Yuan, J., Song, J., & Niu, L. (2012). Facile Preparation of Pt / Polyallylamine / Reduced Graphene Oxide Composites and Their Application in the Electrochemical Catalysis on Methanol Oxidation. *International Journal of Electrochemical Science*, 7(10), 10094–10107.
- Huang, J., Virji, S., Weiller, B., & Kaner, R. (2003). Polyaniline nanofibers: facile synthesis and chemical sensors. *Journal of the American Chemical Society*, 125(2), 314–315.
- Huang, L. M., Liao, W. H., Ling, H. C., & Wen, T. C. (2009). Simultaneous synthesis of polyaniline nanofibers and metal (Ag and Pt) nanoparticles. *Materials Chemistry and Physics*, 116(2–3), 474–478.
- Huang, Y., Liang, J., & Chen, Y. (2012). An overview of the applications of graphene-based materials in supercapacitors. *Small*, 8(12), 1805–1834.
- Iro, Z. S., Subramani, C., & Dash, S. S. (2016). A brief review on electrode materials for supercapacitor. *International Journal of Electrochemical Science*, 11(12), 10628–10643.

- Jampani, P., Manivannan, A., & Kumta, P. N. (2010). Advancing the Supercapacitor Materials and Technology Frontier for Improving Power Quality. *The Electrochemical Society's Interface*, 19(3), 57–62.
- Janata, J., & Josowicz, M. (2003). Conducting polymers in electronic chemical sensors. *Nature Materials*, 2(1), 19–24.
- Jangid, N. K., Singh Chauhan, N. P., Meghwal, K., & Punjabi, P. B. (2014). Conducting polymers and their applications. *Research Journal of Pharmaceutical, Biological and Chemical Sciences*, 5(3), 383–412.
- Jayalakshmi, M., & Balasubramanian, K. (2008). Simple capacitors to supercapacitors-an overview. *Internationa Journal of Electrochemical Sciences*, 3, 1196–1217.
- Jiang, W., Xin, W., Xun, S., Chen, S., Gao, X., Liu, Z., & Tian, J. (2017). Sensors and Actuators B: Chemical Reduced graphene oxide-based optical sensor for detecting specific protein. *Sensors & Actuators: B. Chemical*, 249, 142–148.
- Joon, H., Lee, S., Hoang, L., Su, C., Rae, Y., Rae, K., & Park, S. (2017). Maximizing volumetric energy density of all-graphene-oxide- supercapacitors and their potential applications for energy harvest. *Journal of Power Sources*, 346, 113–119.
- Jung, J. H., Park, H. J., Kim, J., & Hur, S. H. (2014). Highly durable Pt/graphene oxide and Pt/C hybrid catalyst for polymer electrolyte membrane fuel cell. *Journal of Power Sources*, 248, 1156–1162.
- Karthika, P. (2012). Functionalized Exfoliated Graphene Oxide as Supercapacitor Electrodes. *Soft Nanoscience Letters*, 02, 59–66.
- Khan, Q. A., Shaur, A., Khan, T. A., Joya, Y. F., & Awan, M. S. (2017). Characterization of reduced graphene oxide produced through a modified Hoffman method. *Cogent Chemistry*, 3(1), 1-9.

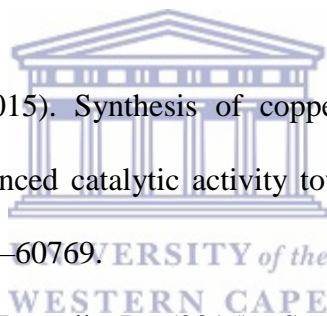
- Khesuoe, M., Matoetoe, M., & Okumu, F. (2016). Potential of Silver Nanoparticles Functionalized Polyaniline as an Electrochemical Transducer. *Journal of Nano Research*, 44, 21–34.
- Khomenko, V., Frackowiak, E., & Béguin, F. (2005). Determination of the specific capacitance of conducting polymer/nanotubes composite electrodes using different cell configurations. *Electrochimica Acta*, 50(12), 2499–2506.
- Kiamahalleh, M. V., Zein, S. H. S., Najafpour, G., Sata, S. A., & Buniran, S. (2012). Multiwalled Carbon Nanotubes Based Nanocomposites for Supercapacitors: a Review of Electrode Materials. *Nano*, 07(02), 1230002.
- Kim, T. Y., Lee, H. W., Stoller, M., Dreyer, D. R., Bielawski, C. W., Ruoff, R. S., & Suh, K. S. (2010). High-performance supercapacitors based on poly(ionic liquid) - modified graphene electrodes. *American Chemical Society*, 5(1), 436-442.
- Köhler, J. M., Abahmane, L., Wagner, J., Albert, J., & Mayer, G. (2008). Preparation of metal nanoparticles with varied composition for catalytical applications in microreactors. *Chemical Engineering Science*, 63(20), 5048–5055.
- Konios, D., Stylianakis, M. M., Stratakis, E., & Kymakis, E. (2014). Dispersion behaviour of graphene oxide and reduced graphene oxide. *Journal of Colloid and Interface Science*, 430, 108–112.
- Kou, R., Shao, Y., Wang, D., Engelhard, M. H., Kwak, J. H., Wang, J., & Liu, J. (2009). Enhanced activity and stability of Pt catalysts on functionalized graphene sheets for electrocatalytic oxygen reduction. *Electrochemistry Communications*, 11(5), 954–957.
- Krehula, S., & Musi, S. (2011). Hydrothermal Synthesis of Platinum Group Metal Nanoparticles, *Croatica Chemica Acta*, 84(4), 465–468.

- Kumar, N. A., Choi, H.-J., Shin, Y.-R., Chang, D. W., Dai, L., & Baek, J.-B. (2012). Polyaniline-Grafted Reduced Graphene Oxide for Efficient Electrochemical. *American Chemical Society Nano*, 25(2), 1715–1723.
- Kurbanoglu, S., Rivas, L., Ozkan, S. A., & Merkoçi, A. (2017). Biosensors and Bioelectronics Electrochemically reduced graphene and iridium oxide nanoparticles for inhibition-based angiotensin-converting enzyme inhibitor detection. *Biosensors and Bioelectronic*, 88, 122–129.
- Lei, C., & Lekakou, C. (2010). Carbon-based nanocomposite EDLC supercapacitors. *Nanotech Conference Expo 2010*, 1, 176–179.
- Lekakou, C., Moudam, O., Markoulidis, F., Andrews, T., Watts, J. F., & Reed, G. T. (2011). Carbon-based fibrous EDLC capacitors and supercapacitors. *Journal of Nanotechnology*, 409382, 1-8.
- Li, J., Fang, K., Qiu, H., Li, S., & Mao, W. (2004). Micromorphology and electrical property of the HCl-doped and DBSA-doped polyanilines. *Synthetic Metals*, 142(1–3), 107–111.
- Li, Y., Gao, W., Ci, L., Wang, C., & Ajayan, P. M. (2010). Catalytic performance of Pt nanoparticles on reduced graphene oxide for methanol electro-oxidation. *Carbon*, 48(4), 1124–1130.
- Li, Y., Zhang, H., Wu, B., & Guo, Z. (2017). Applied Surface Science Improving the oxidation resistance and stability of Ag nanoparticles by coating with multilayered reduced graphene oxide. *Applied Surface Science*, 425, 194–200.
- Lima, A. H., Mendonça, J. P., Duarte, M., Stavale, F., Legnani, C., & Carvalho, G. S. G. De. (2017). Reduced graphene oxide prepared at low temperature thermal treatment as transparent conductors for organic electronic applications. *Organic Electronics*, 49, 165–173.

- Long, N. V., Chien, N. D., Hayakawa, T., Hirata, H., Lakshminarayana, G., & Nogami, M. (2010). The synthesis and characterization of platinum nanoparticles: a method of controlling the size and morphology. *Nanotechnology*, *21*(3), 035605.
- Lota, G., Frackowiak, E., Mittal, J., & Monthieux, M. (2007). High performance supercapacitor from chromium oxide-nanotubes based electrodes. *Chemical Physics Letters*, *434*(1–3), 73–77.
- Lu, P., Xue, D., Yang, H., & Liu, Y. (2012). Supercapacitor and nanoscale research towards electrochemical energy storage. *International Journal of Smart and Nano Materials*, *4*(1), 1–25.
- Madhav, M. R., David, S. E. M., Kumar, R. S. S., Swathy, J. S., Bhuvaneshwari, M., Mukherjee, A., & Chandrasekaran, N. (2017). Toxicity and accumulation of copper oxide (CuO) nanoparticles in different life stages of Artemia salina. *Environmental Toxicology and Pharmacology*, *52*, 227–238.
- Madria, N., Arunkumar, T. A., Nair, N. G., Vadapalli, A., Huang, Y. W., Jones, S. C., & Reddy, V. P. (2013). Ionic liquid electrolytes for lithium batteries: Synthesis, electrochemical, and cytotoxicity studies. *Journal of Power Sources*, *234*, 277–284.
- Mafuné, F., Kohno, J., Takeda, Y., Kondow, T., & Sawabe, H. (2000). Structure and stability of silver nanoparticles in aqueous solution produced by laser ablation. *The Journal of Physical Chemistry B*, *104*(35), 8333–8337.
- Mahmood, N., Zhang, C., Yin, H., & Hou, Y. (2014). Graphene-based nanocomposites for energy storage and conversion in lithium batteries, supercapacitors and fuel cells. *Journal of Materials and Chemistry A*, *2*(1), 15–32.
- Marcano, D. D. C. D., Kosynkin, D. D. V., Berlin, J. M., Sinitskii, A., Sun, Z. Z., Slesarev, A., & Tour, J. M. (2010). Improved synthesis of graphene oxide. *American Chemical Society*, *4*(8), 4806–4814.

- Marcano, D. C., Kosynkin, D. V., Berlin, J. M., Sinitskii, A., Sun, Z., Slesarev, A., & Tour, J. M. (2010a). Improved synthesis of graphene oxide. *American Chemical Society Nano*, 4(8), 4806–4814.
- Mastragostino, M., Arbizzani, C., & Soavi, F. (2001). Polymer-based supercapacitors. *Journal of Power Sources*, 97–98, 812–815.
- Moozarm, P., Meng, P., & Alias, Y. (2017). Applied surface science facile one-step electrochemical deposition of copper nanoparticles and reduced graphene oxide as nonenzymatic hydrogen peroxide sensor. *Applied Surface Science*, 413, 56–65.
- Murata. (2016). High Performance Supercapacitor (EDLC) DMF Series.
- Njagi, E. C., Huang, H., Stafford, L., Genuino, H., Galindo, H. M., Collins, J. B., & Suib, S. L. (2011). Biosynthesis of iron and silver nanoparticles at room temperature using aqueous sorghum bran extracts. *Langmuir*, 27(1), 264–271.
- Oyedotun, K. O., Madito, M. J., Bello, A., Momodu, D. Y., Mirghni, A. A., & Manyala, N. (2017). Investigation of graphene oxide nanogel and carbon nanorods as electrode for electrochemical supercapacitor. *Electrochimica Acta*, 245, 268–278.
- Pandey, G. P., Kumar, Y., & Hashmi, S. A. (2010). Ionic liquid incorporated polymer electrolytes for supercapacitor application. *Indian Journal of Chemistry - Section A Inorganic, Physical, Theoretical and Analytical Chemistry*, 49(5–6), 743–751.
- Portet, C., Taberna, P. L., Simon, P., Flahaut, E., & Laberty-Robert, C. (2005). High power density electrodes for Carbon supercapacitor applications. *Electrochimica Acta*, 50(20), 4174–4181.

- Prusty, R. K., Ghosh, S. K., Rathore, D. K., & Ray, B. C. (2017). Composites : Part A Reinforcement effect of graphene oxide in glass fibre / epoxy composites at in-situ elevated temperature environments: An emphasis on graphene oxide content. *Composites Part A*, 95, 40–53.
- Ravichandran, R., Sundarrajan, S., Venugopal, J. R., Mukherjee, S., & Ramakrishna, S. (2010). Applications of conducting polymers and their issues in biomedical engineering. *Journal of The Royal Society Interface*, 7(5), S559–S579.
- Reynolds, C. (2009). Evolution of supercapacitors. *Electronic Products*, 51(5).
- Robert Pellecchia, Curtis Holmes, G. B. and F. R. S. (2010). Dynamic modelling and control design of advanced energy storage for power system applications, *Dynamic Modelling*, 3, 49-92.
- Sarkar, C., & Dolui, S. K. (2015). Synthesis of copper oxide/reduced graphene oxide nanocomposite and its enhanced catalytic activity towards reduction of 4-nitrophenol. *RSC Advances*, 5(75), 60763–60769.
- Sarkar, K., Sarkar, K. J., & Banerji, P. (2015). Synthesis of graphene oxide–silver nanocomposite with photochemically grown silver nanoparticles to use as a channel material in thin film field effect transistors. *The Royal Society of Chemistry Advanced*, 5(130), 107811–107821.
- Schneuwly, A., & Gallay, R. (2000). Properties and applications of supercapacitors From the state-of-the-art to future trends. *Proceeding PCIM2000*, 1–10.
- Settanni, G., Zhou, J., Suo, T., Schöttler, S., Landfester, K., Schmid, F., & Mailänder, V. (2017). Protein corona composition of PEGylated nanoparticles correlates strongly with amino acid composition of protein surface. *Nanoscale*, 9, 2138-2144.

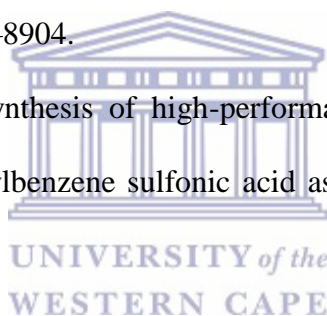


- Shahriary, L., & Athawale, A. a. (2014). Graphene synthesized by using modified Hummers approach. *International Journal of Renewable Energy and Environmental Engineering*, 02(01), 58–63.
- Shao, G., Lu, Y., Wu, F., Yang, C., Zeng, F., & Wu, Q. (2012). Graphene oxide: The mechanisms of oxidation and exfoliation. *Journal of Materials Science*, 47(10), 4400–4409.
- Shao, Y., Wang, H., Zhang, Q., & Li, Y. (2013). High-performance flexible asymmetric supercapacitors based on 3D porous graphene/MnO₂ nanorod and graphene/Ag hybrid thin-film electrodes. *Journal of Materials Chemistry C*, 1(6), 1245.
- Sharma, P., & Bhatti, T. S. (2010). A review on electrochemical double-layer capacitors. *Energy Conversion and Management*, 51(12), 2901–2912.
- Shumba, M., Centane, S., Chindeka, F., & Nyokong, T. (2017). Nanocomposites of sulphur-nitrogen co-doped graphene oxide nanosheets and cobalt mono carboxyphenoxy phthalocyanines for facile electrocatalysis. *Journal of Electroanalytical Chemistry*, 791, 36-48.
- Silwana, B., Horst, C. Van Der, Iwuoha, E., & Somerset, V. (2015). Synthesis , characterisation and electrochemical evaluation of reduced graphene oxide modified antimony nanoparticles. *Thin Solid Films*, 592, 124–134.
- Simon, P. (2012). Formulation of electrolytes based on ionic liquids for supercapacitor applications. *Cirimat*, 508.
- Simon, P., & Gogotsi, Y. (2009). Materials for electrochemical capacitors. *Nanoscience and Technology: A Collection of Reviews from Nature Journals*, 845–854.

- Slistan-Grijalva, A., Herrera-Urbina, R., Rivas-Silva, J. F., Ávalos-Borja, M., Castellón-Barraza, F. F., & Posada-Amarillas, A. (2008). Synthesis of silver nanoparticles in a polyvinylpyrrolidone (PVP) paste, and their optical properties in a film and in ethylene glycol. *Materials Research Bulletin*, 43(1), 90–96.
- Song, J., Wang, X., Chang, C.-T., Song, J., Wang, X., & Chang, C.-T. (2014). Preparation and characterization of Graphene Oxide. *Journal of Nanomaterials*, 2014, 1–6.
- Stević, Z., Rajčić-Vujasinović, M., Bugarinović, S., & Dekanski, A. (2010). Construction and characterisation of double layer capacitors. *Acta Physica Polonica A*, 117(1), 228–233.
- Stoller, M. D., Park, S., Yanwu, Z., An, J., & Ruoff, R. S. (2008). Graphene-based ultracapacitors. *Nano Letters*, 8(10), 3498–3502.
- Suramwar, N. V., Thakare, S. R., & Khaty, N. T. (2016). One pot synthesis of copper nanoparticles at room temperature and its catalytic activity. *Arabian Journal of Chemistry*, 9, S1807–S1812.
- Tang, Y., Yang, X., Wang, R., & Li, M. (2014). Enhancement of the mechanical properties of graphene-copper composites with graphene-nickel hybrids. *Materials Science and Engineering A*, 599, 247–254.
- Veerapandian, M., Lee, M.-H., Krishnamoorthy, K., & Yun, K. (2012). Synthesis, characterization and electrochemical properties of functionalized graphene oxide. *Carbon*, 50(11), 4228–4238.
- Venkataraman, A. (2015). Pseudocapacitors for energy storage. *Dissertations and Theses*, 2486.
- Wan, M. (2008). A template-free method towards conducting polymer nanostructures. *Advanced Materials*, 20(15), 2926–2932.

- Wang, H., Qiao, X., Chen, J., & Ding, S. (2005). Preparation of silver nanoparticles by chemical reduction method. *Colloids and Surfaces A: Physicochemical and Engineering Aspects*, 256(2–3), 111–115.
- Wang, X., Yu, S., & Jin, J. (2016). Application of graphene oxides and graphene oxide-based nanomaterials in radionuclide removal from aqueous solutions. *Science Bulletin*, 61(20), 1583–1593.
- Wang, Y., Sauriat-dorizon, H., & Korri-yousoufi, H. (2017). Sensors and Actuators B : Chemical direct electrochemical DNA biosensor based on reduced graphene oxide and metalloporphyrin nanocomposite. *Sensors & Actuators: B. Chemical*, 251, 40–48.
- Wang, Y., Shi, Z., Huang, Y., Ma, Y., Wang, C., Chen, M., & Chen, Y. (2009). Supercapacitor devices based on graphene materials. *Journal of Physical Chemistry C*, 113, 13103–13107.
- Wu, T.-T. (2013). Preparation and characteristics of graphene oxide and its thin films. *Surface and Coatings Technology*, 231, 487–491.
- Wu, Z. S., Winter, A., Chen, L., Sun, Y., Turchanin, A., Feng, X., & Mallen, K. (2012). Three-dimensional nitrogen and boron co-doped graphene for high-performance all-solid-state supercapacitors. *Advanced Materials*, 24(37), 5130–5135.
- Xu, C., Wang, X., & Zhu, J. (2008). Graphene–metal particle nanocomposites. *The Journal of Physical Chemistry C*, 112(50), 19841–19845.
- Xu, X., Shen, J., Li, N., & Ye, M. (2015). Microwave-assisted in situ synthesis of cobalt nanoparticles decorated on reduced graphene oxide as promising electrodes for supercapacitors. *International Journal of Hydrogen Energy*, 40(38), 13003–13013.
- Yan, Y., Li, B., Guo, W., Pang, H., & Xue, H. (2016). Vanadium based materials as electrode materials for high performance supercapacitors. *Journal of Power Sources*, 329, 148–169.

- Yang, J., & Gunasekaran, S. (2013). Electrochemically reduced graphene oxide sheets for use in high performance supercapacitors. *Carbon*, 51(1), 36–44.
- Yang, J., Yin, H., Jia, J., & Wei, Y. (2011). Facile synthesis of high-concentration, stable aqueous dispersions of uniform silver nanoparticles using aniline as a reductant. *Langmuir*, 27(8), 5047–5053.
- Yang, L., Yan, D., Liu, C., Song, H., & Tang, Y. (2015). Vertically oriented reduced graphene oxide supported dealloyed palladium e copper nanoparticles for methanol electrooxidation. *Journal of Power Sources*, 278, 725–732.
- Yin, B., Ma, H., Wang, S., & Chen, S. (2003). Electrochemical synthesis of silver nanoparticles under protection of poly(n-vinylpyrrolidone). *The Journal of Physical Chemistry B*, 107(34), 8898–8904.
- Yin, H., & Yang, J. (2011). Synthesis of high-performance one-dimensional polyaniline nanostructures using dodecylbenzene sulfonic acid as soft template. *Materials Letters*, 65(5), 850–853.
- Zaaba, N. I., Foo, K. L., Hashim, U., Tan, S. J., Liu, W. W., & Voon, C. H. (2017). Synthesis of graphene oxide using modified Hummers Method: solvent influence. *Procedia Engineering*, 184, 469–477.
- Zainy, M., Huang, N. M., Vijay Kumar, S., Lim, H. N., Chia, C. H., & Harrison, I. (2012). Simple and scalable preparation of reduced graphene oxide-silver nanocomposites via rapid thermal treatment. *Materials Letters*, 89, 180–183.
- Zeki, S. (2015). Gold nanoparticle functionalized graphene oxide modified platinum electrode for hydrogen peroxide and glucose sensing. *Materials Letters*, 150, 20–23.
- Zhang, J., & Zhao, X. S. (2012). Conducting polymers directly coated on reduced graphene oxide sheets as high-performance supercapacitor electrodes. *Journal of Physical Chemistry C*, 116(9), 5420–5426.

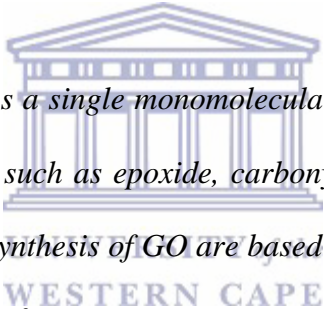


- Zhang, L. L., Zhou, R., & Zhao, X. S. (2009). Carbon-based materials as supercapacitor electrodes. *Journal of Materials Chemistry*, 38(29), 2520–2531.
- Zhang, X., Zhang, D., Chen, Y., Sun, X., & Ma, Y. (2012). Electrochemical reduction of graphene oxide films: Preparation, characterization and their electrochemical properties. *Chinese Science Bulletin*, 57(23), 3045–3050.
- Zheng, J. P., Cygan, P. J., & Jow, T. R. (1995). Hydrous Ruthenium Oxide as an Electrode Material for Electrochemical Capacitors, *142*(8), 9–13.
- Zheng, S., Xue, H., & Pang, H. (2017). Supercapacitors based on metal coordination materials. *Coordination Chemistry Reviews*, 0010-8545.
- Zhou, Y., & Narendran, N. (2005). Photovoltaic-powered light-emitting diode lighting systems. *Optical Engineering*, 44(11), 111311.
- Zhu, Y., Hu, D., Wan, M., Jiang, L., & Wei, Y. (2007). Conducting and superhydrophobic rambutan-like hollow spheres of polyaniline. *Advanced Materials*, 19(16), 2092–2096.
- Zhu, Y., Murali, S., Cai, W., Li, X., Suk, J. W., Potts, J. R., & Ruoff, R. S. (2010). Graphene and graphene oxide: Synthesis, properties, and applications. *Advanced Materials*, 22(35), 3906–3924.
- Zielińska, A., Skwarek, E., Zaleska, A., Gazda, M., & Hupka, J. (2009). Preparation of silver nanoparticles with controlled particle size. *Procedia Chemistry*, 1(2), 1560–1566.

Chapter 3

Synthesis and Evaluation of the Supercapacitor Properties of Graphene Oxide (GO) and Reduced Graphene Oxide

Summary



Graphene oxide (GO) is viewed as a single monomolecular layer of graphite with numerous oxygen containing functionalities such as epoxide, carbonyl, carboxyl and hydroxyl groups. Modern procedures used for the synthesis of GO are based on the Hummers method in which graphite is oxidized by a solution of potassium permanganate in sulphuric acid. Treating GO with hydrazine, a strong reducing agent, reduces GO to reduced graphene oxide (rGO). There are however alternatives that have been used as reducing agents for the reduction of GO to rGO. GO can be reduced as a thin film or in aqueous solution, however, for supercapacitors it is necessary to know which to use for the construction of the electrodes. Therefore the chapter determines which is more proper to use in supercapacitors, GO or rGO. The chapter also discusses the different experimental methods for graphene oxide and graphene and their characterization techniques. Comparison of GO with rGO to determine which is more useful to use in supercapacitors is demonstrated.

Abstract

Graphene oxide (GO) was synthesized by the modified Hummers method and was further reduced to reduced graphene oxide (rGO) by hydrazine monohydrate and ammonia solution. The prepared materials were characterized by different characterization techniques to determine which materials would be suitable for supercapacitors. High resolution scanning electron microscopy (HRSEM) revealed a sheet-like morphology of separated thin sheets and wrinkled edges for GO, whereas rGO was composed of thinner sheets and smaller pores than GO. High resolution transmission electron microscopy (HRTEM) shows light, transparent, and flat nanosheets that appear to be situated at the top of the grid and these nanosheets appeared to be larger than 1.5 μm . Ultraviolet-Visible spectroscopy (UV-Vis) of GO revealed two characteristic bands, the first is a shoulder at ~ 311 nm, which corresponds to an $n\text{-}\pi^*$ plasmon peak. Another characteristic feature appears at 227 nm, and corresponds to a $\pi\text{-}\pi^*$ plasmon peak, however the shoulder band in rGO disappeared and a characteristic band appeared at 264 nm. Fourier transform infrared spectroscopy (FTIR) of GO revealed vibrational bands of O-H stretching vibrations at 3434 cm^{-1} , C-O (carboxylic acid and carbonyl moieties) at 1736 cm^{-1} and the graphitic domains of C-C at 1635 cm^{-1} and C=C-O at 1392 cm^{-1} . The band at $980 - 1250\text{ cm}^{-1}$ contains the C-O (1040 cm^{-1}) and the O-H (1227 cm^{-1}) deformation, respectively, of carboxylic acid groups while rGO revealed that the oxygen bands either disappear or are greatly reduced in intensity while a new band that appears at 656 cm^{-1} is attributed to C-C bonds that are due to thermal annealing. Raman spectroscopy of GO shows a D band (1346 cm^{-1}) a second-order overtone of a different in-plane vibration and corresponds to defects within the sp^2 network, a G band (1595 cm^{-1}) and a 2D band (2689 cm^{-1}) attributed to primary in-plane vibrational mode. For rGO the D band and G band are shifted to lower frequencies due to the incomplete defect healing. X-ray

diffraction (XRD) of GO, revealed a very sharp diffraction band (001) appearing at $2\theta = 11.08^\circ$ which indicates that AB stacking exists in GO with larger interlayer spacing, however, rGO revealed an appearance of a broad band at 26.5° due to (002) reflection of rGO. Electrochemical studies were carried out with Cyclic Voltammetry (CV) which revealed that the materials are ideal double layer capacitance materials capacitance of GO and rGO were calculated from cyclic voltammetry and falling between the range of 100-200 $F g^{-1}$.



3.1 Introduction

Graphene oxide (GO), a single sheet of graphite, is an intermediate during reduced graphene oxide synthesis by the method of oxidation, exfoliation and reduction of graphite powder by strong reducing agents. The method is the mostly used method for the preparation of reduced graphene oxide (rGO) due to its low cost, facile preparation process and large productivity. Due to the oxygen functional groups found on the basal plane of GO, it can therefore be regarded as functionalized rGO. Due to the degradation of the sp^2 hybrid carbon atoms in graphite to sp^2 - sp^3 hybrid atoms, GO possesses less stacking stability, poor conductivity therefore alone as a carbon material, it was claimed that it is not able to directly serve as electrode material for supercapacitors (Gao, 2015; Georgakilas *et al.*, 2012). The first synthesis of rGO was reported to be prepared by the micromechanical cleavage from highly ordered pyrolytic graphite wherein in this synthesis method, a layer from the graphite was peeled off using scotch tape and transferred on to the silicon substrate (Gao, 2015). Recently, the common method mostly used for the preparation of graphene oxide is the modified Hummers method. This method uses a mixture of graphite, a cold solution of sulphuric acid, sodium nitrate and potassium permanganate used in an ice bath. The permanganate is mostly used as an oxidant but the active site is the diamanganese heptoxide and for safety purposes; it should be used with lower temperatures (Gao, 2015; Shahriary & Athawale, 2014). The modified Hummers method involves the treatment of potassium permanganate, sulphuric acid and nitric acid (Wong *et al.*, 2015). The potassium permanganate is added slowly to the reaction, keeping the temperature below 5 °C to prevent overheating and the evolution of gases. The mixture is then stirred at room temperature for five days for proper oxidation to take place. The resulting mixture is then diluted with water and sulphuric acid. To ensure the completion of the reaction with potassium permanganate, the mixture is treated with

hydrogen peroxide and finally washed with hydrochloric acid and water (Shahriary & Athawale, 2014; Stylianakis *et al.*, 2012). To improve the synthesis of GO, Marcano *et al.*, 2010a) enhanced the amount of the potassium permanganate and performed the reaction in a ratio of 9:1 mixture of sulphuric acid or phosphoric acid instead of the sodium nitrate. This method increases the amount of hydrophilic oxidized graphene material and improves the efficiency of the oxidation process. This improved method does not involve large exothermic reactions and produces no toxic gases therefore it is more advantageous than the other methods. GO can be reduced by many techniques such as thermal annealing reduction (Dzukarnain *et al.*, 2016) which involves the reduction of GO by heat treatment (Khamaj, 2017). Chemical reduction involves treating GO with chemical reagents which are based on their reactions with GO (Li *et al.*, 2009). The reduction is obtained at room temperature or by reasonable heating (Gao, 2015; Pei & Cheng, 2011).



3.2 Experimental

3.2.1 Chemicals and sample preparation

All chemicals used in the experiments were of analytical grade and were used as purchased without further purification. Graphite (1-2 micron), sodium nitrate NaNO_3 , sulphuric acid H_2SO_4 ($\geq 98\%$), potassium permanganate KMnO_4 ($\geq 99\%$), hydrogen peroxide ($\geq 30\%$), hydrochloric acid ($\geq 37\%$), acetone ($\geq 99.9\%$), hydrazine monohydrate, reagent grade (98%) were all purchased from Sigma-Aldrich, Cape Town, South Africa.

3.2.2 Instrumentation

Electrochemical measurements were performed using a 273A Potentiostat/Galvanostat (Princeton Applied Research), wherein glassy carbon electrode, platinum wire and Ag/AgCl (3 M NaCl) acted as the working electrode, the counter electrode and the reference electrode, respectively. A mass of 20 mg of sample (GO or rGO) was dissolved in deionized water (1 mg/mL) and sonicated for an hour. A volume of 25 μL of mixture was drop coated on a glassy carbon electrode and was left to dry on air. A volume of 10 μL of nafion was drop coated on the already dried electrode and was left to dry in air. Nafion is used as binder to help the material stick easily on the surface of the electrode. The electrode was then used for electrochemical reactions. Cyclic voltammetry (CV) experiments were performed over a potential range of -1.0 V to +1.0 V and scan rate of 50 mV/s. Ultraviolet-visible (UV-Vis) absorption measurements for the prepared GO and rGO were obtained using 1 cm quartz cuvette on a Nicolet Evolution 100 UV-Visible spectrophotometer (Thermo Electron, UK) over a wavelength range of 200 to 800 nm. Fourier transform infrared (FTIR) spectra were recorded on a Perkin Elmer FTIR model 100 spectrophotometer, operating between 400 and 4000 cm^{-1} in order to characterize the presence of specific features of GO and rGO. The high-resolution scanning electron microscopy micrographs (HRSEM) of GO and rGO were imaged using a Ziess Auriga SEM operating at 50kV and high resolution-transmission electron microscope (HR-TEM) equipped with an energy-dispersed spectroscopy (EDS) detector which was used to study the size and morphology of samples. Copper grid (Cu) was used as sample holder for the immobilization of (2 μL) solution of GO and rGO and the micrographs were recorded at room temperature. X-ray Diffraction using Diffractometer D8 Advance manufactured by Bruker AXS in Germany was done to determine the crystal

structure of the samples. Raman spectroscopy was taken with a Renishaw inVia Raman Microscope made in Germany and a Class 1 Laser product was used.

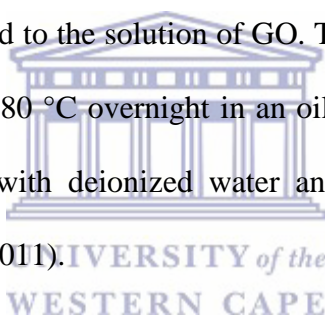
3.2.3 *Synthesis of GO*

GO was prepared using a modified Hummers method. Specifically, 0.5 g of graphite powder was added to a cold solution of 40 mL of concentrated sulfuric acid (H_2SO_4 , 98%) and 0.375 g of sodium nitrate (NaNO_3) under vigorous stirring for 1 hour in an ice bath. 2.25 g potassium permanganate (KMnO_4) was added portion wise to the solution while it was stirring and the mixture was to remain for a further 2 hours in an ice bath, to cool the mixture below $10\text{ }^\circ\text{C}$. The mixture took on a green brown color and remained stirring for 5 days in order to ensure complete oxidation of the graphite. After completion of the reaction, 70 mL of dilute aqueous solution of 5% H_2SO_4 was added to the mixture to cleave the formed precipitate salts due to oxidation. The mixture was heated at $98\text{ }^\circ\text{C}$ for 1 hour while it was being stirred. The heating was removed and 2 mL 30% H_2O_2 peroxide was added to the mixture (after it was let to cool down to $60\text{ }^\circ\text{C}$). The mixture was stirred for a further 2 hours. Subsequently, in order to remove residues of KMnO_4 and derivatives such as Mn_2O_7 , the following procedure was followed. The mixture was centrifuged for 10 min at 4000 rpm, washed with 600 mL aqueous solution of 3% H_2SO_4 and 0.5% H_2O_2 and then placed in an ultrasonic bath for 10 min. The process was repeated a number of times to get rid of the salts. Then, the mixture was washed and purified with 150 mL of aqueous 3% HCl for 2-3 times by mixing and centrifugation, to eliminate any metal ions. Then washed with distilled water until the pH increased, due to the HCl , to the value 7 (average of 4 times) and thereby remove any remaining acidic entirety. Finally, the solution was washed with acetone and dried at $60\text{ }^\circ\text{C}$ in a vacuum oven for 12 hours. After drying, the GO was obtained in the form of a shell,

followed by grinding, weighing and collecting the product. The sample was named GO (Stylianakis *et al.*, 2012) .

3.2.4 Reduction of graphene oxide (GO)

The prepared GO was reduced to rGO by using hydrazine monohydrate as the reducing agent. 100 mg of GO was dispersed in 200 mL of deionized water and ultra-sonicated for three hours through which the bulk GO powders were transformed into GO sheets. The obtained brown precipitation/dispersion was centrifuged at 3000 rpm for 30 min to remove any excess un-exfoliated GO. A volume of 200 μ L of hydrazine monohydrate and 3 mL of ammonia solution were then added to the solution of GO. The mixture was stirred vigorously for 10 to 20 min and refluxed at 80 °C overnight in an oil bath. The final product was then centrifuged or filtered, washed with deionized water and dried under vacuum overnight (Konios *et al.*, 2014; Park *et al.*, 2011).



3.2.5 Fabrication of the electrode

3.2.5.1 Preparation of the electrode

The materials used in the experiment for fabrication of the electrode consisted of 40 mg active material, 5 mg of carbon black, 5 mg (3 drops) of isopropanol and 8 mg of polytetrafluoroethylene (PTFE) binder. The active material consisted of the graphene oxide. The carbon black and GO were mixed together and crushed to ensure that they were correctly mixed. For a given electrode, relevant materials were mixed together in a 10 mL small beaker to form dough. The dough was transferred onto a flat glass plate. A stainless steel/Teflon rod was used to roll the dough into mm thick flexible thin films. When making the thin film the

dough was rolled many times with constant addition of three drops of isopropanol to ensure that the material was correctly mixed in the thin film. The thin film was then placed in an oven and was allowed to bake at 80 ° C under vacuum. Once the thin film was dried it was then cut into small wafers for the construction of the electrode (Njomo *et al.*, 2014).

3.2.5.2 Construction of supercapacitor cell

A single electrode was assembled with three parts; electrode material, stainless steel mesh current collector and stainless steel wire. The electrode was assembled by cutting the stainless steel mesh current collector into a 1 cm × 4 cm rectangular shape. The collector was then cleaned by shaking it in ethanol, drying it and then weighing. Approximately 1 cm² wafer was placed on the stainless steel mesh and pressed at a pressure of 20 MPa for 5 min. The electrode was then weighed and the difference in mass was used as the active mass of the electrode. The stainless steel wire was tightly held onto the current collector for external circuit connection and acted as cathode. The active material was GO and acted as anode. The stainless steel wire and active material were used to make a two-electrode asymmetric supercapacitor cell. The cell system was fabricated using a solution of 1 M H₂SO₄ as the electrolyte and tested for supercapacitor parameters using the BST8-3 eight-channel battery testing machine. The cell was fabricated by holding together the two single electrodes (cathode and anode) with a porous and electronically non-conductive separator sandwiched between them to form the cell configuration (Njomo *et al.*, 2014).

3.3 Results and Discussion

3.3.1 Particle size properties of GO

GO prepared from the modified Hummers method is characterized using different techniques and HRTEM is aimed to provide information on the structural properties of the material including particle size, particle shape and chemical composition of GO (Song *et al.*, 2014). The GO micrograph observed in Figure 3.1 (a) which demonstrates the efficient exfoliation of the layered structure of graphite (Karthika, 2012) shows that GO retains a graphene-like lattice substructure due to sonication. The nanosheets are observed to be light and transparent and appear to be situated on top of the copper grid (Sarлак & Meyer, 2017). These nanosheets can also be observed to be flat and appear to be larger than 1.5 μm , the wrinkles and the bends were due to the numerous defects and functional groups of sp^3 hybridized carbon atoms during the oxidation process (Bhattacharya *et al.*, 2017). In general, GO nanosheets tend to be assembled with each other and forms multilayer agglomerates (Mane *et al.*, 2015; Zaaba *et al.*, 2017), however, in the HRTEM image, the existence of topological features along the surface with overlapping area of GO nanosheets reveals that they are extremely dispersed in water (Marcano *et al.*, 2010b; Shalaby *et al.*, 2015; Wilson *et al.*, 2009). Figure 3.1 (b) shows the EDX spectrum of GO whereby GO's elemental composition is determined and it confirms the presence of the functional groups, carbon and oxygen, found in GO (Stankovich *et al.*, 2007; Xu *et al.*, 2011). However, the presence of copper is attributed to the copper grid used upon sample preparation.

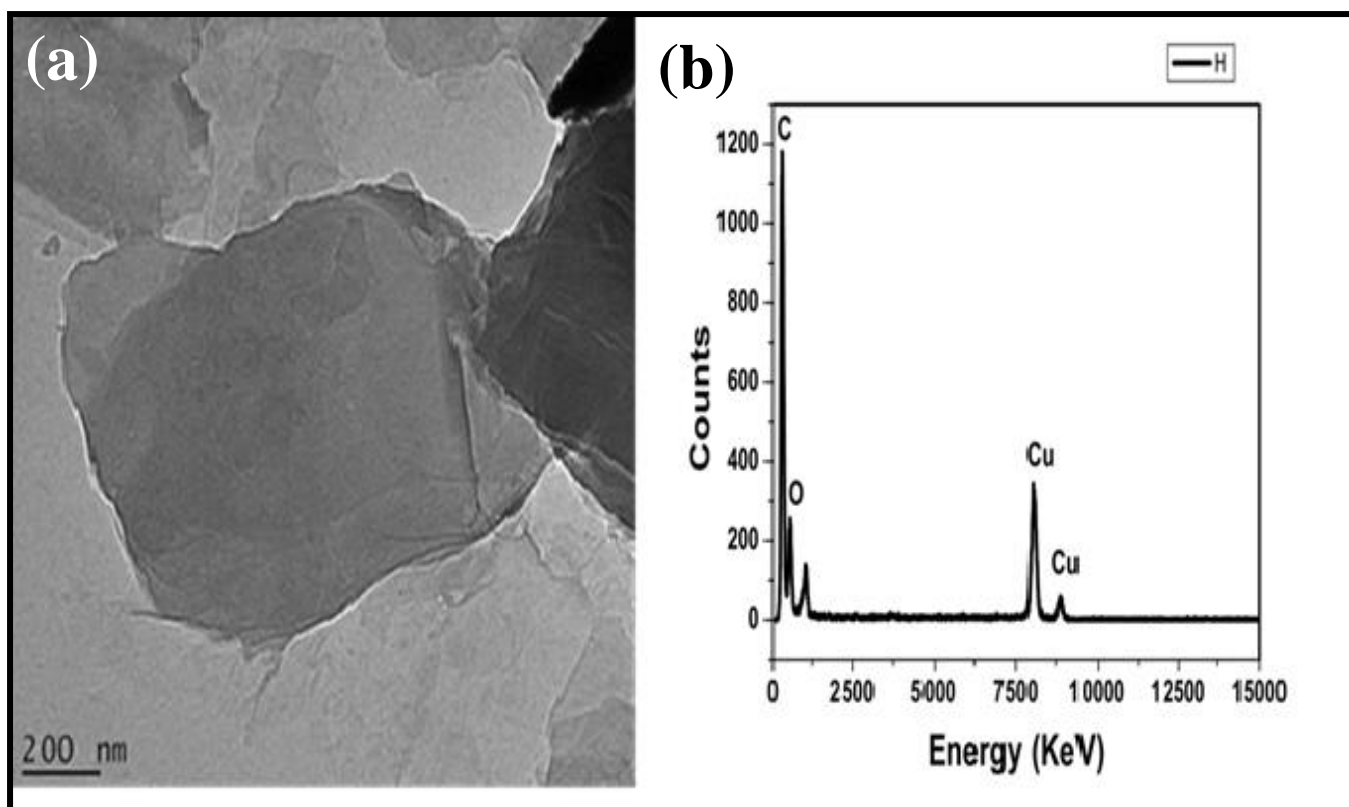
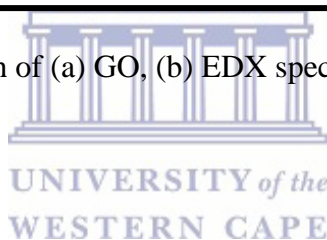


Figure 3. 1: HR-TEM micrograph of (a) GO, (b) EDX spectrum of GO.



3.3.2 Morphological properties of GO and rGO

High resolution SEM is an important technique that provides information of the surface morphology of materials including the roughness, particle shape and size, and absorbency of the material. Both GO and rGO were efficiently exfoliated to form separated thin sheets and wrinkled to form porous structures as shown in Figure 3.2 (a) and (b) (Shahriary & Athawale, 2014). HRSEM images form an absorbent network that resembles a loose sponge like structure of the GO due to the well-defined and interlinked three-dimensional graphene sheets, (Stankovich *et al.*, 2007; Xu *et al.*, 2011). On comparison, rGO was composed of thinner sheets and smaller pores than GO (Drewniak *et al.*, 2016). The GO nanosheets exhibit to some extent the stacking structure with a sheet-like morphology of large thickness

(Hashemi *et al.*, 2018), smooth surfaces and wrinkled edges (Park *et al.*, 2011) while rGO shows thin layered structure of minimum sheet thickness (Li *et al.*, 2017; Xu *et al.*, 2011).

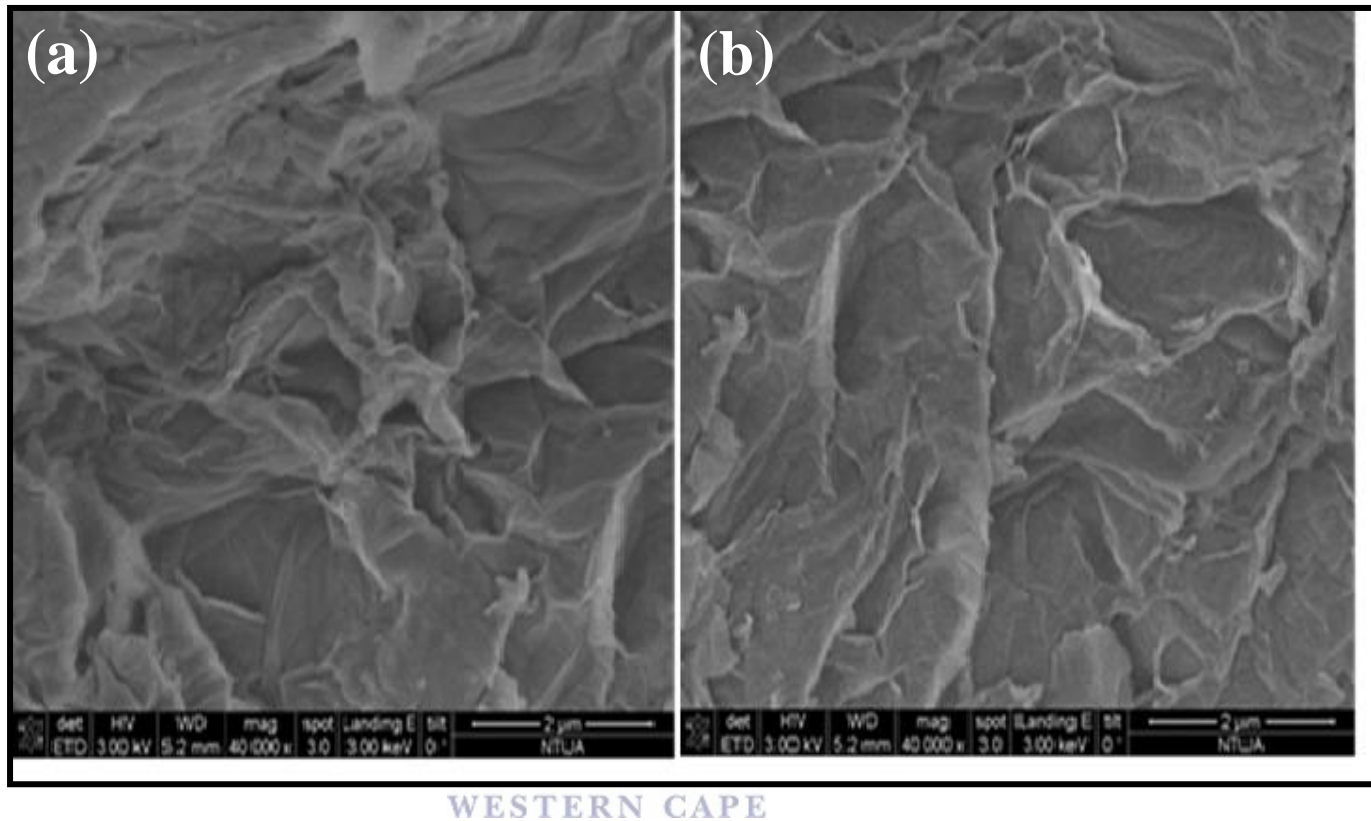


Figure 3. 2: HR-SEM micrographs of (a) GO at 2 μm (b) rGO at 2 μm .

3.3.3 *Optical properties of GO and rGO.*

GO has unique optical properties that can be integrated to different applications. UV-Vis spectra of aqueous GO (i) dispersions are presented in Figure 3.3 (a) at increasingly concentrated aqueous solutions. Two kinds of characteristic features were observed in these spectra to identify GO: the first is a shoulder band at ~ 311 nm, which corresponds to an $n-\pi^*$ plasmon band. The shoulder bands observed for all of the samples are similar. Another characteristic feature appears at 227 nm, and corresponds to a $\pi-\pi^*$ plasmon band (Faust,

1997; Gilje *et al.*, 2008). From UV-Vis spectroscopic studies, it can be concluded that the optical absorption of GO is dominated by the π - π^* plasmon band near 227 nm (Lai *et al.*, 2012b). The π - π^* plasmon band depends on nanometer-scale sp^2 clusters and from linking chromophore units such as C=C, C=O and C–O bonds (Alam *et al.*, 2017; Lai *et al.*, 2012a) .

The UV-Vis spectrum of rGO (ii) in Figure 3.3 (b) exhibits a characteristic band at 264 nm, indicating the restoration of the extensive conjugated sp^2 carbon network (Bhunja & Jana, 2014; Guo *et al.*, 2005; Udayabhaskar *et al.*, 2017). The absorption band shifts to lower absorption wavelengths due to the reduction of oxygen functional groups and an increase in aromatic rings causing electrons to be easily excited to a lower frequency (Jariwala *et al.*, 2011).



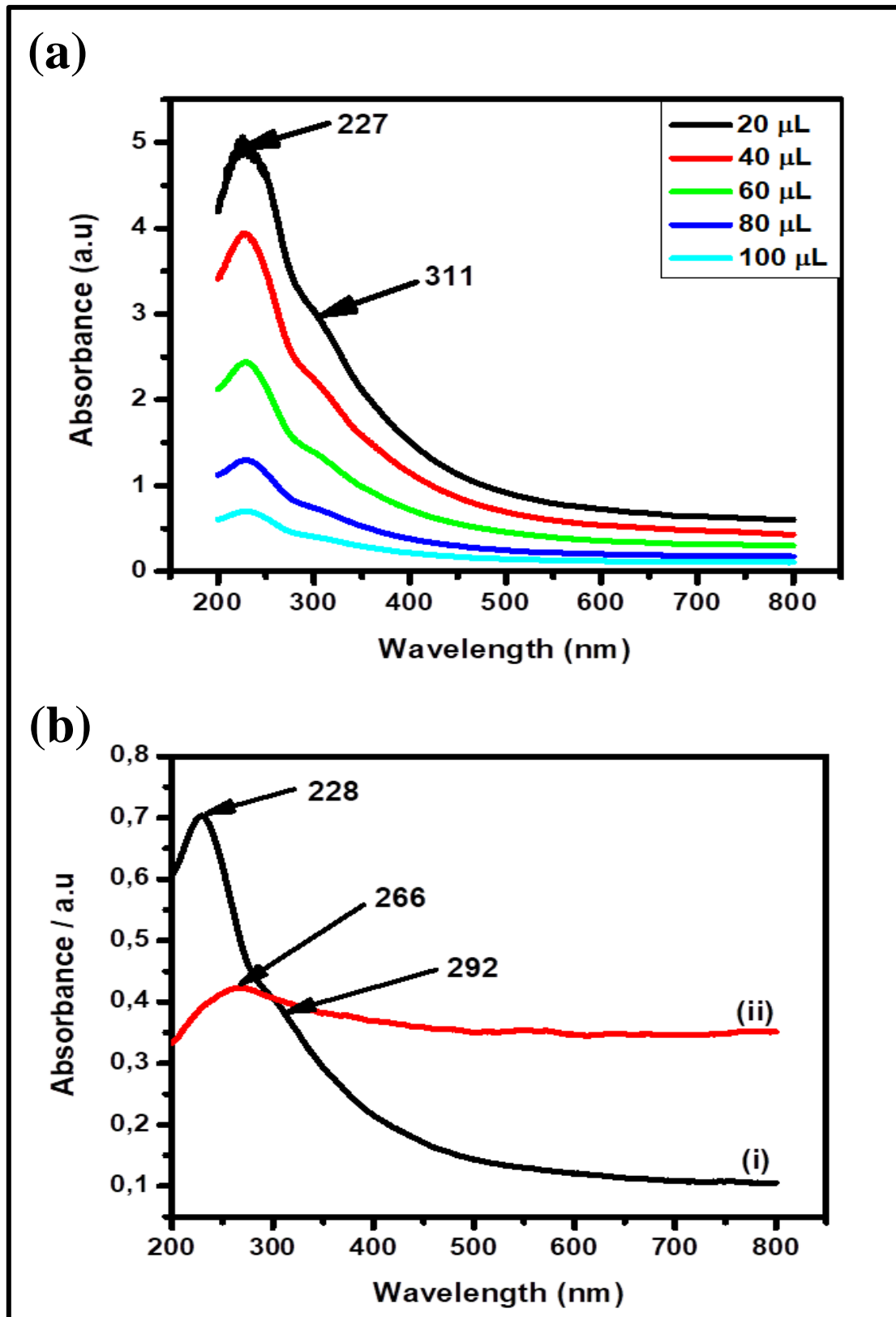
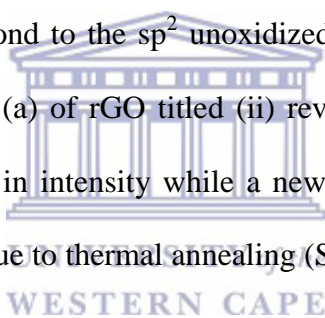


Figure 3. 3: UV-Visible spectra of (a) GO from increasingly concentrated aqueous solutions, 20, 40, 60, 80 and 100 μL in the region (200-800 nm) in de-ionized water (b) (i) GO and (ii) rGO at concentration of 20 μL in the region (200-800 nm) in de-ionized water.

3.3.4 Structural properties of GO and rGO

Further characterization of samples by FTIR was performed to assess the structural properties of GO and rGO. Figure 3.4 (a) displays the FTIR spectra of GO titled (i) and shows the vibrational bands of O-H stretching vibrations at 3431 cm^{-1} , C=O (carboxylic acid and carbonyl moieties) at 1731 cm^{-1} and the graphitic domains of C=C at 1644 cm^{-1} and O=C-O at 1394 cm^{-1} . The band from $980 - 1250\text{ cm}^{-1}$ contains the C-O (1059 cm^{-1}) and the CO-H (1227 cm^{-1}) deformation, respectively, of carboxylic acid groups (Alam *et al.*, 2017; Njomo *et al.*, 2014). The characteristic bands of GO's functional groups confirm the oxidation of graphite (Shahriary & Athawale, 2014). The band found at 1644 cm^{-1} results from the vibration of the aromatic C=C bond to the sp^2 unoxidized network (Wan *et al.*, 2017; Wu, 2013) as observed in Figure 3.4 (a) of rGO titled (ii) reveals that the oxygen bands either disappear or are greatly reduced in intensity while a new peak that appears at 656 cm^{-1} is attributed to C-C bonds that are due to thermal annealing (Sarkar & Dolui, 2015; Shahriary & Athawale, 2014).



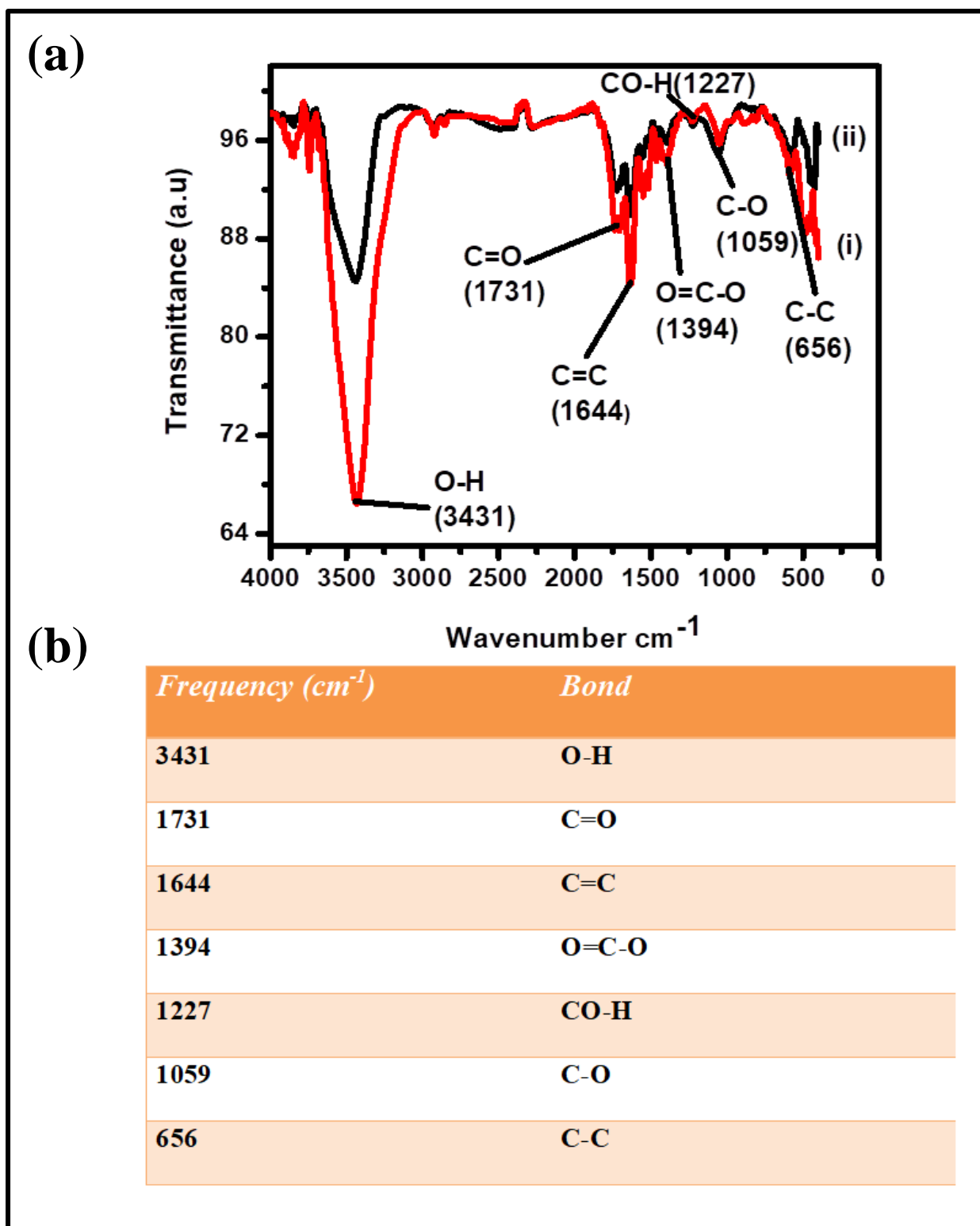


Figure 3. 4: (a) FTIR spectra of GO (i) and rGO (ii) and (b) table showing the frequencies and their respective bonds found in GO.

3.3.5 Internal Structural properties of GO and rGO

Raman spectroscopy is a tool used widely to analyze carbon materials, especially seeing that conjugated and C=C bonds lead to high Raman intensities (Prud *et al.*, 2008). In GO and rGO, the Stokes phonon energy shift caused by laser excitation creates two main bands (D and G) in the Raman spectrum (Shahriary & Athawale, 2014). In Figure 3.5 (a) GO (i) shows a D band (1346 cm^{-1}) a second-order overtone of a different in-plane vibration and corresponds to defects within the sp^2 network, a G band (1595 cm^{-1}) and a 2D band (2689 cm^{-1}) attributed to primary in-plane vibrational mode (Childres *et al.*, 2013; Zhao *et al.*, 2013; Prud *et al.*, 2008). In Figure 3.5 (a) rGO (ii) the D band and G band are shifted to lower frequencies due to the incomplete defect healing and because of added forces from the interactions between layers of AB-stacked graphene. The spectrum changes from that of single-layer graphene as the number of rGO layers increases, (Ferrari, 2007). This therefore splits the 2D band into an increasing number of modes that can combine to give a wider, shorter and higher frequency band (Eda *et al.*, 2008; Khan *et al.*, 2017). The G band also experiences a small red shift from the result of the increased number of layers. The number of layers are derived from the band intensities I_{2D}/I_G ratio as well as the position and shape of these bands for the AB-stacked rGO (Ferrari, 2007; Wahab *et al.*, 2015).

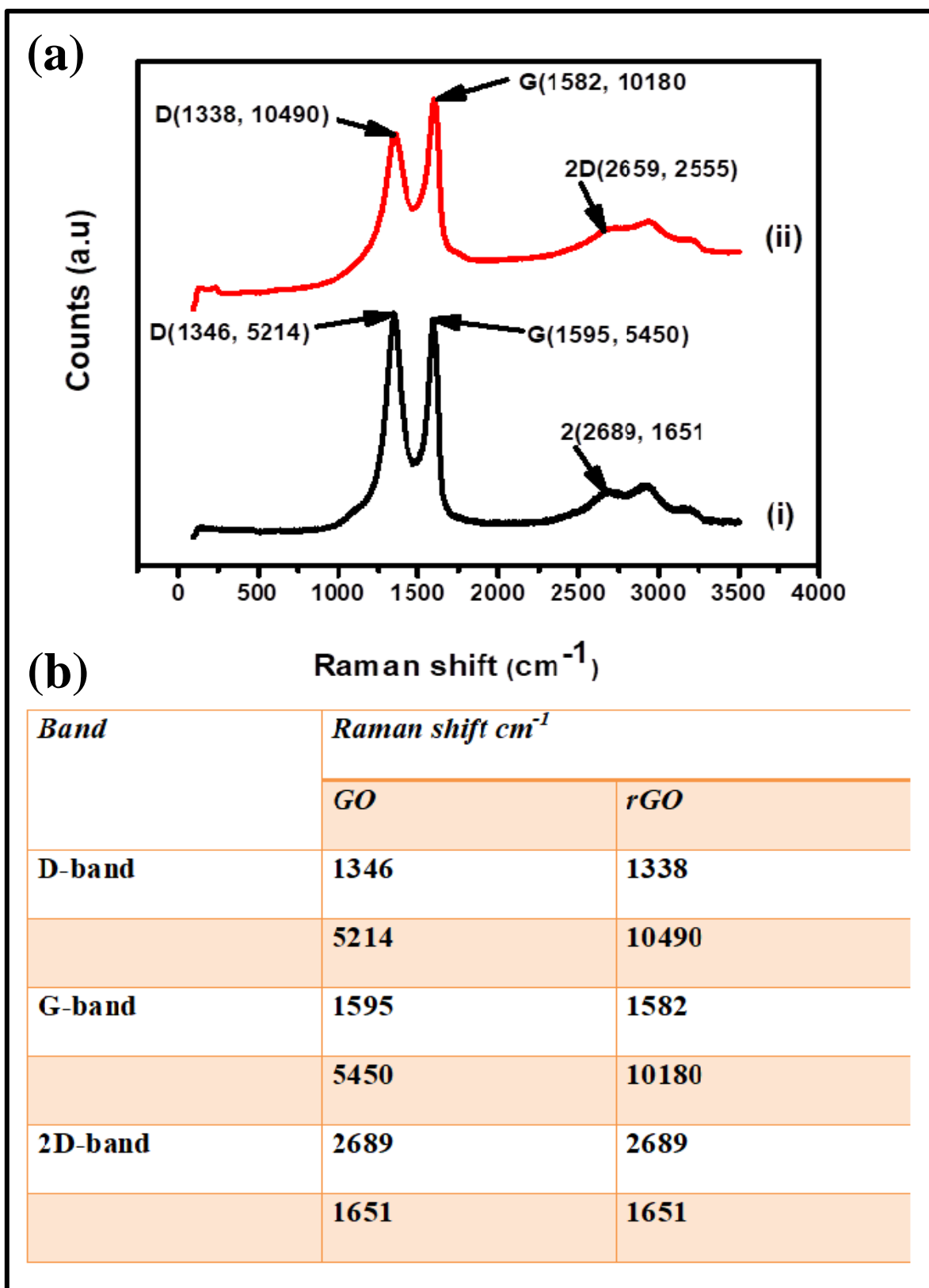


Figure 3. 5: (a) Raman spectroscopy of (i) GO and (ii) rGO (b) Table showing the bands and their respective Raman shift in cm^{-1} found in GO and rGO.

3.3.6 Crystal properties of GO and rGO

A wide angle X-ray diffraction pattern of the powder samples was taken in order to estimate the degree of exfoliation that can be quantitatively estimated from the relative band intensity. Figure 3.6 (a) shows the XRD patterns of GO, revealing a very sharp diffraction band (001) appearing at $2\theta = 11.08^\circ$ (Song *et al.*, 2014). This band indicates that AB stacking exists in GO with larger interlayer spacing (Blanton & Majumdar, 2012) and this value can depend on the method of preparation and on the number of layers of water in the gallery space of the material. The rGO was reduced in the presence of hydrazine monohydrate and there was an appearance of a broad band at 26.5° due to (002) reflection of rGO. This band is very broad indicating the poorly ordered free graphene nanosheets and that significant portion of GO has been greatly reduced (Mu *et al.*, 2013). Furthermore, the broad nature of the reflection in rGO indicates poor ordering of the sheets along the stacking direction (Anwer *et al.*, 2013; Karthika, 2012), giving an implication that the sample could have been completely exfoliated to contain mostly a single layer, a few layers and/or even loosely stacked layers (Blanton & Majumdar, 2012; Kumar *et al.*, 2012; Møller *et al.*, 2016)

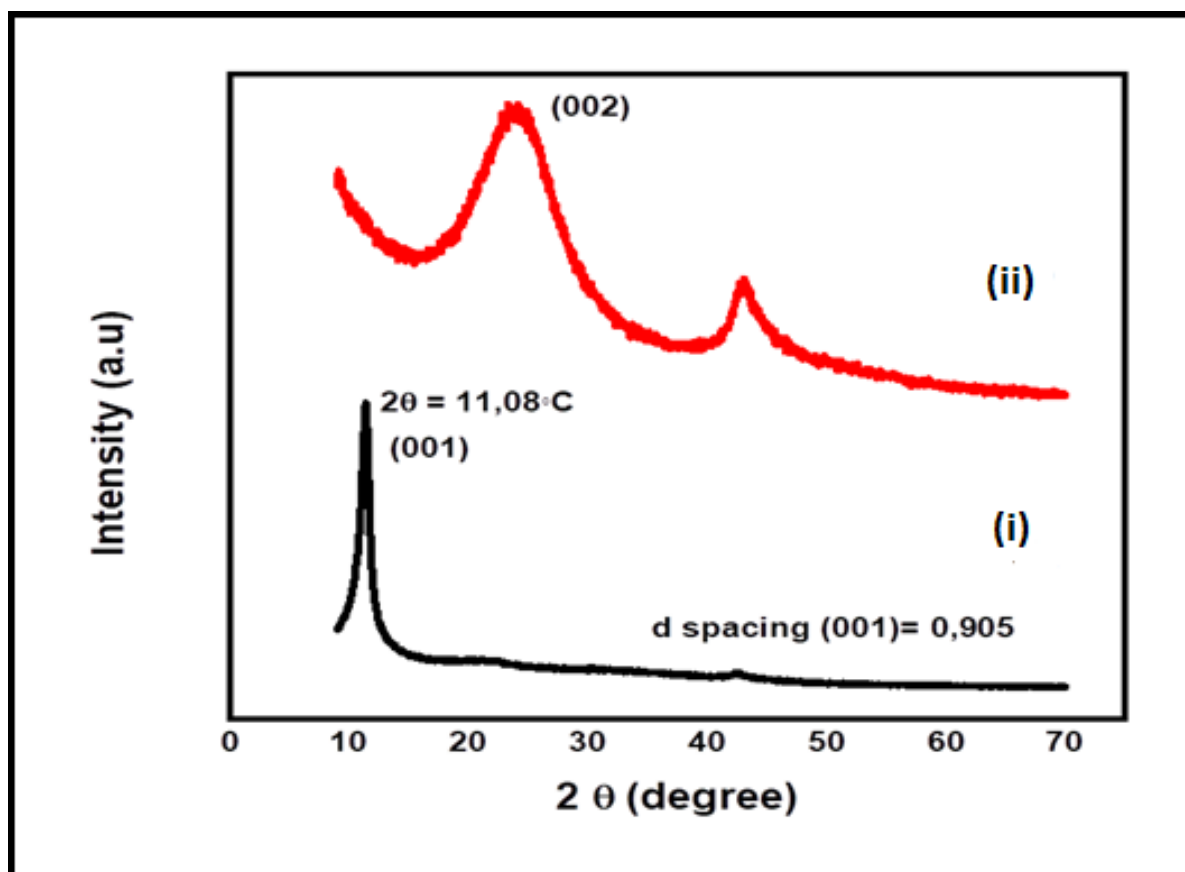
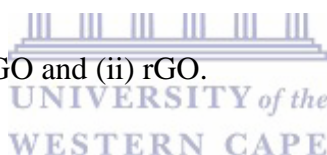


Figure 3. 6: XRD patterns of (i) GO and (ii) rGO.

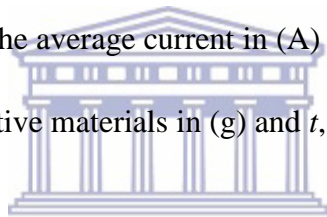


3.4 Electrochemical properties of GO and rGO

3.4.1 Electrochemistry of GO and rGO

Cyclic voltammetry is the most widely used technique for acquiring qualitative information about electrochemical reactions. The electrochemical performances of GO and rGO were measured in a symmetrical two-electrode cell in the potential range of -1.0 V to +1.0 V in 1.0 M H₂SO₄. Figure 3.7 (a) exhibits the cyclic voltammogram of GO in which one anodic peak (i) and one cathodic peak (ii) are observed during the process. The persistent increase of the peak currents shown with successive potential scans as observed in Figure 3.7 (a), indicates that the deposition of GO on GCE has been achieved. Figure 3.7 (b), shows that the deposited

glassy carbon electrode (GCE) modified with the material GO displays anodic peak (i) and cathodic peak (ii) which are attributed to the large number of electrochemical active oxygen containing groups of GO planes that are too stable (Chen *et al.*, 2011; Kim *et al.*, 2017). The calibration curve drawn from linear regression is shown in Figure 3.7 (c) and (e) which show that the materials are ideal double layer capacitor materials (Shao *et al.*, 2010). The calibration curve can also be used to determine the capacitance of the material by using the current under the curve. Figure 3.8 (a), (b) and (d) show that the current under the curve is slowly increased with the scan rate of cyclic voltammetry which then reveals that voltammetric current is directly proportional to the scan rates of CV, (Zoladek *et al.*, 2017). The capacitance, C , can be calculated by the following equations where, Q , is the positive voltammetric charge in (V), I , is the average current in (A) and $\frac{dV}{dt}$ is the voltage scanning rate in (mV/s), m is the mass of the active materials in (g) and t , is the time in (s).



UNIVERSITY of the
WESTERN CAPE (1)

$$C = \frac{Q}{V}$$

$$C = \frac{I}{\frac{dV}{dt}} \times m \quad (2)$$

The calculated capacitance for graphene oxide is 180 F g^{-1} which falls between the ranges of $100\text{--}200 \text{ F g}^{-1}$ determined by other researchers. The same behavior as GO can be observed with rGO. The same parameters were used i.e. the same electrolyte and potential window for Figure 3.7 (d) and Figure 3.7 (e). The anodic peak (i) and cathodic peak (ii) are credited to the electrochemically active oxygen functional groups of reduced planes of GO (Cells, 2013; Njomo *et al.*, 2014; Sharma *et al.*, 2017).

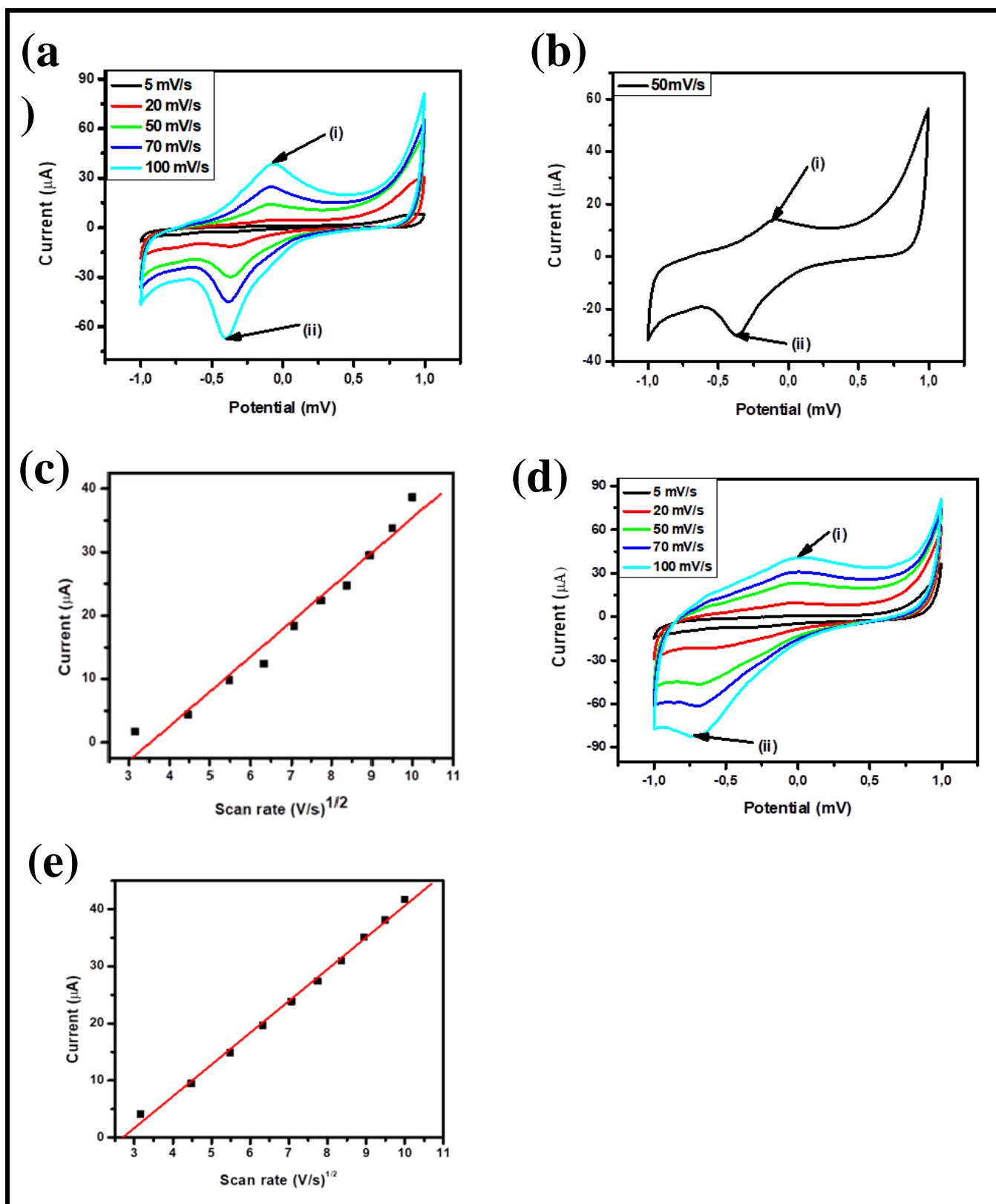


Figure 3. 7: CV behavior of (a) GO, (b) CV behavior of GO at scan rate 50 mV/s (c) calibration curve of rGO (d) CV behavior of rGO (e) Calibration curve of rGO. The

electrochemical behavior of GO and rGO was studied in the potential window of +1.0 V to -1.0 V in 0.1 M H₂SO₄ and the calibration curves were drawn from a linear region.

3.4.2 Testing GO as a supercapacitor material using Galvanostatic-charge discharge

The capacitive behavior of GO is given by the galvanostatic/charge discharge curve as shown in Figure 3.8. Galvanostatic charge/discharge is a standard technique used to test the performance and cycle life of capacitors and batteries (Xu *et al.*, 2011). At lower potentials, the voltage-time curves of GO depict an ideal linear shape with only a little deviation. Again at lower potentials, the deviations of the cyclic voltammetry and voltage-time curves are connected to Faradaic reactions which are due to the additional oxygen functional groups, especially epoxy and alkoxy, at the surface of the carbon (García-gómez *et al.*, 2016). Graphene oxide shows a large current density in CV curves as well as a longer charge-discharge time in V-t curves, which then implies a larger capacitance.

The mass of the thin film of GO was 5.2 g and the first cycle charge and discharge capacities obtained were 44.2 Ah g⁻¹. The voltage range was [0 to -0.9 V] vs. Ag/AgCl. Cycling was done at a current density of 50 A g⁻¹ in an aqueous solution of 1 M H₂SO₄. The specific charge/discharge current density was found to be 45.7 A g⁻¹. The specific capacitance C_{sp} can be calculated where, I , is the current density measured in (A), t , is the time measured in seconds and, V , is the voltage scanning rate in (mV/s).

$$C = \frac{It}{V} \quad (3)$$

Therefore specific capacitance, C_{sp} , can be calculated:

$$\begin{aligned} C_{sp} &= \frac{45.7 \times 3.6}{0.9} \\ &= 182.8 \text{ F g}^{-1} \end{aligned}$$

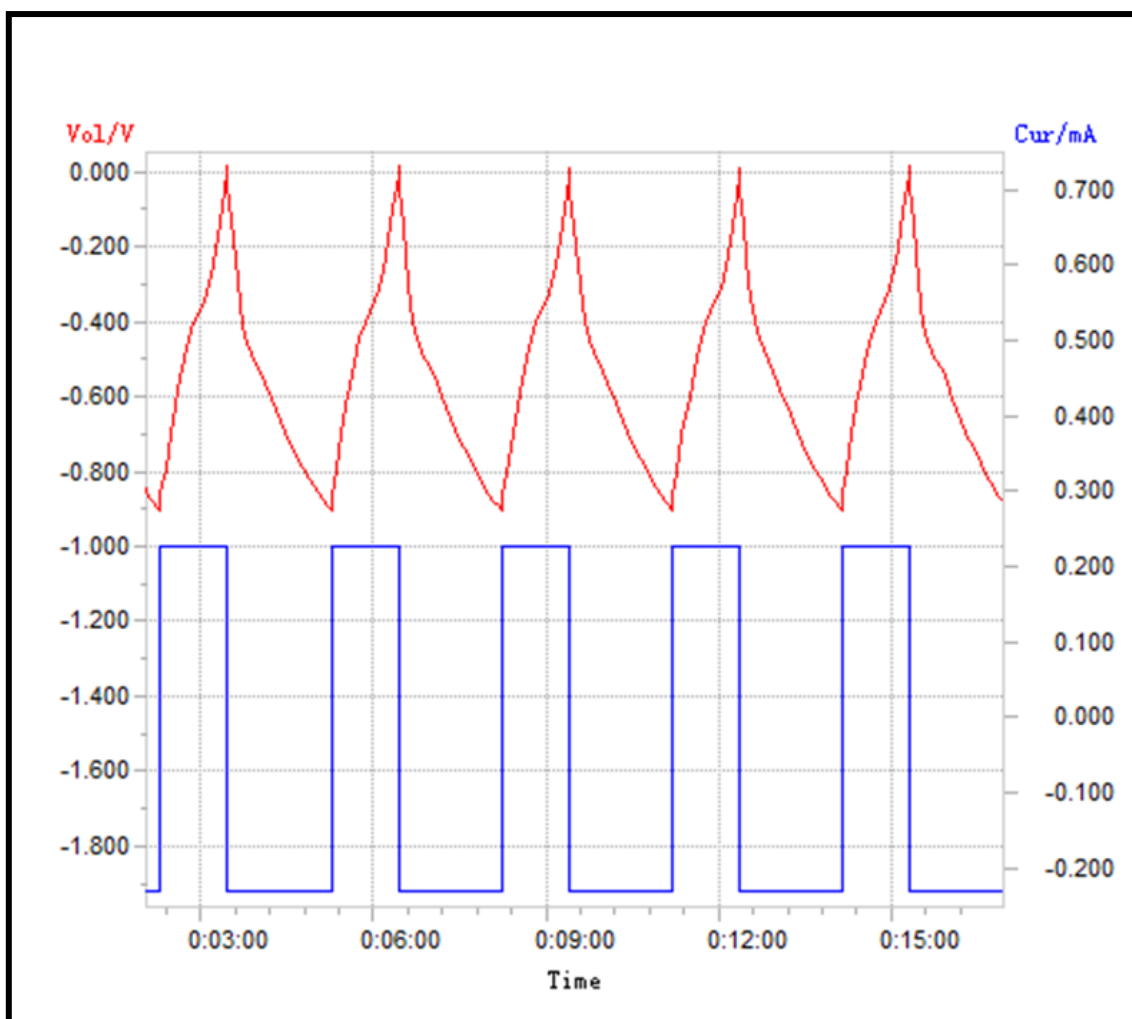


Figure 3. 8: Voltage/time cycling plot of GO voltage range (0 to -0.9 V v Ag/AgCl) at 50 A g⁻¹ in 1 M H₂SO₄ (aq). Specific charge/discharge current density = 45.7 A g⁻¹. Specific capacitance = (45.7 x 3.6)/0.9 = 182.8 F g⁻¹.

3.4.3 Testing rGO as a supercapacitor material using Galvanostatic-charge discharge

The capacitive behavior of rGO is given by the galvanostatic charge-discharge as shown in Figure 3.9. The voltage-time curves of rGO at lower potentials, shows ideal linear shape with only a small deviation. Due to the reduction of the oxygen functional groups, mostly the epoxy and alkoxy, at the surface of the carbon, the deviations of the CV and voltage-time

curves are not entirely connected to faradaic reactions (García-gómez *et al.*, 2016). The rGO shows a smaller current density in CV curves as well as shorter charge-discharge when compared to GO, which then implies a lower capacitance. The mass of the thin film of rGO was 5.2 g and the first cycle charge and discharge capacities obtained were 44.2 Ah g⁻¹. The voltage range was [0 to -0.9 V] vs. Ag/AgCl. Cycling was done at a current density of 50 A g⁻¹ in an aqueous solution of 1 M H₂SO₄. The specific charge/discharge current density was found to be 41.2 A g⁻¹. The specific capacitance, C_{sp} , is calculated according to equation (3) as follows:

$$C_{sp} = \frac{41.2 \times 3.6}{0.9}$$
$$= 164.8 \text{ F g}^{-1}$$



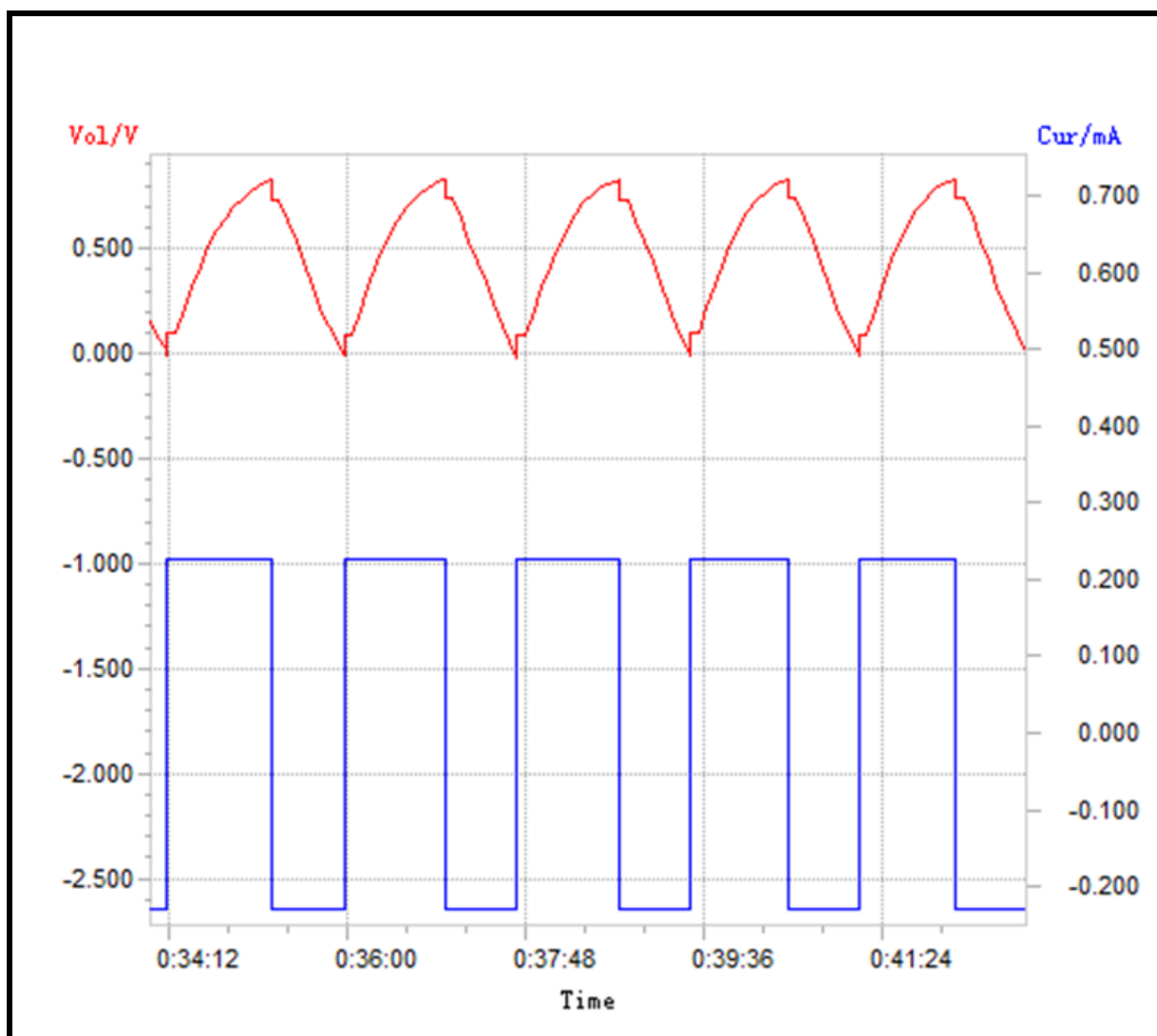


Figure 3. 10: Voltage/time cycling plot of rGO voltage range (0 to -0.9 V v Ag/AgCl) at 50 A g⁻¹ in 1 M H₂SO₄ (aq). Specific charge/discharge current density = 45.7 A g⁻¹. Specific capacitance = (45.7 x 3.6)/0.9 = 182.8 F g⁻¹.

3.5 Conclusions

In summary, GO and rGO have been compared to determine which is more ideal for supercapacitors. The good structural, morphological, crystal and electrochemical properties of GO make it a very good material in many applications. Also, the abundant oxygen

containing functional groups presenting at the surface of GO provide GO with additional pseudocapacitance therefore resulting in a higher capacitance, up to 182.8 F g^{-1} when compared to rGO of 164.8 F g^{-1} . Taking its higher capacitance, lower cost and shorter processing time into consideration, the results indicate that graphene oxide may be a better choice than reduced graphene oxide as an electrode material for supercapacitors.

References

- Alam, S. N., Sharma, N., & Kumar, L. (2017). Synthesis of graphene oxide (GO) by modified Hummers method and its thermal reduction to obtain reduced graphene oxide (rGO). *Graphene*, 06(01), 1–18.
- Anwer, T., Ansari, M. O., & Mohammad, F. (2013). Dodecylbenzenesulfonic acid micelles assisted in situ preparation and enhanced thermoelectric performance of semiconducting polyaniline-zirconium oxide nanocomposites. *Journal of Industrial and Engineering Chemistry*, 19(5), 1653–1658.
- Bhattacharya, S., Ghosh, P., & Basu, B. (2017). Graphene oxide (GO): An efficient carbocatalyst for the benign synthesis of functionalized 1,4-benzothiazines. *Tetrahedron Letters*, 58(10), 926–931.
- Bhunia, S. K., & Jana, N. R. (2014). Reduced graphene oxide-silver nanoparticle composite as visible light photocatalyst for degradation of colorless endocrine disruptors. *American Chemical Society Applied Materials and Interfaces*, 6(22), 20085–20092.
- Blanton, T. N., & Majumdar, D. (2012). X-ray diffraction characterization of polymer intercalated graphite oxide. *Powder Diffraction*, 27(2), 104–107.

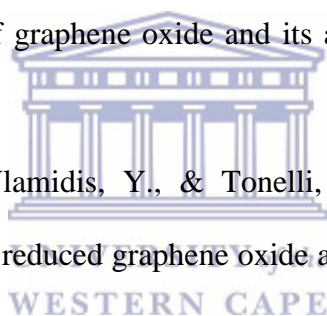
- Cells, S. (2013). Electrochemically Reduced Graphene Oxide Multilayer Films as Efficient Counter Electrode for Dye-Sensitized, *Scientific Reports*, 3, 1–7.
- Chen, L., Tang, Y., Wang, K., Liu, C., & Luo, S. (2011). Direct electrodeposition of reduced graphene oxide on glassy carbon electrode and its electrochemical application. *Electrochemistry Communications*, 13(2), 133–137.
- Childres, I., Jauregui, L., Park, W., Cao, H., & Chen, Y. (2013). Raman spectroscopy of graphene and related materials. *New Developments in Photon and Materials Research*, 1–20.
- Drewniak, S., Muzyka, R., Stolarczyk, A., Pustelny, T., Kotyczka-Morańska, M., & Setkiewicz, M. (2016). Studies of reduced graphene oxide and graphite oxide in the aspect of their possible application in gas sensors. *Sensors*, 16(1), 103.
- Dzukarnain, M. Z. B., Takami, T., Imai, H., & Ogino, T. (2016). Highly conductive , monolayer and large-area reduced graphene oxide fi lms fabricated by electrical connection at the two-dimensional boundaries between the tiled graphene oxide fl akes. *Thin Solid Films*, 615, 247–255.
- Eda, G., Fanchini, G., & Chhowalla, M. (2008). Large-area ultrathin films of reduced graphene oxide as a transparent and flexible electronic material. *Nature Nanotechnology*, 3(5), 270–274.
- Faust, B. (1997). Ultraviolet/visible spectroscopy. *Modern Chemical Techniques*, 3(1), 92–115.
- Ferrari, A. C. (2007). Raman spectroscopy of graphene and graphite: Disorder, electron-phonon coupling, doping and nonadiabatic effects. *Solid State Communications*, 143(1–2), 47–57.

- Fu, C., Zhao, G., Zhang, H., & Li, S. (2013). Evaluation and Characterization of Reduced Graphene Oxide Nanosheets as Anode Materials for Lithium-Ion Batteries. *International Journal of Electrochemical Sciences*, 8, 6269–6280.
- Gao, W. (2015). The chemistry of graphene oxide. *Graphene Oxide: Reduction Recipes, Spectroscopy, and Applications*, 61–95.
- García-gómez, A., Eugénio, S., Duarte, R. G., Silva, T. M., Carmezim, M. J., & Montemor, M. F. (2016). Applied surface science electrodeposited reduced-graphene oxide / cobalt oxide electrodes for charge storage applications. *Applied Surface Science*, 382, 34–40.
- Georgakilas, V., Otyepka, M., Bourlinos, A. B., Chandra, V., Kim, N., Kemp, K. C., & Kim, K. S. (2012). Functionalization of graphene: Covalent and non-covalent approaches, derivatives and applications. *Chemical Reviews*, 112(11), 6156–6214.
- Gilje, S., Kaner, R. B., Wallace, G. G., Li, D. A. N., Mu, M. B., Muller, M. B., & Wallace, G. G. (2008). Processable aqueous dispersions of graphene nanosheets. *Nature Nanotechnology*, 3(2), 101–105.
- Guo, Q., Yi, C., Zhu, L., Yang, Q., & Xie, Y. (2005). Chemical synthesis of cross-linked polyaniline by a novel solvothermal metathesis reaction of p-dichlorobenzene with sodium amide. *Polymer*, 46(9), 3185–3189.
- Hashemi, M., Omidi, M., Muralidharan, B., Tayebi, L., Herpin, M. J., Mohagheghi, M. A., ... Milner, T. E. (2018). Layer-by-layer assembly of graphene oxide on thermosensitive liposomes for photo-chemotherapy. *Acta Biomaterialia*, 65, 376–392.
- Jariwala, D., Srivastava, A., & Ajayan, P. M. (2011). Graphene Synthesis and Band Gap Opening. *Journal of Nanoscience and Nanotechnology*, 11(8), 6621–6641.
- Karthika, P. (2012). Functionalized Exfoliated Graphene Oxide as Supercapacitor Electrodes. *Soft Nanoscience Letters*, 02, 59–66.

- Khamaj, J. A. (2017). Effect of heat treatment in electrical transport characteristics of graphene-oxide transistor. *Applied Materials Today*, 6, 62–65.
- Khan, Q. A., Shaur, A., Khan, T. A., Joya, Y. F., & Awan, M. S. (2017). Characterization of reduced graphene oxide produced through a modified Hoffman method. *Cogent Chemistry*, 3(1).
- Kim, Y., Jang, H., & Kang, K. (2017). Facile and controllable fabrication of multifunctional nanohybrid films composed of reduced graphene oxide and titanium dioxide through layer-by-layer assembly. *Thin Solid Films*, 636, 359–366.
- Konios, D., Stylianakis, M. M., Stratakis, E., & Kymakis, E. (2014). Dispersion behaviour of graphene oxide and reduced graphene oxide. *Journal of Colloid and Interface Science*, 430, 108–112.
- Kumar, N. A., Choi, H.-J., Shin, Y.-R., Chang, D. W., Dai, L., & Baek, J.-B. (2012). Polyaniline-Grafted Reduced Graphene Oxide for Efficient Electrochemical. *American Chemical Society Nano*, 25(2), 1715–1723.
- Lai, Q., Zhu, S., Luo, X., Zou, M., Huang, S., Lai, Q., & Huang, S. (2012a). Ultraviolet-visible spectroscopy of graphene oxides, *AIP Advances*, 2(032146), 3–8.
- Lai, Q., Zhu, S., Luo, X., Zou, M., Huang, S., Lai, Q., & Huang, S. (2012b). Ultraviolet-visible spectroscopy of graphene oxides, *AIP Advances*, 2(032146), 3–8.
- Li, X., Cai, W., Jung, I., An, J., Yang, D., Velamakanni, A., & Duoff, R. S. (2009). Synthesis, Characterization, and Properties of Large-Area Graphene Films. *Electrochemical Chemical Society Transactions*, 19(5), 41–52.
- Li, Y., Li, H., Du, A., Wang, M., & Zeng, J. (2017). Morphology and isothermal crystallization of graphene oxide reinforced biodegradable poly (butylene succinate), *Polymer Testing*, 59, 1–9.

- Mane, A. T., Navale, S. T., Mane, R. S., Naushad, M., & Patil, V. B. (2015). Synthesis and structural, morphological, compositional, optical and electrical properties of DBSA-doped PPy-WO₃ nanocomposites. *Progress in Organic Coatings*, 87, 88–94.
- Marcano, D. C., Kosynkin, D. V., Berlin, J. M., Sinitskii, A., Sun, Z., Slesarev, A., & Tour, J. M. (2010). Improved Synthesis of Graphene Oxide, *American Chemical Society*, 4(8), 4806-4814.
- Møller, M., Johnsen, R. E., & Norby, P. (2016). Journal of Solid State Chemistry In situ X-ray powder diffraction studies of the synthesis of graphene oxide and formation of reduced graphene oxide. *Journal of Solid State Chemistry*, 240, 49–54.
- Mu, S. J., Su, Y. C., Xiao, L. H., Liu, S. D., Hu, T., & Tang, H. B. (2013). X-ray diffraction pattern of graphite oxide. *Chinese Physics Letters*, 30(9), 10–13.
- Njomo, N., Waryo, T., Masikini, M., Ikpo, C. O., Mailu, S., Tovide, O., & Iwuoha, E. I. (2014). Graphenated tantalum(IV) oxide and poly(4-styrene sulphonic acid)-doped polyaniline nanocomposite as cathode material in an electrochemical capacitor. *Electrochimica Acta*, 128, 226–237.
- Park, S., An, J., Potts, J. R., Velamakanni, A., Murali, S., & Ruoff, R. S. (2011). Hydrazine-reduction of graphite- and graphene oxide. *Carbon*, 49(9), 3019–3023.
- Pei, S., & Cheng, H. (2011). The reduction of graphene oxide. *Carbon*, 50(9), 1–19.
- Prud, R. K., Aksay, I., & Car, R. (2008). Raman Spectra of Graphite Oxide and Functionalized Graphene Sheets. *Nano Letters*, 8(1), 1–6.
- Sarkar, C., & Dolui, S. K. (2015). Synthesis of copper oxide/reduced graphene oxide nanocomposite and its enhanced catalytic activity towards reduction of 4-nitrophenol. *The Royal Society of Chemistry Advances*, 5(75), 60763–60769.

- Sarlak, N., & Meyer, T. J. (2017). Fabrication of completely water soluble graphene oxides graft poly citric acid using different oxidation methods and comparison of them. *Journal of Molecular Liquids*, 243, 654–663.
- Shahriary, L., & Athawale, A. a. (2014). Graphene oxide synthesized by using Modified Hummers approach. *International Journal of Renewable Energy and Environmental Engineering*, 02(01), 58–63.
- Shalaby, A., Nihtianova, D., Markov, P., Staneva, A. D., Iordanova, R. S., & Dimitriev, Y. B. (2015). Structural analysis of reduced graphene oxide by transmission electron microscopy. *Bulgarian Chemical Communications*, 47(1), 291–295.
- Shao, Y., Wang, J., Engelhard, M., Wang, C., & Lin, Y. (2010). Facile and controllable electrochemical reduction of graphene oxide and its applications. *Journal of Materials Chemistry*, 20, 743.
- Sharma, V. V., Gualandi, I., Vlamidis, Y., & Tonelli, D. (2017). Electrochimica Acta Electrochemical behavior of reduced graphene oxide and multi-walled carbon nanotubes composites for catechol and dopamine oxidation. *Electrochimica Acta*, 246, 415–423.
- Song, J., Wang, X., Chang, C.-T., Song, J., Wang, X., & Chang, C.-T. (2014). Preparation and Characterization of Graphene Oxide. *Journal of Nanomaterials*, 2014, 1–6.
- Stankovich, S., Dikin, D. A., Piner, R. D., Kohlhaas, K. A., Kleinhammes, A., Jia, Y., & Ruoff, R. S. (2007). Synthesis of graphene-based nanosheets via chemical reduction of exfoliated graphite oxide. *Carbon*, 45(7), 1558–1565.
- Stylianakis, M. M., Spyropoulos, G. D., Kymakis, E., & Stratakis, E. (2012). Solution-processable graphene linked to 3, 5-dinitrobenzoyl as an electron acceptor in organic bulk heterojunction photovoltaic devices. *Carbon*, 50(15), 5554–5561.



- Udayabhaskar, R., Mangalaraja, R. V, Pandiyarajan, T., Karthikeyan, B., & Contreras, D. (2017). Spectroscopic investigation on graphene-copper nanocomposites with strong UV emission and high catalytic activity, *Carbon*, 124, 256–262.
- Wahab, H. S., Ali, S. H., & Hussein, A. M. A. (2015). Synthesis and Characterization of Graphene by Raman Spectroscopy, *Journal of Materials Sciences and Applications*, 1(3), 130–135.
- Wan, L., Du, C., & Yang, S. (2017). Synthesis of graphene oxide / polybenzoxazine-based nitrogen-containing porous carbon nanocomposite for enhanced supercapacitor properties. *Electrochimica Acta*, 251, 12-24.
- Wilson, N. R., Wilson, N. R., Pandey, P. A., Pandey, P. A., Beanland, R., Beanland, R., & Sloan, J. (2009). Graphene oxide: structural analysis and application as a highly transparent support for electron microscopy. *American Chemical Society Nano*, 3(9), 2547–2556.
- Wong, C. P. P., Lai, C. W., Lee, K. M., & Abd Hamid, S. B. (2015). Advanced chemical reduction of reduced graphene oxide and its photocatalytic activity in degrading reactive black 5. *Materials*, 8(10), 7118–7128.
- Wu, T.-T. (2013). Preparation and characteristics of graphene oxide and its thin films. *Surface and Coatings Technology*, 231, 487–491.
- Xu, B., Yue, S., Sui, Z., Zhang, X., Hou, S., Cao, G., & Yang, Y. (2011). What is the choice for supercapacitors: graphene or graphene oxide? *Energy & Environmental Science*, 4(8), 2826.
- Zaaba, N. I., Foo, K. L., Hashim, U., Tan, S. J., Liu, W. W., & Voon, C. H. (2017). Synthesis of graphene oxide using modified Hummers Method: Solvent influence. *Procedia Engineering*, 184, 469–477.

Zhu, Y., Murali, S., Cai, W., Li, X., Suk, J. W., Potts, J. R., & Ruoff, R. S. (2010). Graphene and graphene oxide: Synthesis, properties, and applications. *Advanced Materials*, 22(35), 3906–3924.

Zoladek, S., Rutkowska, I. A., Blicharska, M., Miecznikowski, K., Ozimek, W., Orłowska, J., & Kulesza, P. J. (2017). Electrochimica Acta Evaluation of reduced-graphene-oxide-supported gold nanoparticles as catalytic system for electroreduction of oxygen in alkaline electrolyte. *Electrochimica Acta*, 233, 113–122.



Chapter 4

Platinum, Silver and Copper Nanoparticles-Doped Graphene Oxide Based Supercapacitors

Summary

Graphene oxide, GO, as a carbon based material is viewed as a single layer of graphite containing many oxygen functional groups such as epoxide, carbonyl, carboxyl and hydroxyl groups. Numerous modern procedures used for the synthesis of GO are founded on the method first reported by Hummers in which graphite is oxidized by a solution of potassium permanganate in sulphuric acid over a certain period of time. Metal nanoparticles have been used in many applications and fields due to their unique properties. Recently, carbon black, carbon nanotubes, graphene have been widely used in combination of support with these nanoparticles and used as electrodes. The chapter discusses the different experimental methods for graphene oxide intercalated or decorated with platinum, silver and copper nanoparticles and their properties are determined by different characterization techniques. Their electrochemical properties are also determined.

Abstract

A simple one step method was developed to load small sized platinum Pt, silver Ag and copper Cu nanoparticles (NPs) in large quantities on graphene oxide (GO) by the electrostatic self-assembly. The method includes the functionalization of GO by a cationic polyelectrolyte acting as a surfactant cetyl trimethylammonium bromide (CTAB) and an anionic poly (sodium 4-styrenesulfonate) (PSS) polyelectrolyte. Furthermore, ethylene glycol plays an important role as the reducing agent and stabilizer for the Pt, Ag, Cu nanoparticles without damaging the graphite structures of GO. The materials were characterized with high resolution scanning electron microscopy (HRSEM) which revealed very rough surfaces with small nanoparticles being observed to spread out on the surface of GO. High resolution transmission electron microscopy (HRTEM) showed uniformly dispersed small-sized nanoparticles of platinum, silver and copper on surface of GO with mean particle sizes of 2.3 ± 0.2 nm and 2.6 ± 0.3 nm and 3.5 ± 0.5 nm respectively. These small NPs suggest a strong interaction between the GO and metal atoms, because there was no aggregation of the NPs upon heat treatment. Fourier transform infrared spectroscopy (FTIR) revealed a decrease in vibrational band intensity of the functional groups of epoxide and carbonyl which indicates the incomplete reduction of GO. Raman spectroscopy showed a shift of the D and G-band to lower frequencies. The D and G bands exhibited a shift toward lower frequencies (D: from 1348 cm^{-1} for GO, 1346 cm^{-1} for GO/Pt NPs, G: from 1601 cm^{-1} for GO, 1599 cm^{-1} for GO/Pt NPs). X-ray fluorescence (XRF) confirmed the loading of the nanoparticles on the surface of GO with the metals appearing in abundance. X-ray diffraction (XRD) revealed three diffraction bands indexed to the (111), (200) and (220) diffraction planes of metallic Pt, Ag and Cu.

4.1 Introduction

Graphene oxide's properties include large surface areas, unique thermal and chemical stabilities, excellent mechanical strength, superior electrical conductivities etc. (Abdolmaleki *et al.*, 2017). The properties have made GO a potential component in many fields such as solar cells, storage devices, energy conversion, sensors etc. (Cruz-silva *et al.*, 2016). Over the years, the synthesis of GO has been studied and GO can be synthesized using different techniques such as Brodie, Staudenmaier, or Hummers method, or some variation of these methods. All three methods involve oxidation of graphite to various levels, but recently a modified Hummers method has been used for the synthesis of GO (Alam *et al.*, 2017; Gao, 2015; Shahriary & Athawale, 2014). Due to the exceptional properties and unique performance of metal nanoparticles, they have attracted attention over the years (Grinou *et al.*, 2012). Recently GO has been anchored with metal nanoparticles which could potentially exhibit novel catalytic, magnetic and optoelectronic properties (Lightcap *et al.*, 2010). Well-dispersed small sized nanoparticles are expected to enhance activity and selectivity for catalytic reactions (Ha *et al.*, 2011). GO has been successfully used as a material that hosts other materials to prepare hybrids of reduced GO and metal nanoparticles. This is attributed to the easy exfoliation and excellent intercalation properties of GO (Lin *et al.*, 2015). This work reports a simple process for preparing well-dispersed nanoparticles of Pt, Ag and Cu with small particle size in large quantities loaded on the surface of graphene oxide (GO).

4.2 Experimental

4.2.1 Chemicals and sample preparation

All chemicals used in the experiments were of analytical grade and were used as purchased without further purification. Graphite (1-2 micron), sodium nitrate NaNO_3 ($\geq 99\%$), sulphuric

acid H_2SO_4 ($\geq 98\%$), potassium permanganate KMnO_4 ($\geq 99\%$), hydrogen peroxide ($\geq 30\%$), hydrochloric acid HCl ($\geq 37\%$), hexachloroplatinic acid $\text{H}_2\text{PtCl}_6 \cdot 6\text{H}_2\text{O}$ ACS reagent ($\geq 37.50\%$) Pt basis, silver nitrate AgNO_3 ACS reagent ($\geq 99.0\%$), sodium hydroxide NaOH BioXtra ($\geq 98\%$) acidimetric, pellets (anhydrous), cetyl trimethylammonium bromide CTAB (98%), poly (sodium 4-styrenesulfonate) PSS (70 000) powder, sodium acetate NaAc ($\geq 99\%$) FCC FG, poly-ethylene glycol (PEG) (400 powder), ethylene glycol anhydrous (99.8%), acetone ($\geq 99.9\%$) were all purchased from Sigma Aldrich.

4.2.2 Instrumentation

Ultraviolet–visible (UV–Vis) absorption measurements for the prepared GO and rGO were obtained using 1 cm quartz cuvette on a Nicolet Evolution 100 UV-Visible spectrophotometer (Thermo Electron, UK) over a wavelength range of 200 to 800 nm. Fourier transform infrared (FTIR) spectra were recorded on a Perkin Elmer FTIR model 100 spectrophotometer, operating between 400 and 4000 cm^{-1} in order to characterize the presence of specific features of GO and rGO. The high-resolution scanning electron micrographs (HRSEM) of the produced materials were imaged using a Zeiss Auriga SEM operating at 50kV and high resolution-transmission electron microscope (HR-TEM) equipped with an energy-dispersed spectroscopy (EDS) detector was used to study the size, morphology and composition of samples. Copper grid (Cu) was used as sample holder for the immobilization of (2 μL) solution of the hybrids of GO and rGO with metal nanoparticles and the micrographs were recorded at room temperature. X-ray Diffraction using Diffractometer D8 Advance manufactured by Bruker AXS in Germany was done to determine the crystal

structure identification of the samples. Raman spectroscopy was taken with a Renishaw inVia Raman Microscope made in Germany and a Class 1 Laser product was used.

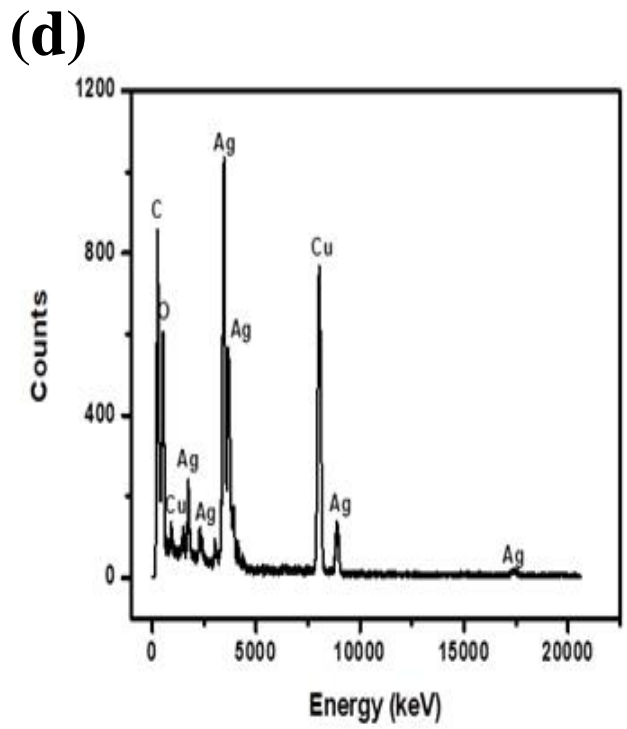
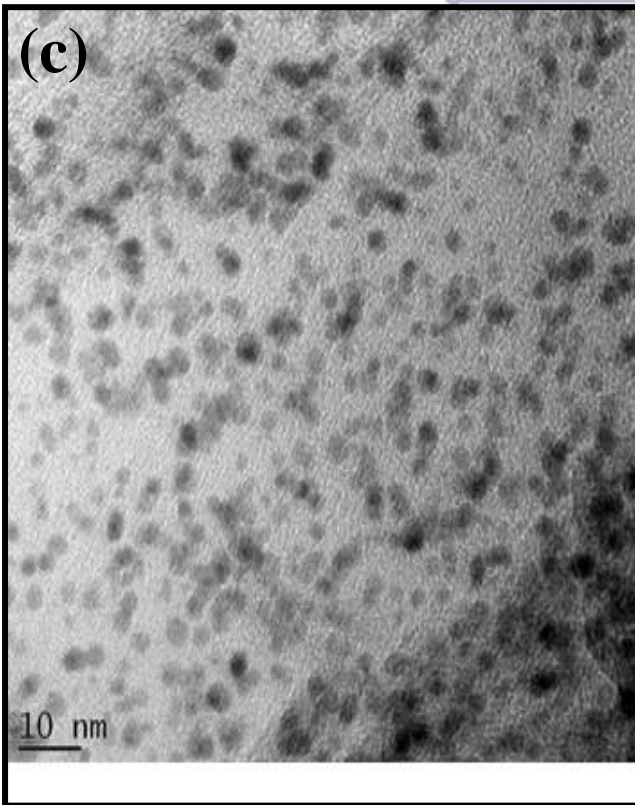
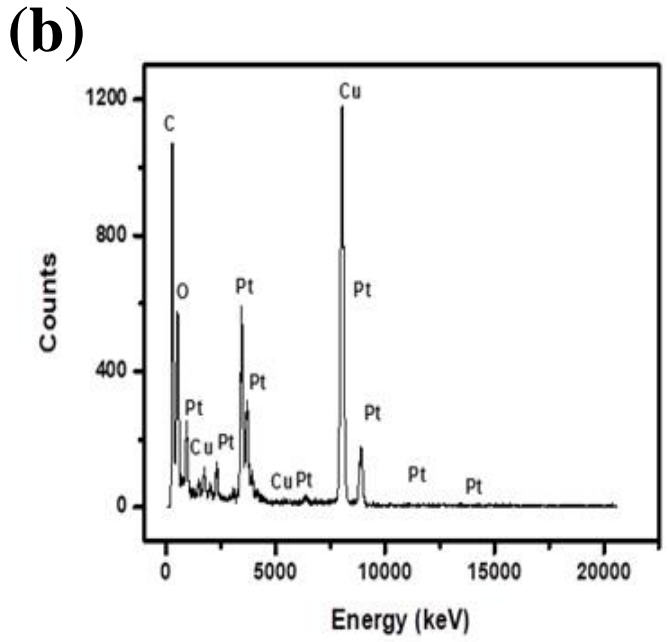
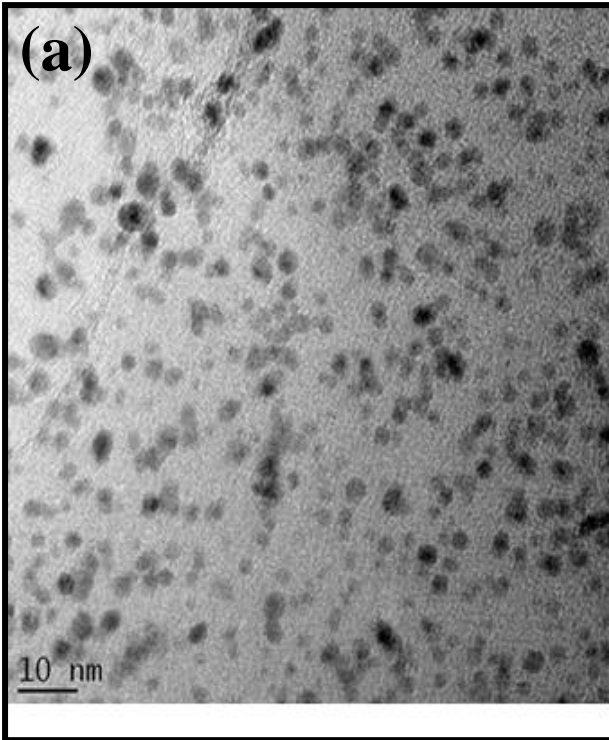
4.2.3 Synthesis of graphene oxide loaded with Pt, Ag and Cu NPs

GO was synthesized according to the steps mentioned in Chapter 3, Section 3.2.3. The loading of platinum, silver and copper NPs onto GO nanosheets was carried out by electrostatic self-assembly. Initially, GO was functionalized by cetyl trimethylammonium bromide (CTAB) a cationic polyelectrolyte which acts as a surfactant and poly (sodium 4-styrenesulfonate) (PSS) an anionic polyelectrolyte. 30 mg of GO was homogeneously dispersed in 40 mL of an aqueous solution of 1% wt. CTAB using ultra-sonication for 30 min followed by centrifugation to remove the remaining excess CTAB. The functionalized GO was then dispersed in 40 mL of an aqueous solution of 1% wt. PSS by stirring and ultra-sonication for 30 min and the mixture was stored overnight. After 12 hours, the excess PSS was removed by centrifugation and the prepared material was subjected to ultrasonic agitation in 40 mL of ethylene glycol (EG) for 30 min. Consequently, 0.2 g of hexachloroplatinic acid ($\text{H}_2\text{PtCl}_6 \cdot 6\text{H}_2\text{O}$) for platinum nanoparticles, silver nitrate (AgNO_3) for silver nanoparticles, copper acetate $\text{Cu}(\text{CH}_3\text{COO})_2$ for copper nanoparticles, respectively, were dissolved in the 40 mL dispersion of EG/functionalized GO and the mixture was sonicated for 30 min to form a stable suspension. At this point 3.6 g of sodium acetate (NaAc) and 1.0 g of poly-ethylene glycol (PEG) were added under continuous stirring for a further 30 min. The suspension was then sealed in a Teflon autoclave of stainless steel (capacity 200 mL) and heated at 200 °C for 12 hours followed by natural cooling to room temperature. A black precipitate was obtained by filtration, washed by de-ionized water and acetone and dried in a vacuum oven at 60° C for 12 hours.

4.3 Results and Discussion

4.3.1 Particle size analysis of GO/Pt NPs, GO/Ag NPs and GO/Cu NPs

Figure 4.1 (a), (c) and (e) shows HR-TEM images of GO/Pt NPs, GO/Ag NPs and GO/Cu NPs, respectively. The Pt NPs and Ag NPs that are loaded on the surface of GO are small and dispersed uniformly with mean particle sizes of 2.3 ± 0.2 nm and 2.6 ± 0.3 nm for Pt and Ag NPs, respectively. These small NPs suggest a strong interaction between the GO and platinum and silver atoms, because there was no aggregation of the NPs upon heat treatment (Xin *et al.*, 2016). However, the Cu NPs loaded on the surface of GO were large and not uniformly dispersed, with mean particle size of 3.5 ± 0.5 nm. This is due to the aggregation of the Cu NPs upon heat treatment and the weak interaction between the GO and copper atoms (Li *et al.*, 2010). Figure 4.1 (b), (d), (f) show the EDS spectra of GO/Pt NPs, GO/Ag NPs and GO/Cu NPs, respectively. This confirms the presence of the metal nanoparticles loaded on the surface of GO (Fakhri *et al.*, 2014; Khan *et al.*, 2016; Xie *et al.*, 2017). However, the presence of copper is attributed to the copper grid used upon sample preparation for the GO/Pt NPs, GO/Ag NPs, therefore, in the case of GO/Cu NPs; a nickel grid was used so as to observe the presence of Cu NPs.



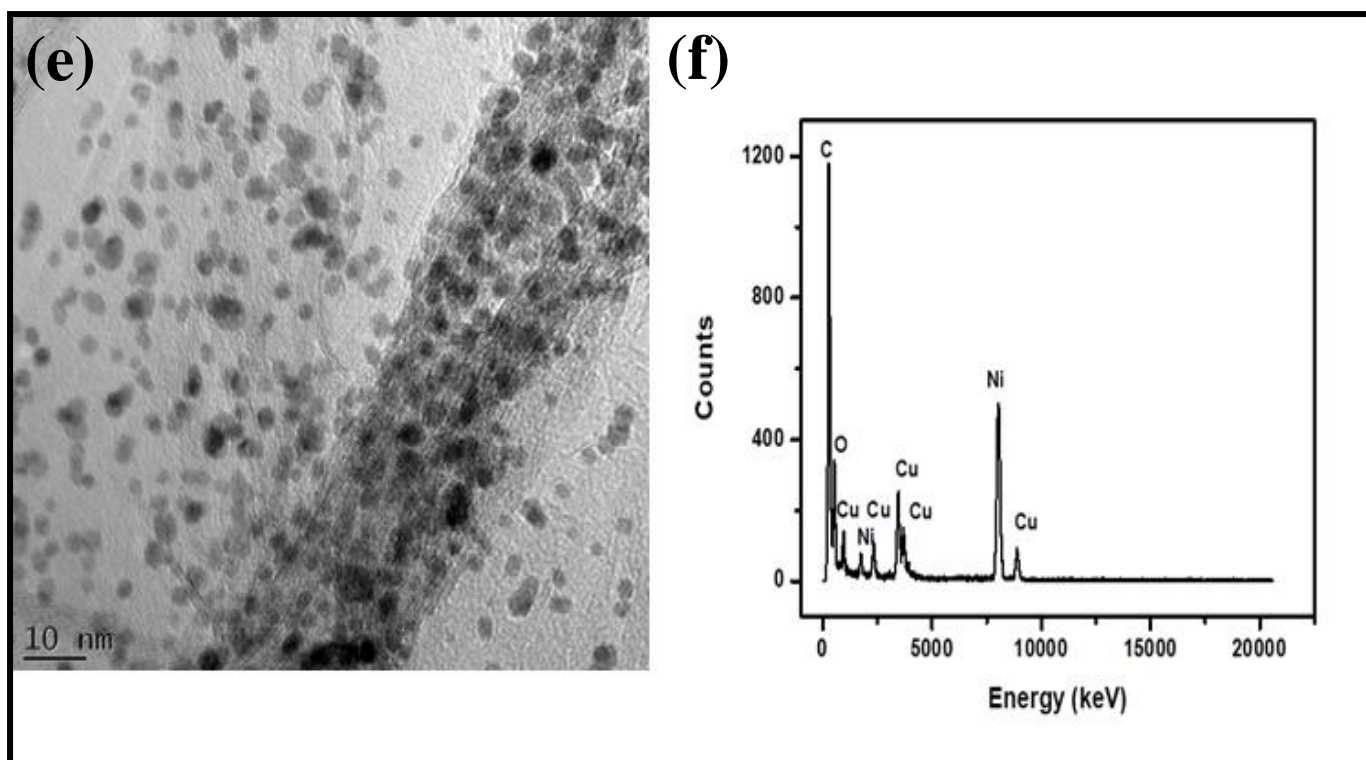
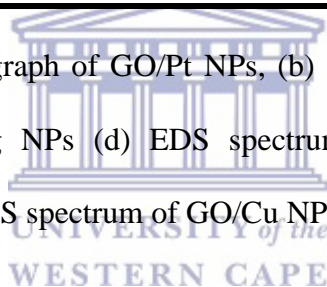


Figure 4. 1: (a) HRTEM micrograph of GO/Pt NPs, (b) EDS spectrum of GO/Pt NPs, (c) HRTEM micrograph of GO/Ag NPs (d) EDS spectrum of GO/Ag NPs, (e) HRTEM micrograph of GO/Cu NPs (f) EDS spectrum of GO/Cu NPs.



4.3.2 Morphological properties of GO/Pt NPs, GO/Ag NPs and GO/Cu NPs

Figure 4.2 (a)-(c) show the SEM images of GO/Pt NPs, GO/Ag NPs and GO/Cu NPs, respectively. When the nanoparticles were loaded on the surface of GO, the surface of GO altered from smooth to rough with small particles observed on the surface. A uniform dispersion of the nanoparticles was observed and when magnified, the nanoparticles appeared to have been spread out on the surface of GO. This confirms that GO was loaded with the different nanoparticles of Pt, Ag and Cu (Dong *et al.*, 2010; Li *et al.*, 2017; Mallakpour *et al.*, 2017).

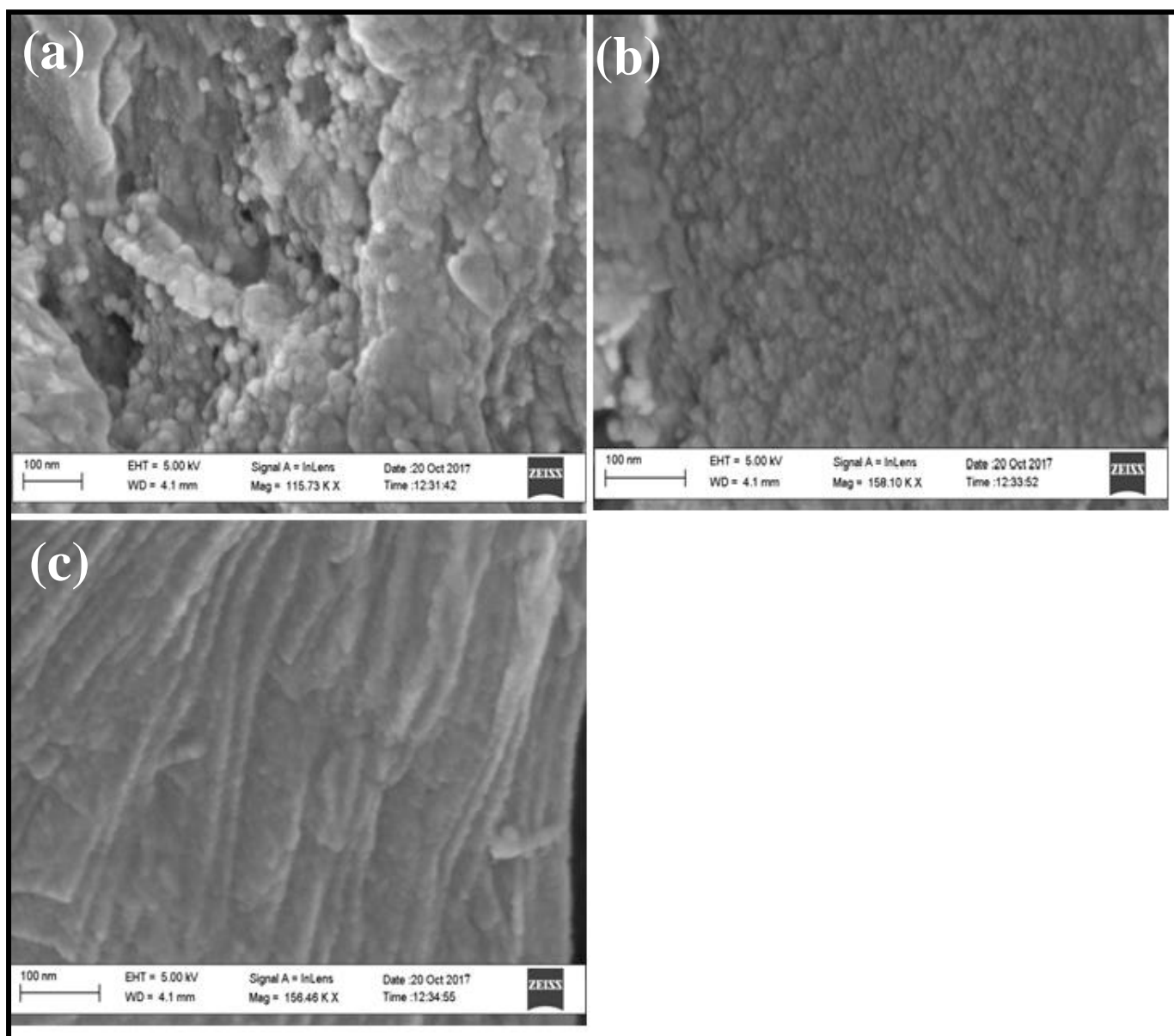
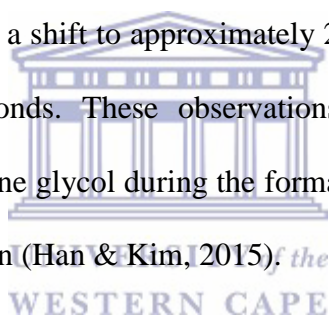


Figure 4. 2: HRSEM micrographs of (a) GO/Pt NPs, (b) GO/Ag NPs, (c) GO/Cu NPs.

4.3.3 *Optical properties of GO/Ag NPs*

Figure 4.3 (a) shows the UV-Vis spectrum of silver nanoparticles synthesized by the polyol method using a solution of silver nitrate AgNO_3 and PVP. The UV-Vis spectrum revealed a broad surface plasmon resonance (SPR) band spanning between 315 and 406 nm, consisting of a sharp band centered on 315 nm and a shoulder peak appearing at 430 nm. In general,

anisotropic silver NPs are indicated by presence of two or more SPR bands (Bhui *et al.*, 2009), therefore, the presence of a broad band consisting of two bands can be attributed to the formation of a thin layer of silver oxide (Ag_2O) formed on the surface of silver NPs by its surface oxidation (Shahverdi *et al.*, 2007). The sharp band around 315 nm is indicative of Ag NPs without Ag_2O layers, and the absorption band at 406 nm suggested the existence of Ag/ Ag_2O core-shell structures (Budhiraja *et al.*, 2013b). Hence it was observed that the prepared colloids were the mixture of Ag NPs with and without Ag_2O layers (Ahmad *et al.*, 2003; Pal *et al.*, 2009). The attachment of Ag NPs to the GO surface shown in Figure 4.3 (b) was confirmed primarily through the detection of a band at 406 nm, which was attributed to the plasmon resonance of Ag NPs. Furthermore, the GO-Ag NPs UV-Vis spectrum showed that the shoulder disappeared and a shift to approximately 263 nm attributed to the electronic transitions of C=C aromatic bonds. These observations suggest that GO sheets were simultaneously reduced by ethylene glycol during the formation of the Ag NPs, resulting in a partial restoration of π -conjugation (Han & Kim, 2015).



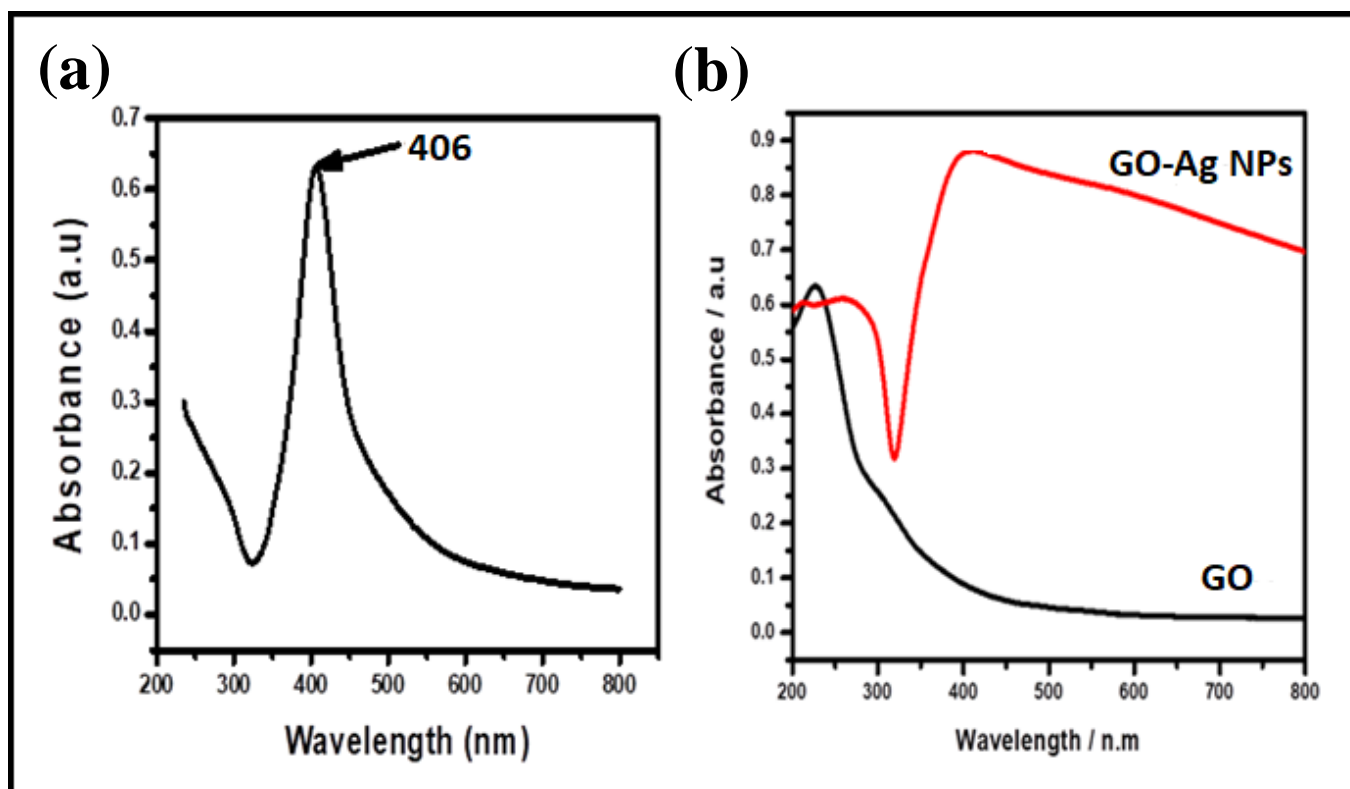
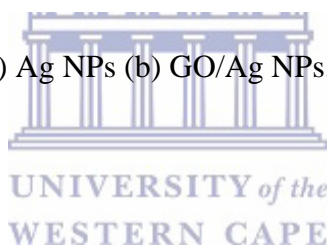


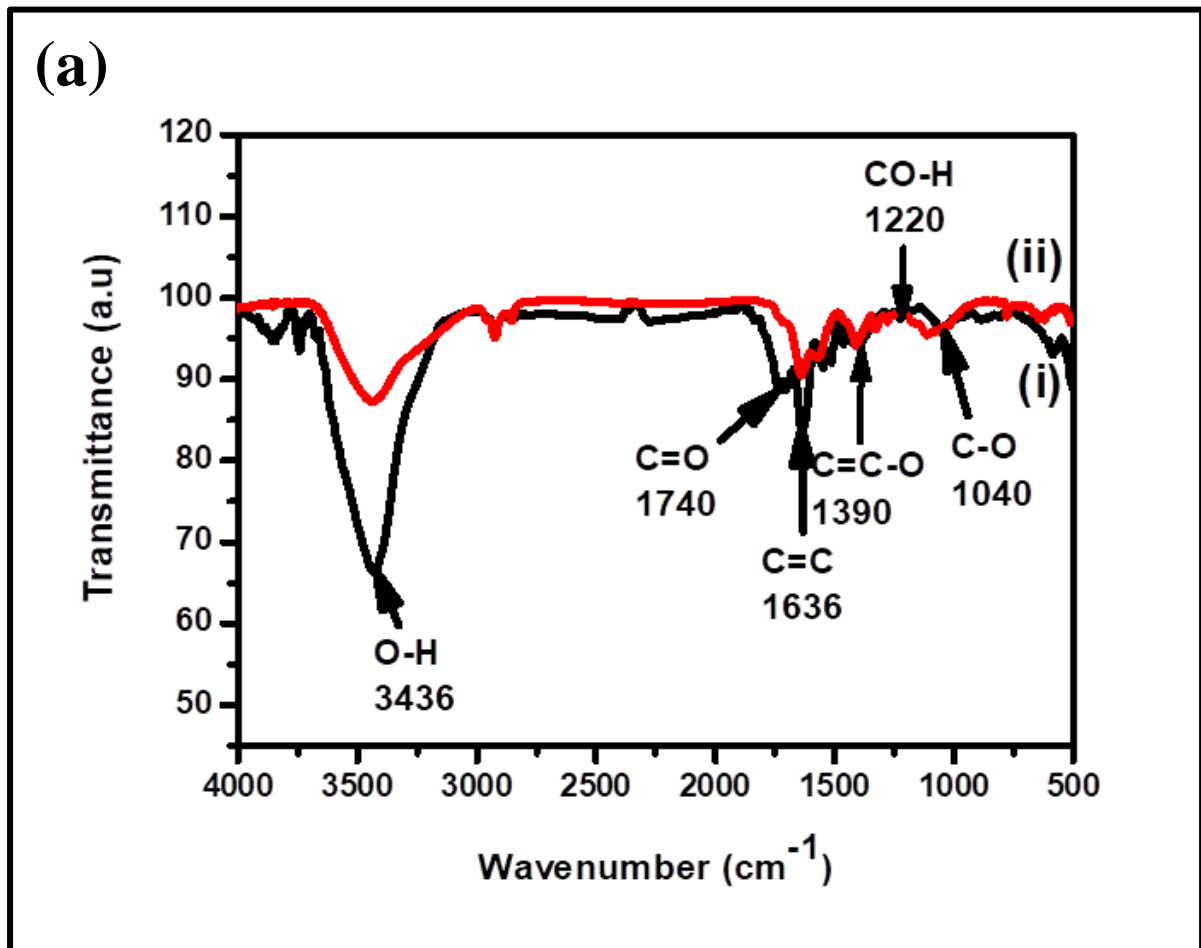
Figure 4. 3: UV-Vis spectra of (a) Ag NPs (b) GO/Ag NPs.



4.3.4 Structural properties of GO/Pt NPs, GO/Ag NPs and GO/Cu NPs

Figure 4.4 (a)-(c) show the FTIR spectra of GO/Pt NPs, GO/Ag NPs and GO/Cu NPs, respectively compared with the GO spectrum (black color) in all spectra. GO contains functional groups mainly O-H at 3436 cm^{-1} attributed to the carboxylic acid functionality, C=O at 1740 cm^{-1} , C=C at 1636 cm^{-1} , C-O-H at 1390 cm^{-1} , CO-H at 1220 cm^{-1} attributed to the functionality of graphene sheets and C-O at 1040 cm^{-1} was related to the vibration of epoxide functionality (Nasehnia *et al.*, 2016). The appearance of all these vibrational bands indicates the presence of rich oxygen containing functionalities in graphene oxide (Wang *et al.*, 2017). When the ethylene glycol was introduced in the synthesis process it reduced all metal precursors and GO simultaneously to generate Pt, Ag and Cu metallic NPs on rGO. A

closer inspection of the FTIR scans of all the three GO/Pt NPs, GO/Ag NPs and GO/Cu NPs revealed a decrease in the band intensities of the functional groups of epoxide and carbonyl which indicates the incomplete reduction of GO(Singh *et al.*, 2013; Zoladek *et al.*, 2017).



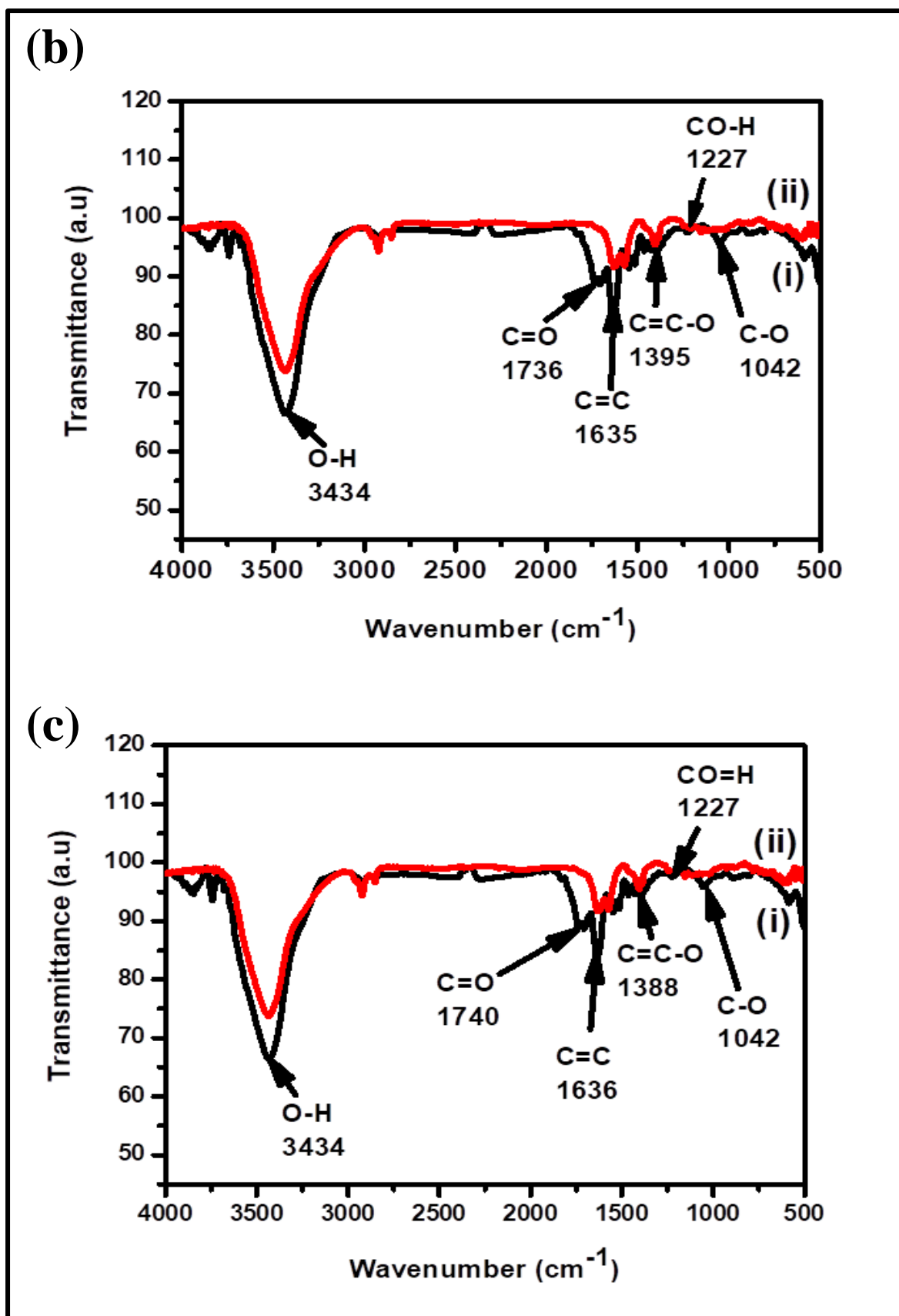
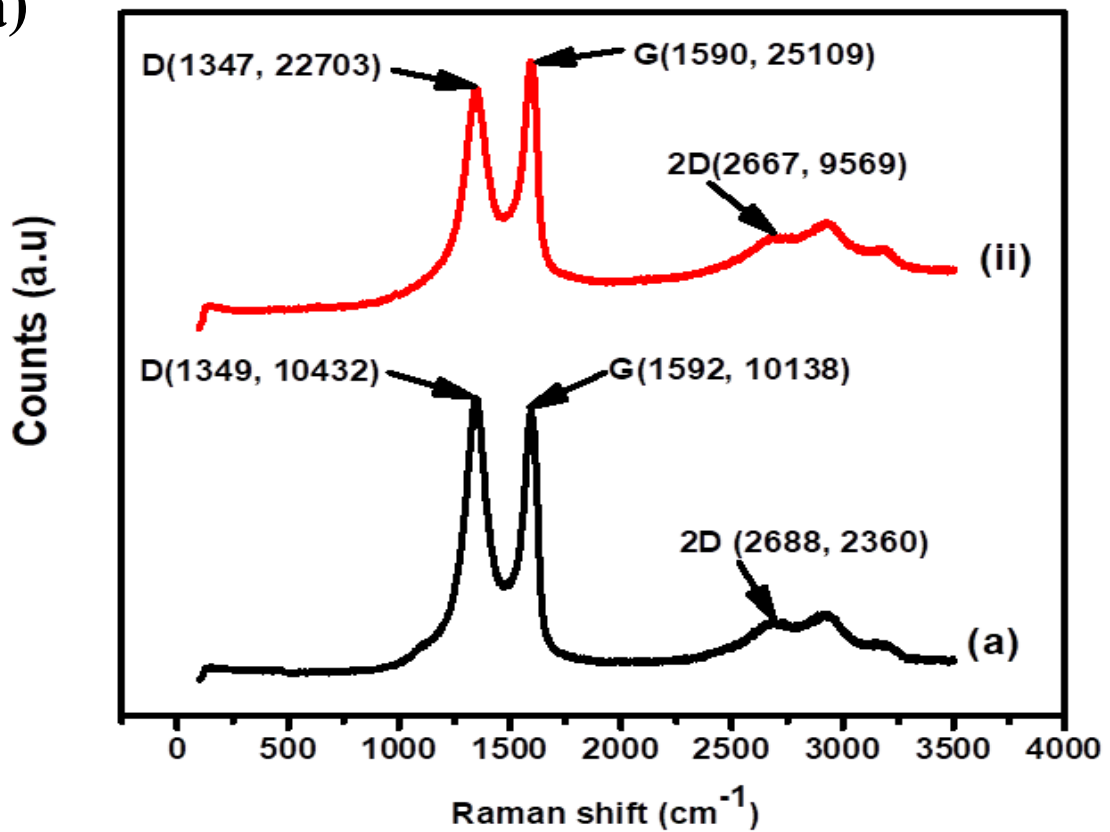


Figure 4. 4: FTIR spectra of (a) GO/Pt NPs (b) GO/Ag NPs (c) GO/Cu NPs. For comparison reasons, the FTIR spectra of GO is presented as (i) in all three spectra.

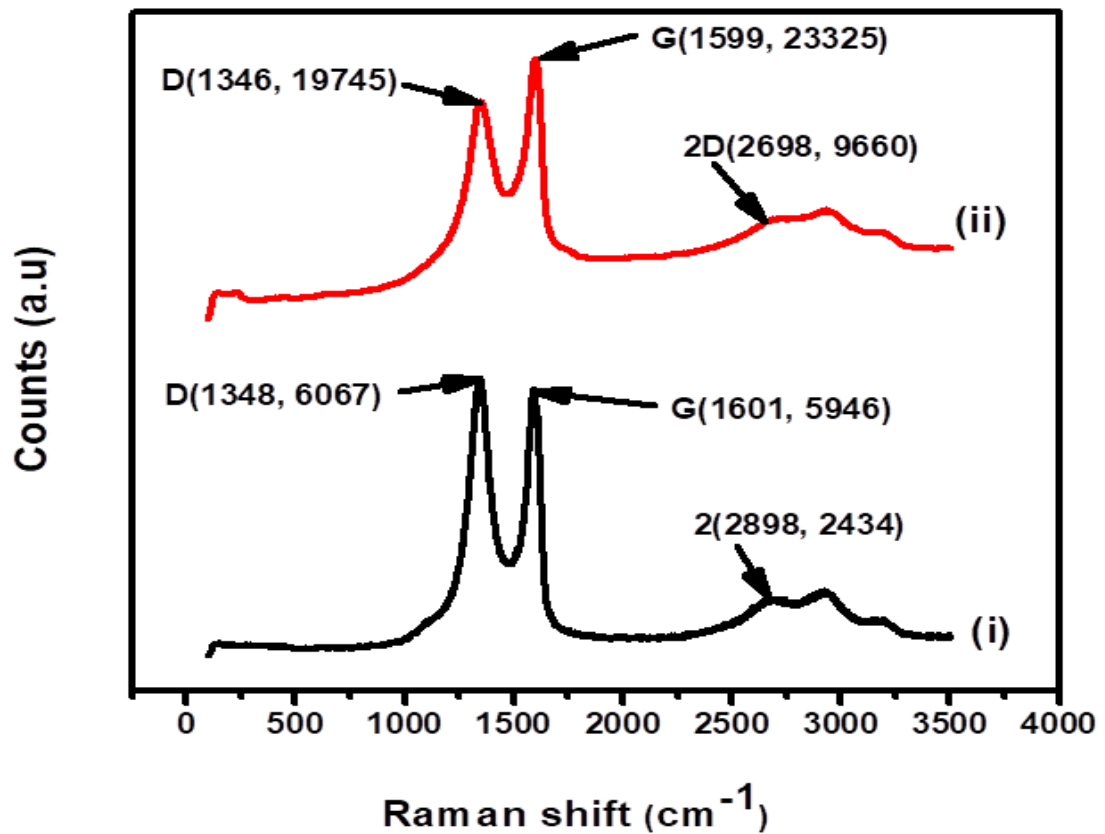
4.3.5 Internal Structural properties of GO/Pt NPs, GO/Ag NPs, GO/Cu NPs

Fig 4.5 shows the Raman spectra of (a) GO/Pt NPs (b) GO/Ag NPs (c) GO/Cu NPs, respectively. The two protruding peaks of D band which is due to the doubly degenerate E_{2g} mode at the Brillouin zone center and G band which arises from the defect mediated zone-edge phonons, near K-point are observed in all samples (Herrera *et al.*, 2013; Fu *et al.*, 2012). GO labeled (i) shows a D band ($\sim 1346\text{ cm}^{-1}$) a second-order overtone of a different in-plane vibration and corresponds to defects within the sp^2 network, a G band ($\sim 1595\text{ cm}^{-1}$) and a primary in-plane vibrational mode 2D band ($\sim 2689\text{ cm}^{-1}$) for all the Raman spectra's (Chen *et al.*, 2013; Zhang, 2012; Zhang *et al.*, 2015). D and 2D band positions are dispersive (dependent on the laser excitation energy). However, the GO loaded with nanoparticles displays a decrease in intensity ratio of D/G (0.85) in nanoparticle compared to that of GO (0.95) due to the increase in intensity of the G band. This indicates a decrease in average size of sp^2 domain upon the reduction of GO. Meanwhile, the D and G bands exhibit a shift toward lower frequencies from GO to GO/Pt NPs, GO/Ag NPs and GO/Cu NPs nanocomposites (D: from 1348 cm^{-1} for GO, 1346 cm^{-1} for GO/Pt NPs, G: from 1601 cm^{-1} for GO, 1599 cm^{-1} for GO/Pt NPs) (Song & Chen, 2014; Zhang, 2012; Zhao *et al.*, 2012). The same behavior can be observed on the Raman spectra for silver and copper nanoparticles where the D and G bands are shifted to lower frequencies. This is an indication of the interaction between Pt, Ag and Cu nanoparticles and GO sheets (Chen *et al.*, 2010; Tang *et al.*, 2013; Zhang *et al.*, 2015; Zhao *et al.*, 2012).

(a)



(b)



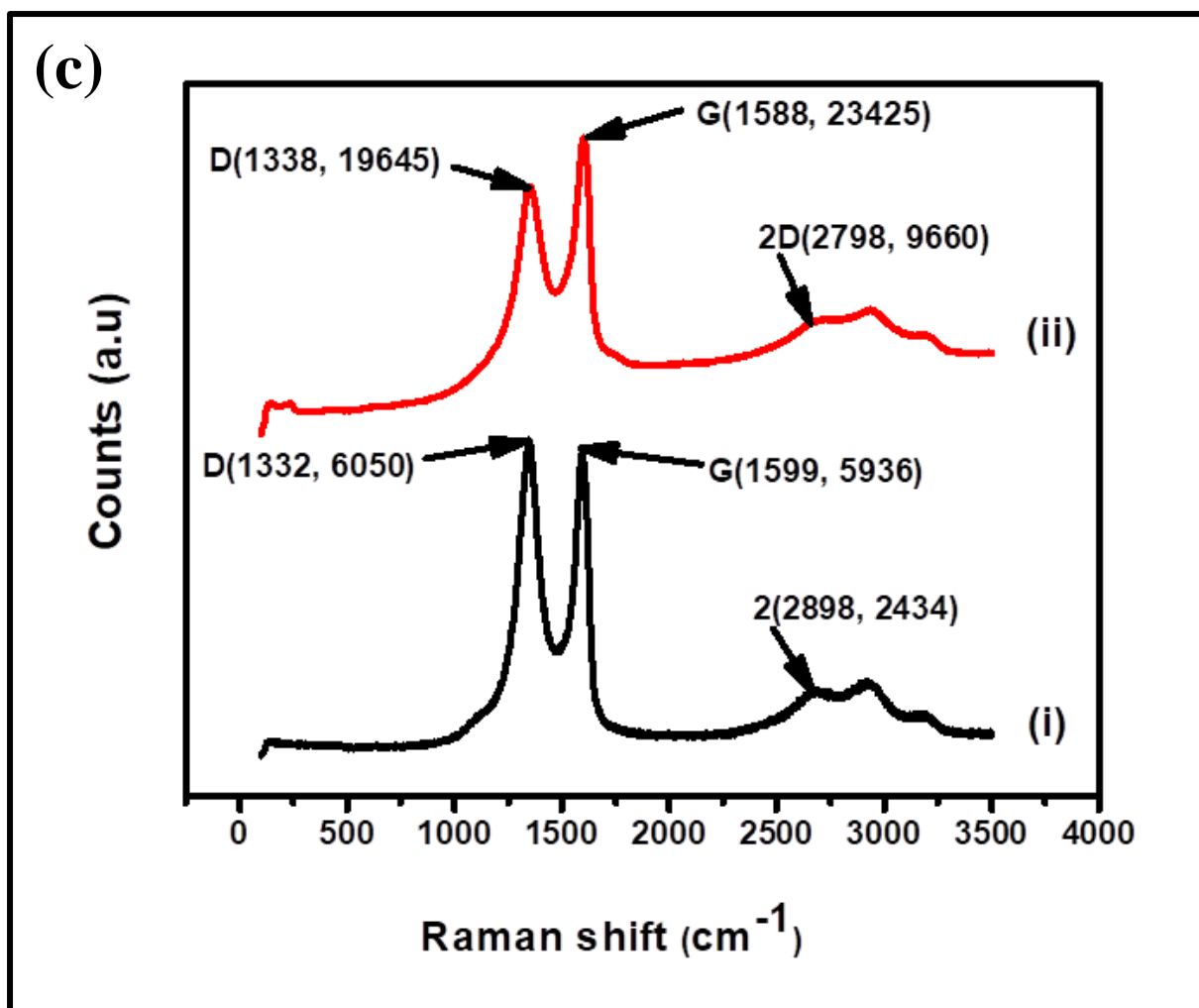
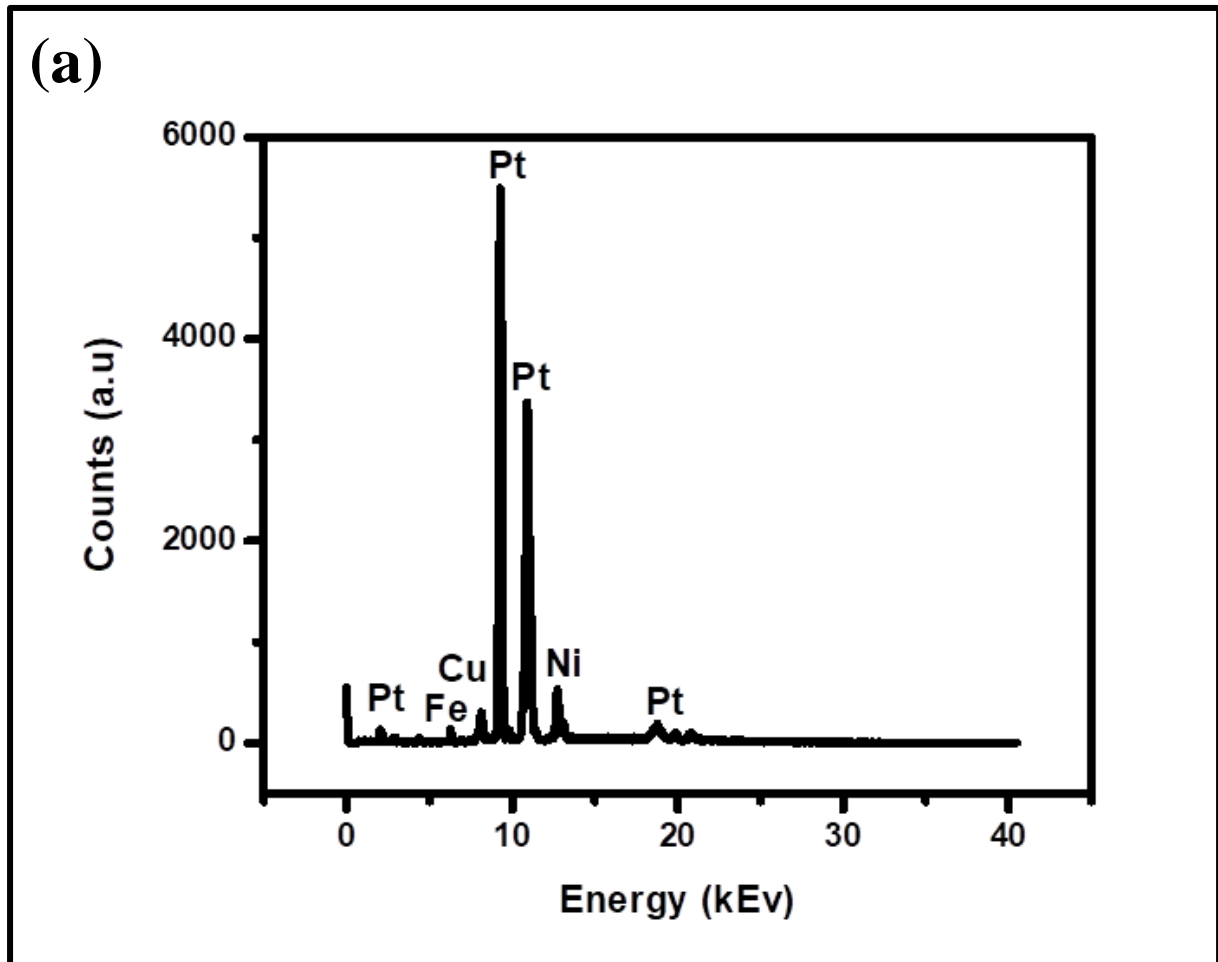


Figure 4. 5: Raman spectra of (a) GO/Pt NPs (b) GO/Ag NPs (c) GO/Cu NPs. For comparison reasons, the Raman spectra of GO is presented as (i) in all three spectras.

4.3.6 Elemental composition studies of GO/Pt NPs, GO/Ag NPs and GO/Cu NPs

X-Ray Fluorescence (XFR) is an analytical technique that is used to determine the elemental composition within a material (Advisor, Francisco, & Food, 2015). Figure 4.6 (a)-(c) show the XRF spectra of GO/Pt NPs, GO/Ag NPs and GO/Cu NPs, respectively. It shows that Pt, Ag and Cu are present in the samples that were prepared. The GO has been successfully supported or loaded with the platinum, silver and copper nanoparticles. The other elements

that are present in the samples such as Fe, Ni, Br, Zn etc. are due to impurities in the materials.



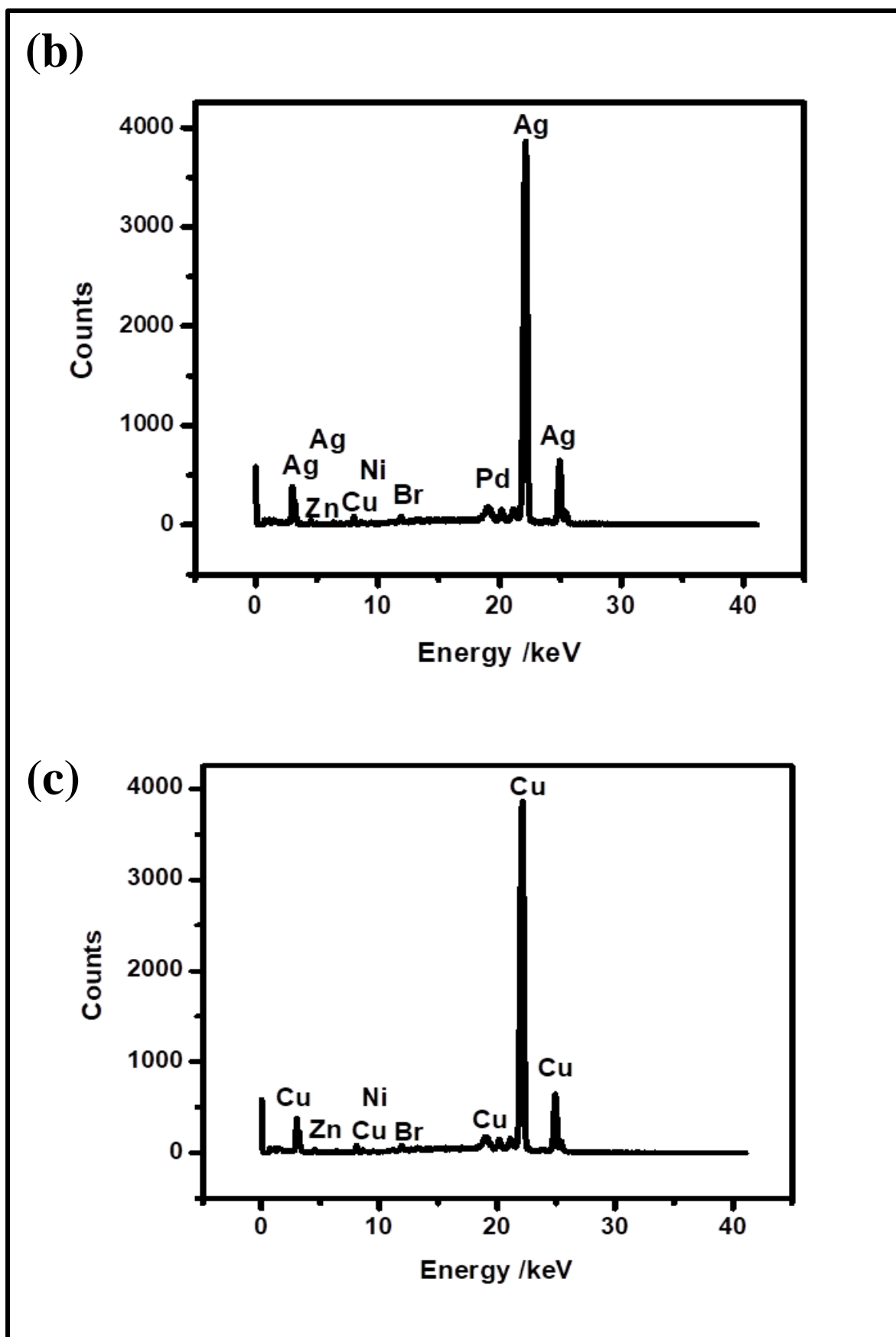
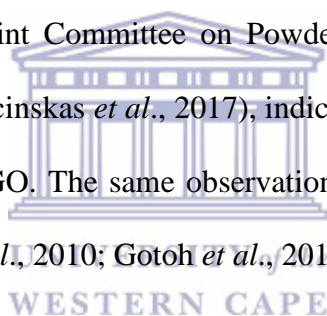
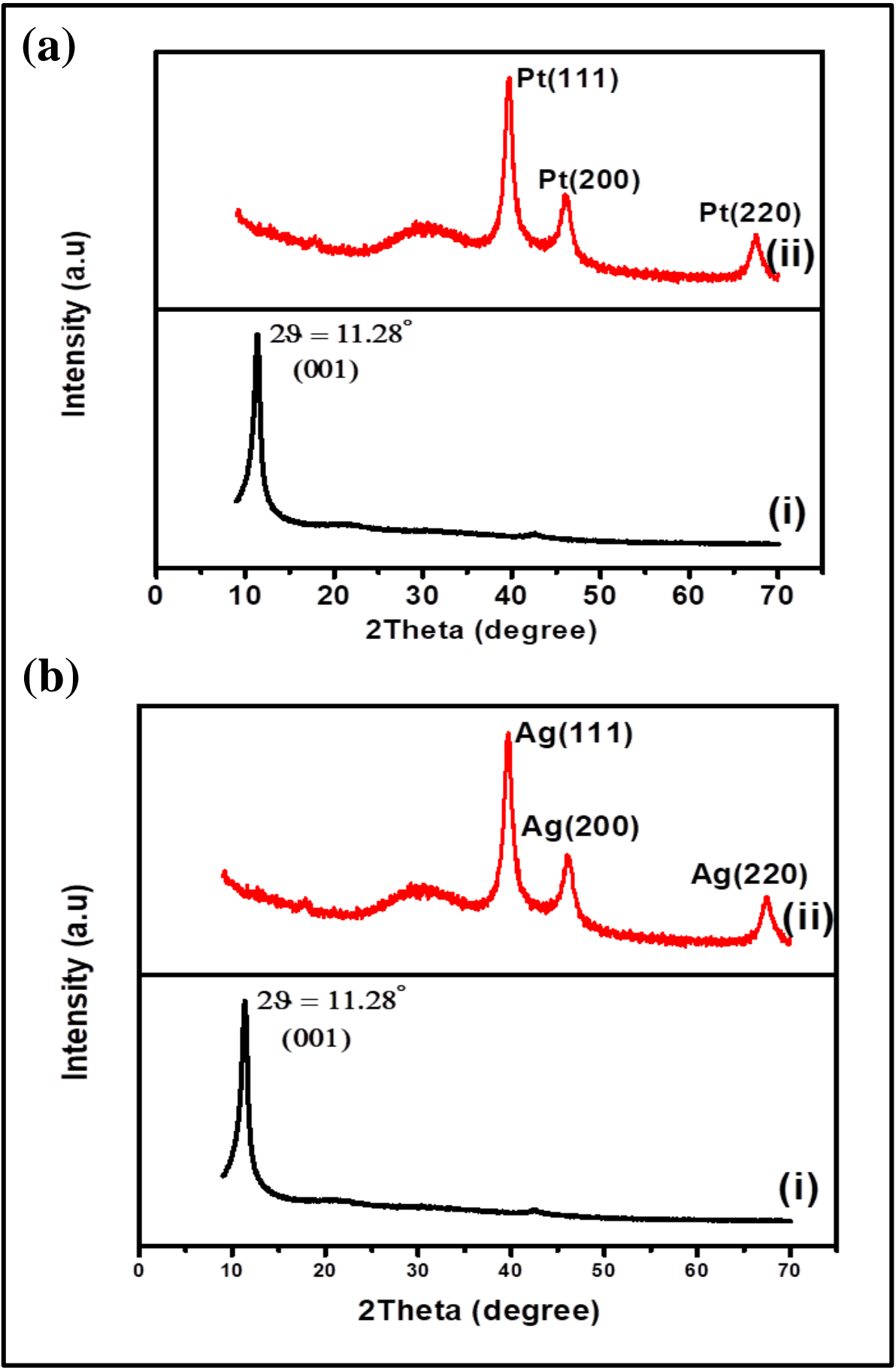


Figure 4. 6: XRF spectra of (a) GO/Pt NPs (b) GO/Ag NPs (c) GO/Cu NPs.

4.3.7 Crystallographic properties of GO/Pt NPs, GO/Ag NPs and GO/Cu NPs

Figure 4.7 (a) – (c) show the XRD patterns of GO (i) compared with the XRD patterns of GO/Pt NPs, GO/Ag NPs and GO/Cu NPs, respectively. GO reveals a very sharp diffraction band (001) appearing at $2\theta = 11.28^\circ$ (Fakhri *et al.*, 2014; Ye *et al.*, 2014). This band indicates that AB stacking exists in GO with larger interlayer spacing and this value depends on the method of preparation and on the number of layers of water in the gallery space of the material. When GO was loaded with the nanoparticles, three diffraction bands appeared with Pt NPs, Ag NPs and Cu NPs at 39.5° , 46.0° and 67° indexed to the (111), (200) and (220) diffraction planes of metallic Pt, Ag and Cu, respectively. These diffraction bands fall in line with the angles found in the Joint Committee on Powder Diffraction Standards (JCPDS) (Blanton & Majumdar, 2013; Vilcinskas *et al.*, 2017), indicating strongly the formation of the nanoparticles on the surface of GO. The same observations were observed for all the XRD patterns of the spectra (Dubal *et al.*, 2010; Gotoh *et al.*, 2010; Xu *et al.*, 2015).





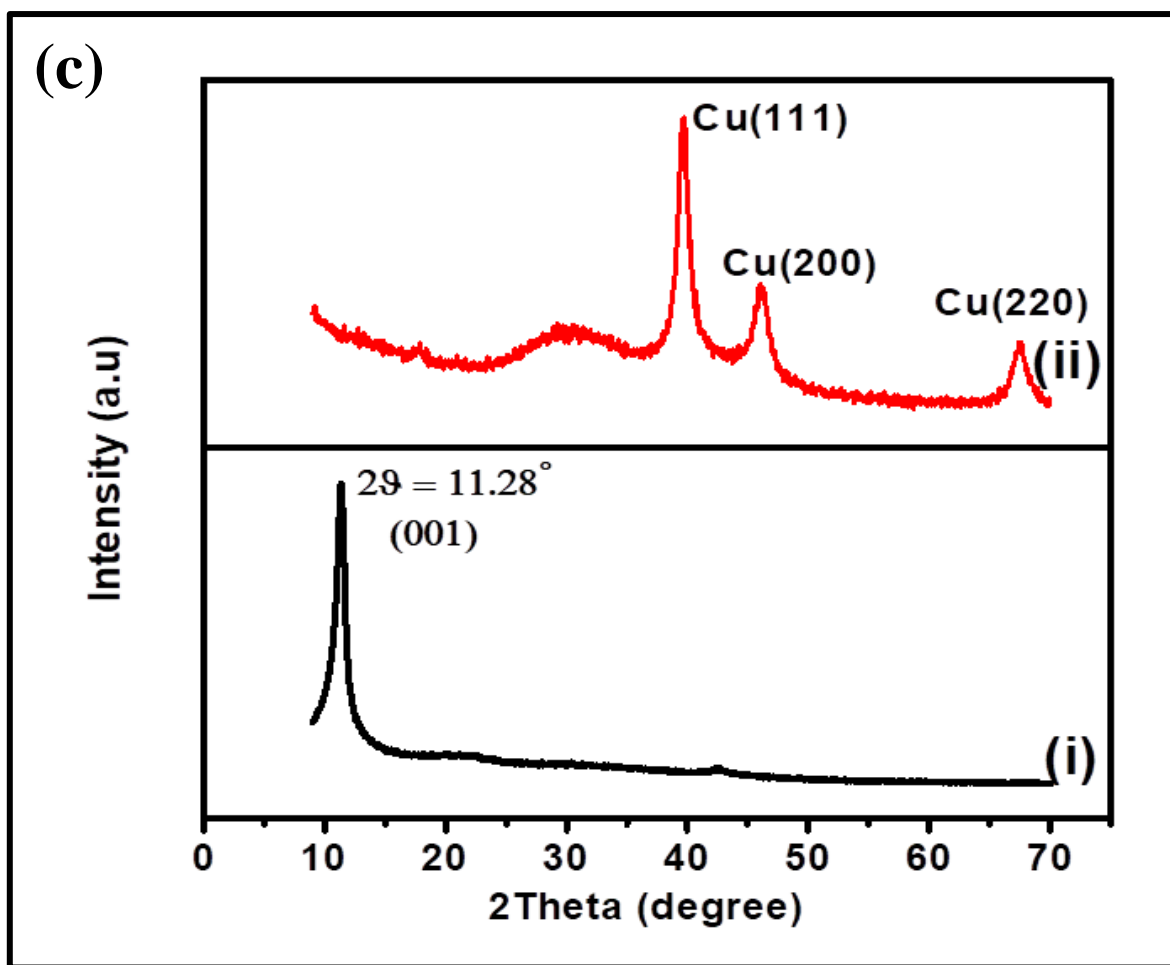


Figure 4. 7: XRD patterns of (a) GO/Pt NPs, (b) GO/Ag NPs and (c) GO/Cu NPs. For comparison reasons, the XRD pattern of GO is presented.

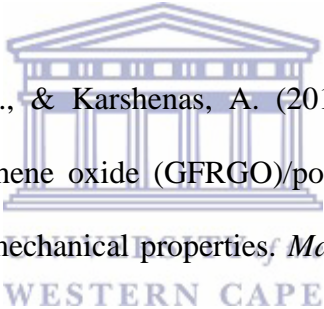
4.4 Conclusions

GO was synthesized by the modified Hummers method. It was then loaded with Pt, Ag and Cu NPs by the electrostatic self-assembly method. HRTEM images of GO/Pt NPs and GO/Ag NPs show that Pt NPs and Ag NPs were successfully loaded on the surface of GO. The NPs were small and were uniformly dispersed with mean particle sizes of 2.3 ± 0.2 nm and 2.6 ± 0.3 nm, respectively. However, Cu NPs were loaded on the surface of GO but were large and were uniformly dispersed with mean particle size of 5.5 ± 0.5 nm. The EDS spectra

confirmed the presence of the metal nanoparticles Pt, Ag and Cu loaded on the surface of GO. HRSEM images of GO loaded with nanoparticles showed rough surfaces with small particles observed on the surface of GO and when magnified a uniform distribution of the NPs was observed. This confirms the presence of the nanoparticles on the GO and metal nanoparticle. The UV-Vis spectra of silver nanoparticles shows a broad surface plasmon resonance (SPR) band bridging between 385 and 406 nm, a sharp band centered at 315 nm and a shoulder band at 430 nm. The attachment of silver nanoparticles on the GO surface was confirmed when a band at 406 nm was detected which is then attributed to the plasmon resonance of Ag NPs. GO contains functional groups mainly O-H at 3434 cm^{-1} attributed to the carboxylic acid functionality, C=O at 1736 cm^{-1} , C=C at 1635 cm^{-1} , C=O-H at 1392 cm^{-1} , CO-H at 1227 cm^{-1} attributed to the functionality of graphene sheets and C-O at 1040 cm^{-1} was attributed to the vibration of epoxide functionality as shown by FTIR graphs. However, on close inspection of the FTIR scans of all the three GO/Pt NPs, GO/Ag NPs and GO/Cu NPs the functional group's intensity of the bands were decreased indicating the incomplete reduction of GO. GO/Pt, GO/Ag, and GO/Cu NPs observed in the Raman spectroscopy exhibit an increased D/G intensity ratio (1.16) of nanoparticles compared to GO (0.95) which indicates a decrease in average size of sp^2 domain during the reduction of GO. The D and G bands exhibit a shift toward lower frequencies from GO to GO/Pt NPs, GO/Ag NPs and GO/Cu NPs (D: from 1348 cm^{-1} for GO, 1336 cm^{-1} for GO/Pt NPs, G: from 1605 cm^{-1} for GO, 1586 cm^{-1} for GO/Pt NPs). This is an indication that the GO/Pt, GO/Ag and GO/Cu NPs nanocomposite displays an interaction between the Pt, Ag and Cu nanoparticles and GO sheets, demonstrating that the GO sheets are hybridized with nanoparticles successfully. The XRF spectra of GO/Pt NPs, GO/Ag NPs and GO/Cu NPs show that Pt, Ag and Cu were present in the samples that were prepared. The GO has been successfully supported or loaded with the platinum, silver and copper nanoparticles. XRD patterns of GO compared with

GO/Pt NPs, GO/Ag NPs and GO/Cu NPs. GO reveals a very sharp diffraction band (001) appearing at $2\theta = 11.28^\circ$. When GO was supported with the Pt, Ag and Cu NPs, three diffraction bands appeared at 39.5° corresponding to (111), 46.0° corresponding to (200) and 67° corresponding to (220) diffraction planes of metallic Pt, Ag and Cu, respectively. We can then conclude that the simple one step method which was developed to load small sized Pt, Ag and copper Cu nanoparticles in large quantities on graphene oxide was a success as can be observed from the results.

References

- 
- Abdolmaleki, A., Mallakpour, S., & Karshenas, A. (2017). Facile synthesis of glucose-functionalized reduced graphene oxide (GFRGO)/poly(vinyl alcohol) nanocomposites for improving thermal and mechanical properties. *Materials Science & Engineering B*, 217, 26–35.
- Advisor, S., Francisco, S., & Food, U. S. (n.d.). Introduction to Energy Dispersive X-Ray Fluorescence (XRF) - An analytical chemistry perspective. *Journal of Chemistry Education*, 88(7), 868-872
- Ahmad, A., Mukherjee, P., Senapati, S., Mandal, D., Khan, M. I., Kumar, R., & Sastry, M. (2003). Extracellular biosynthesis of silver nanoparticles using the fungus *Fusarium oxysporum*. *Colloids and Surfaces B: Biointerfaces*, 28(4), 313–318.
- Alam, S. N., Sharma, N., & Kumar, L. (2017). Synthesis of graphene oxide (GO) by modified Hummers method and its thermal reduction to obtain reduced graphene oxide (rGO). *Graphene*, 06(01), 1–18.

- Bhui, D. K., Bar, H., Sarkar, P., Sahoo, G. P., De, S. P., & Misra, A. (2009). Synthesis and UV-vis spectroscopic study of silver nanoparticles in aqueous SDS solution. *Journal of Molecular Liquids*, 145(1), 33–37.
- Blanton, T., & Majumdar, D. (2013). Characterization of X-ray Irradiated graphene oxide coatings using X-ray diffraction, X-ray photoelectron spectroscopy, and atomic force microscopy. *Power Diffraction*, 28(2), 68-71.
- Budhiraja, N., Sharma, A., Dahiya, S., & Parmar, R. (2013). Synthesis and optical characteristics of silver nanoparticles on different substrates. *International Letters of Chemistry, Physics, and Astronomy*, 14(80–88).
- Chen, C., Long, M. C., Wu, H., & Cai, W. M. (2013). One-step synthesis of Pt nanoparticles/reduced graphene oxide composite with enhanced electrochemical catalytic activity. *Science China Chemistry*, 56(3), 354–361.
- Chen, S., Zhu, J., Wu, X., Han, Q., & Wang, X. (2010). Graphene oxide-MnO₂ nanocomposites for supercapacitors. *American Chemical Society Nano*, 4(5), 2822–2830.
- Cruz-silva, R., Barandiar, J. M., & García-guti, D. I. (2016). Magnetic properties of thermally reduced graphene oxide decorated with PtNi nanoparticles, *Journal of Alloys and Compounds*, 678, 541-548.
- Dong, L., Gari, R. R. S., Li, Z., Craig, M. M., & Hou, S. (2010). Graphene-supported platinum and platinum-ruthenium nanoparticles with high electrocatalytic activity for methanol and ethanol oxidation. *Carbon*, 48(3), 781–787.
- Dubal, D. P., Dhawale, D. S., Salunkhe, R. R., Jamdade, V. S., & Lokhande, C. D. (2010). Fabrication of copper oxide multilayer nanosheets for supercapacitor application. *Journal of Alloys and Compounds*, 492(1–2), 26–30.

- Fakhri, P., Jaleh, B., & Nasrollahzadeh, M. (2014). Synthesis and characterization of copper nanoparticles supported on reduced graphene oxide as a highly active and recyclable catalyst for the synthesis of formamides and primary amines. *Journal of Molecular Catalysis A: Chemical*, 383–384, 17–22.
- Gao, W. (2015). The chemistry of graphene oxide. *Graphene Oxide: Reduction Recipes, Spectroscopy, and Applications*, 61–95.
- Gotoh, K., Kinumoto, T., Fujii, E., Yamamoto, A., & Hashimoto, H. (2010). Exfoliated graphene sheets decorated with metal/metal oxide nanoparticles: Simple preparation from cation exchanged graphite oxide. *Carbon*, 4, 1–8.
- Grinou, A., Yun, Y. S., Cho, S. Y., Park, H. H., & Jin, H. J. (2012). Dispersion of Pt nanoparticle-doped reduced graphene oxide using aniline as a stabilizer. *Materials*, 5(12), 2927–2936.
- Ha, H., Kim, Y., Hwang, S., & Ruoff, R. S. (2011). One-Pot Synthesis of Platinum Nanoparticles Embedded on Reduced Graphene Oxide for Oxygen Reduction in Methanol Fuel Cells, *Electrochemical and Solid State-Letters*, 14(7), 73–76.
- Han, J. W., & Kim, J. (2015). Reduced graphene oxide – silver nanoparticle nanocomposite : a potential anticancer nanotherapy. *International Journal of Nanomedicine*, 10, 6257–6276.
- Herrera, G. M., Padilla, A. C., & Hernandez-rivera, S. P. (2013). Surface enhanced Raman Scattering (SERS) studies of gold and silver nanoparticles prepared by laser ablation, *Nanomaterials*, 3(1), 158–172.
- Khan, S., Ali, J., Husain, M., & Zulfequar, M. (2016). Synthesis of reduced graphene oxide and enhancement of its electrical and optical properties by attaching Ag nanoparticles. *Physica E: Low-Dimensional Systems and Nanostructures*, 81, 320–325.

- Li, M., Zhou, S., & Xu, M. (2017). Graphene oxide supported magnesium oxide as an efficient cathode catalyst for power generation and wastewater treatment in single chamber microbial fuel cells. *Chemical Engineering Journal*, 328, 106–116.
- Li, Y., Gao, W., Ci, L., Wang, C., & Ajayan, P. M. (2010). Catalytic performance of Pt nanoparticles on reduced graphene oxide for methanol electro-oxidation. *Carbon*, 48(4), 1124–1130.
- Lightcap, I. V., Kosel, T. H., & Kamat, P. V. (2010). Anchoring semiconductor and metal nanoparticles on a two-dimensional catalyst mat. storing and shuttling electrons with reduced graphene oxide. *Nano Letters*, 10(2), 577–583.
- Lin, X.-Q., Deng, H.-H., Wu, G.-W., Peng, H.-P., Liu, A.-L., Lin, X.-H., ... Chen, W. (2015). Platinum nanoparticles/graphene-oxide hybrid with excellent peroxidase-like activity and its application for cysteine detection. *The Analyst*, 140(15), 5251–5256.
- Mallakpour, S., Abdolmaleki, A., & Karshenas, A. (2017). Graphene oxide supported copper coordinated amino acids as novel heterogeneous catalysts for epoxidation of norbornene. *Catalysis Communications*, 92, 109–113.
- Nasehnia, F., Mohammadpour Lima, S., Seifi, M., & Mehran, E. (2016). First principles study on optical response of graphene oxides: From reduced graphene oxide to the fully oxidized surface. *Computational Materials Science*, 114, 112–120.
- Pal, A., Shah, S., & Devi, S. (2009). Microwave-assisted synthesis of silver nanoparticles using ethanol as a reducing agent. *Materials Chemistry and Physics*, 114(2–3), 530–532.
- Shahriary, L., & Athawale, A. a. (2014). Graphene Oxide Synthesized by using Modified Hummers Approach. *International Journal of Renewable Energy and Environmental Engineering*, 02(01), 58–63.

- Shahverdi, A. R., Minaeian, S., Shahverdi, H. R., Jamalifar, H., & Nohi, A. A. (2007). Rapid synthesis of silver nanoparticles using culture supernatants of Enterobacteria: A novel biological approach. *Process Biochemistry*, 42(5), 919–923.
- Singh, K., Ohlan, A., Pham, V. H., R, B., Varshney, S., Jang, J., & Chung, J. S. (2013). Nanostructured graphene/Fe₃O₄ incorporated polyaniline as a high performance shield against electromagnetic pollution. *Nanoscale*, 5(6), 2411–20.
- Song, Y., & Chen, S. (2014). Graphene quantum-dot-supported platinum nanoparticles: Defect-mediated electrocatalytic activity in oxygen reduction. *American Chemical Society Applied Materials and Interfaces*, 6(16), 14050–14060.
- Tang, X. Z., Li, X., Cao, Z., Yang, J., Wang, H., Pu, X., & Yu, Z. Z. (2013). Synthesis of graphene decorated with silver nanoparticles by simultaneous reduction of graphene oxide and silver ions with glucose. *Carbon*, 59, 93–99.
- Vilcinskis, K., Mulder, F. M., Picken, S. J., & Koper, G. J. M. (2017). In situ X-ray diffraction studies of graphite oxidation reaction indicating different exfoliation mechanism than ex site studies. *Chemical Physics*, 31(15).
- Wang, Y., Zhao, S., Li, M., Li, W., Zhao, Y., Qi, J., & Cui, X. (2017). Graphene quantum dots decorated graphene as an enhanced sensing platform for sensitive and selective detection of copper (II). *Journal of Electroanalytical Chemistry*, 797, 113–120.
- Xie, F., Hu, W., Ning, D., Zhuo, L., Deng, J., & Lu, Z. (2017). ZnO nanowires decoration on carbon fiber via hydrothermal synthesis for paper-based friction materials with improved friction and wear properties. *Ceramics International*, 44(4), 4204–4210.
- Xin, L., Yang, F., Rasouli, S., Qiu, Y., Li, Z. F., Uzunoglu, A., & Xie, J. (2016). Understanding Pt Nanoparticle Anchoring on Graphene Supports through Surface Functionalization. *ACS Catalysis*, 6(4), 2642–2653.

- Xu, X., Shen, J., Li, N., & Ye, M. (2015). Microwave-assisted in situ synthesis of cobalt nanoparticles decorated on reduced graphene oxide as promising electrodes for supercapacitors. *International Journal of Hydrogen Energy*, 40(38), 13003–13013.
- Ye, L., Li, Z., Zhang, L., Lei, F., & Lin, S. (2014). A green one-pot synthesis of Pt/TiO₂/Graphene composites and its electro-photo-synergistic catalytic properties for methanol oxidation. *Journal of Colloid and Interface Science*, 433, 156–162.
- Zhang, K. (2012). Applied Surface Science Fabrication of copper nanoparticles / graphene oxide composites for surface-enhanced Raman scattering. *Applied Surface Science*, 258(19), 7327–7329.
- Zhang, X., Xu, S., Jiang, S., Wang, J., Wei, J., & Xu, S. (2015). Applied Surface Science Growth graphene on silver – copper nanoparticles by chemical vapor deposition for high-performance surface-enhanced Raman scattering. *Applied Surface Science*, 353, 63–70.
- Zhao, H., Fu, H., Zhao, T., Wang, L., & Tan, T. (2012). Fabrication of small-sized silver NPs/graphene sheets for high-quality surface-enhanced Raman scattering. *Journal of Colloid and Interface Science*, 375(1), 30–34.
- Zoladek, S., Rutkowska, I. A., Blicharska, M., Miecznikowski, K., Ozimek, W., Orłowska, J., & Kulesza, P. J. (2017). Electrochimica Acta Evaluation of reduced-graphene-oxide-supported gold nanoparticles as catalytic system for electroreduction of oxygen in alkaline electrolyte. *Electrochimica Acta*, 233, 113–122.

Chapter 5

Synthesis and Supercapacitor Applications of Pt, Ag and Cu Nanoparticles- Doped Graphene Oxide/Polyanilino-Dodecylbenzenesulphonic Acid Composite

Electrodes

Summary

Graphene oxide (GO) a carbon material with exceptional properties such as good electrical, mechanical, thermal properties and high surface area makes it a good material in fields such as energy devices, polymer composites, sensors, biomedical etc.. Over the years there have been many techniques used for the synthesis of GO and many methods for its reduction. Metal nanoparticles have attracted a lot of attention due to their unique performance in magnetic, optical, catalytic and energy performances and other fields. Currently GO is being supported or loaded with metal nanoparticles to enhance its properties for applications in many fields. High surface carbon materials, metal oxides or metal nanoparticles and conducting polymers have been studied as possible materials for application in energy related devices. PANI is an excellent biological conductor with good environmental stability and biocompatibility and has been used in combination with carbon based materials to develop supercapacitor electrodes and sensors. GO was then loaded with platinum (Pt), silver (Ag) and copper (Cu) nanoparticles. This material was then anchored on dodecylbenzenesulphonic acid doped polyaniline (DBSA doped PANI).

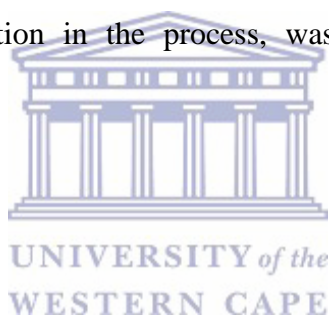
Abstract

A simple one step method to anchored dodecylbenzenesulphonic acid (DBSA) doped polyaniline (PANI) was developed. This method makes use of materials such as aniline and ammonium persulphate. Anchoring the GO with DBSA doped PANI revealed that single GO sheets were embedded into the polymer latex, which causes the DBSA-PANI particles to become adsorbed on their surfaces. This process then appeared as dark regions in the high resolution transmission electron microscopy (HRTEM) images. Morphological studies by high resolution scanning electron microscopy (HRSEM) also support that single GO sheets are embedded into the polymer latex as composite formation appeared aggregated and as bounded particles with smooth and toothed edges. The Fourier transform infrared (FTIR) spectroscopy studies revealed that the anchored GO with DBSA doped polyaniline exhibited broad adsorption bands at around 3144 cm^{-1} attributed to polyaniline N-H stretching vibrations and two vibrational peaks centered at 1557 and 1464 cm^{-1} attributed to the stretching frequencies of quinoid and benzenoid rings of polyaniline. The band that is produced at 1297 cm^{-1} belongs to the C-N stretching of secondary amide group and the band that appears at 1135 cm^{-1} is attributed to in-plane bending of the C-H bond and bands at, 1044 and 1004 cm^{-1} are due to SO_3^- group (O=S=O and S-O stretching) of DBSA. The composites were tested for application as suitable supercapacitor materials and specific capacitances were determined as 227.2, 206.4 and 192.8 F g^{-1} which correspond to GO/Pt/DBSA-PANI, GO/Ag/DBSA-PANI and GO/Cu/DBSA-PANI, respectively. GO/Pt/DBSA-PANI behaved better than the other composites as it can be observed to have given higher capacitances when compared to GO/Ag/DBSA-PANI and GO/Cu/DBSA-PANI.

5.1 Introduction

Graphene oxide (GO) is defined as a single sheet of graphite oxide and is also an intermediate during the synthesis of reduced graphene oxide (Gao, 2015). The synthesis method includes oxidation, exfoliation and reduction of graphite powder and this method has been widely used due to its low cost and large productivity (Zhang *et al.*, 2017). Graphene oxide has considerable exceptional properties such as good mechanical, electronic, optical etc. which renders graphene oxide a good candidate for use in energy storage devices (Gao, 2015; Mahmood *et al.*, 2014; Zhu *et al.*, 2010). Due to GO's unique nanostructure and extremely attractive properties, graphene sheets can be required as potential building blocks for new materials (Li & Kaner, 2008). Metal nanoparticles have attracted a lot of attention due to their performance in electronic, magnetic, optical and catalytic applications. Recently, metal nanoparticles such as Pt, Pd, Au, Ag etc. have been supported on the surface of GO (Bonet *et al.*, 1999; Grinou *et al.*, 2012). It is most likely that NPs supported on graphene sheet possibly display novel catalytic, magnetic, and optoelectronic properties (He & Gao, 2011). Well-dispersed small-sized nanoparticles are expected to exhibit enhanced activity and selectivity for catalytic reactions (Yang *et al.*, 2015). However, the uniform dispersion of small sized nanoparticles in large quantities onto the surface of GO remains a great challenge (Watson, 2014). Conducting polymers have been used to maintain the need for high electrical conductivity of materials for a myriad of applications including energy-related devices. High surface carbon materials in combination with noble metals and conducting polymers have been extensively studied, however due to the poor conductivity of some often limit their use in high performance devices (Snook *et al.*, 2011; Xu *et al.*, 2010). However, there has been much interest in polyaniline -based materials because of their low cost and they can easily be synthesized. Since polyaniline is an excellent organic conductor with good environmental

stability and biocompatibility (Trchová & Stejskal, 2011), it has been used often to produce materials or composites with carbon materials for supercapacitor electrodes or sensor applications (Kumar *et al.*, 2012). The ability to hybridize carbon-based nanomaterials with conducting polymers to produce nanocomposites is of great importance and has generated lots of interest. When graphene oxide nanosheets are compounded with conducting polymers enhances higher electrical conductivity and mechanical strength of resulting nanocomposites (Imran *et al.*, 2014; Wang *et al.*, 2009). These characteristics therefore enable graphene oxide-based conducting polymer nanocomposites to be considered for many applications and many more other applications and in many more other fields (Kumar *et al.*, 2012; Zhang & Zhao, 2012). Dodecylbenzenesulphonic acid (DBSA) was used as a dopant to enable the polymer-organic solvent interaction in the process, was used for the doping of PANI (Castillo-Castro *et al.*, 2007).



5.2 Experimental

5.2.1 Chemicals and sample preparation

All chemicals used in the experiments were of analytical grade and were used as purchased without further purification. Graphite (1-2 micron), sodium nitrate NaNO_3 ($\geq 99\%$), sulphuric acid H_2SO_4 ($\geq 98\%$), potassium permanganate KMnO_4 ($\geq 99\%$), hydrogen peroxide ($\geq 30\%$), hydrochloric acid HCl ($\geq 37\%$), hexachloroplatinic acid $\text{H}_2\text{PtCl}_6 \cdot 6\text{H}_2\text{O}$, ACS reagent ($\geq 37.50\%$) Pt basis, silver nitrate AgNO_3 , ACS reagent ($\geq 99.0\%$), copper acetate ACS reagent, ($\geq 99.0\%$), sodium hydroxide NaOH , BioXtra ($\geq 98\%$) acidimetric, pellets (anhydrous), cetyl trimethylammonium bromide CTAB (98%), poly (sodium 4-styrenesulfonate) PSS ($\sim 70\ 000$) powder, sodium acetate NaAc , poly-ethylene glycol (PEG)

(400 powder), ethylene glycol anhydrous (99.8%), acetone ($\geq 99.9\%$), dodecylbenzenesulphonic acid ($\geq 98\%$), aniline ACS reagent ($\geq 99.5\%$), ammonium persulphate ACS reagent ($\geq 98.0\%$), methanol ($\geq 99.9\%$) and isopropanol ($\geq 99.7\%$) were all purchased from Sigma Aldrich.

5.2.2 Instrumentation

The cell system was fabricated using 1 M H_2SO_4 solution as the electrolyte and tested for supercapacitor parameters using the BST8-3 eight-channel battery testing machine. Fourier transform infrared (FTIR) spectra were recorded on a Perkin Elmer FTIR model 100 spectrophotometer, operating between 400 and 4000 cm^{-1} in order to characterize the presence of specific features of GO and rGO. The high-resolution scanning electron microscopy (HRSEM) of GO and rGO were imaged using a Zeiss Auriga SEM operating at 50kV and high resolution-transmission electron microscope (HR-TEM) equipped with an energy-dispersive spectroscopy (EDS) detector was used to study the size, morphology and composition of samples. Copper grid (Cu) was used as sample holder for the immobilisation of (2 μL) solution of GO and rGO and the micrographs were recorded at room temperature.

5.2.3 Synthesis of GO/NPs, GO/AgNPs and GO/Cu NPs anchored DBSA doped PANI

Graphene oxide was synthesized according to the steps mentioned in Chapter 3, Section 3.2.3. It was also loaded with platinum, silver and copper nanoparticles according to the method mentioned in Chapter 4, Section 4.2.3. A mass of 0.5 g GO/Pt NPs, GO/Ag NPs and GO/Cu NPs was sonicated in 400 mL of 1M DBSA solution prepared in 1M HCl for 5 hours as reported earlier. DBSA, an anionic surfactant was used as dopant as well as to disperse the

graphene oxide loaded with nanoparticles in the solution. Thereafter, 5 mL of double distilled aniline and solution of ammonium persulphate (12.53 g of $(\text{NH}_4)_2\text{S}_2\text{O}_8$ in 100 mL of 1 M HCl) was added drop-wise to the previous solution of DBSA for in situ oxidative polymerization of aniline with graphene oxide loaded nanoparticles under stirring condition in ice bath for 6.5 hours. A greenish black precipitate was obtained which was washed thoroughly with double distilled water and methanol to remove any traces of reactants and polyaniline oligomers until the filtrate had to become transparent. Thus, prepared nanocomposite was dried at 60 °C and stored in a desiccator for further experiments (Kumar *et al.*, 2013). The materials were named GO/Pt/DBSA-PANI, GO/Ag/DBSA-PANI and GO/Cu/DBSA-PANI, respectively.

5.2.4 Fabrication of the electrode material

5.2.4.1 Preparation of the electrode materials



The materials used in the experiment for fabrication of the electrode consisted of 40 mg active material, 5 mg of carbon black, 5 mg (3 drops) of isopropanol and 8 mg of polytetrafluoroethylene (PTFE) binder. The active material consisted of the GO/Pt NPs anchored DBSA doped PANI (GO/Pt/DBSA-PANI). The carbon black and GO/Pt NPs anchored DBSA doped PANI (GO/Pt/DBSA-PANI) were mixed together and crushed to ensure that they were correctly mixed. For a given electrode, relevant materials were mixed together in a 10 mL small beaker to form dough. The dough was transferred onto a flat glass plate. A stainless steel/Teflon rod was used to roll the dough into mm thick flexible thin films. When making the thin film the dough was rolled many times with constant addition of three drops of isopropanol to ensure that the material was correctly mixed in the thin film. The thin film was then placed in an oven and was allowed to bake at 80° C under vacuum.

Once the thin film was dried it was then cut into small wafers for the construction of the electrode. The same principle was used for GO/Ag NPs anchored dbsa doped PANI (GO/Ag/DBSA-PANI) and GO/Cu NPs anchored dbsa doped PANI (GO/Cu/DBSA-PANI) composites, respectively (Njomo *et al.*, 2014).

5.2.4.2 Construction of supercapacitor cell

A single electrode was assembled with three parts; electrode material, stainless steel mesh current collector and stainless steel wire. The electrode was assembled by cutting the stainless steel mesh current collector into a 1 cm × 4 cm rectangular shape. The collector was then cleaned by shaking it in ethanol, dried and then weighed. The approximately 1 cm² wafer was placed on the stainless steel mesh and pressed at a pressure of 20 MPa for 5 min. The electrode was then weighed and the difference in mass was used as the active mass of the electrode. The stainless steel wire was tightly held onto the current collector for external circuit connection and acted as cathode. The active material was GO/Pt NPs anchored DBSA doped PANI (GO/Pt/DBSA-PANI) and acted as anode. The stainless steel wire and active material were used to make a two-electrode asymmetric supercapacitor cell. The cell system was fabricated using 1M H₂SO₄ solution as the electrolyte and tested for the supercapacitor parameters using the BST8-3 eight-channel battery testing machine. The cell was fabricated by holding together the two single electrodes (cathode and anode) with a porous and electronically non-conductive separator sandwiched between them to form the cell configuration (Njomo *et al.*, 2014).

5.3 Results and Discussion

5.3.1 Structural analysis of GO/Pt/DBSA-PANI, GO/Ag/DBSA-PANI and GO/Cu/DBSA-PANI

Figures 5 (a) to (c) shows the surface of structures, GO/Pt/DBSA-PANI, GO/Ag/DBSA-PANI and GO/Cu/DBSA-PANI, respectively, with more dark surfaces. This observations are due to the presence of GO in the matrix. DBSA acts as a surfactant and binding agent, and appears to assist the binding between PANI and GO (Calheiros *et al.*, 2017). The single GO sheets may also be embedded into the polymer latex, which causes the DBSA-PANI particles to become adsorbed on their surfaces. This process may appear as dark regions in the HRTEM images of GO/Pt/DBSA-PANI, GO/Ag/DBSA-PANI and GO/Cu/DBSA-PANI, as a whole (Afzal & Akhtar, 2012). Moreover, as observed from the HRTEM image analysis of the GO/Pt/DBSA-PANI, GO/Ag/DBSA-PANI and GO/Cu/DBSA-PANI composite, the easier formation of a micellar structure, as well as the surfactant nature of DBSA, can stabilize the PANI particles found attached to the surface of the GO (Chang *et al.*, 2007). DBSA hydrophobic tails are arranged in such a way that they turn to one another. On the other hand, the hydrophilic groups of the free DBSA turn to the aqueous phase and may even attach to the surface of GO (Castillo-Castro *et al.*, 2007). As a result, the interactions in the GO/Pt/DBSA-PANI, GO/Ag/DBSA-PANI and GO/Cu/DBSA-PANI composites (DBSA-PANI in association with GO particles) generate some kind of aggregated structure and appear in the form of agglomerates, which appear as dark regions in the HRTEM images (Ashokan *et al.*, 2015). Morphological studies also support that single GO sheets are embedded into the polymer latex and DBSA-PANI particles are adsorbed onto the surfaces of the GO sheets (Haba *et al.*, 2000; Long *et al.*, 2010). This structure is possible because GO

sheets have a large surface area. Consequently, more active sites may be generated for the charge transfer in the polymer composite formed by GO and DBSA with the PANI matrix (Ansari & Mohammad, 2012; Castillo-Castro *et al.*, 2007; Kumar *et al.*, 2013).

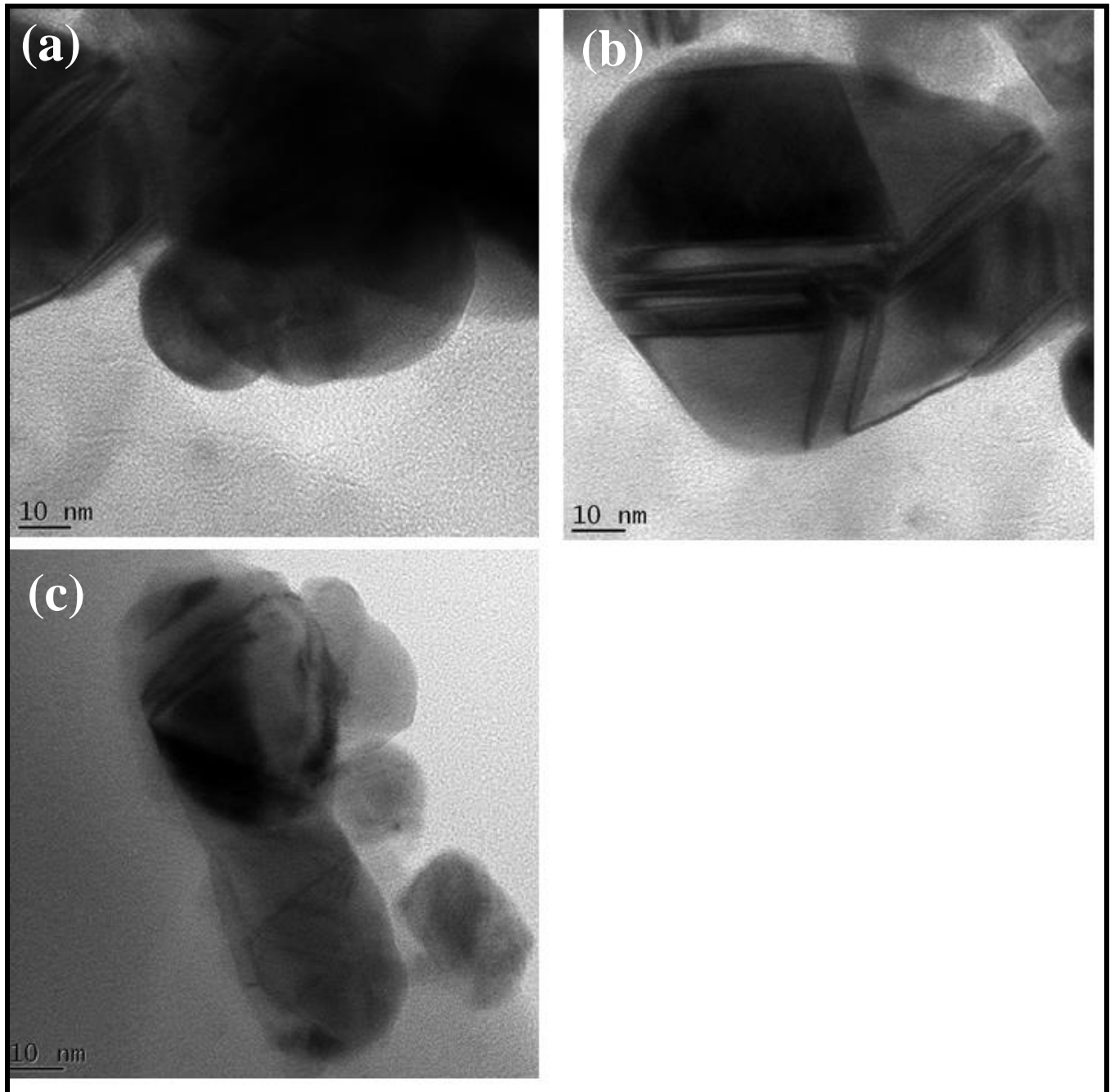
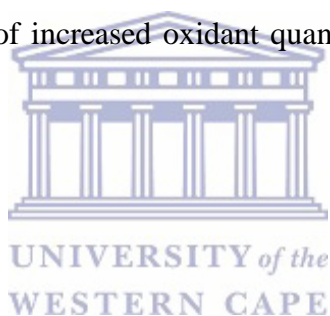


Figure 5. 1: HRTEM images of (a) GO/Pt/DBSA-PANI, (b) GO/Ag/DBSA-PANI and (c) GO/Cu/DBSA-PANI.

5.3.2 Morphological properties of GO/Pt/DBSA-PANI, GO/Ag/DBSA-PANI and GO/Cu/DBSA-PANI

The high resolution scanning electron micrographs (HRSEM) of the GO/Pt/DBSA-PANI, GO/Ag/DBSA-PANI and GO/Cu/DBSA-PANI composites are shown in Figure 5.2(a) to (c), respectively. It can be seen that the composite formation are aggregated and bounded particles (Castillo-Castro *et al.*, 2007). It is clear that the surfaces of glassy nature are smooth, and the edges are toothed. The morphologies of the GO/Pt/DBSA-PANI, GO/Ag/DBSA-PANI and GO/Cu/DBSA-PANI composites have been changed with the addition of oxide at increased oxidant ratio. The enhanced polymer formation with decreased particle roughness is possible through the addition of increased oxidant quantity (Chew *et al.*, 2015; Li *et al.*, 2004; Yin & Ruckenstein, 2000)



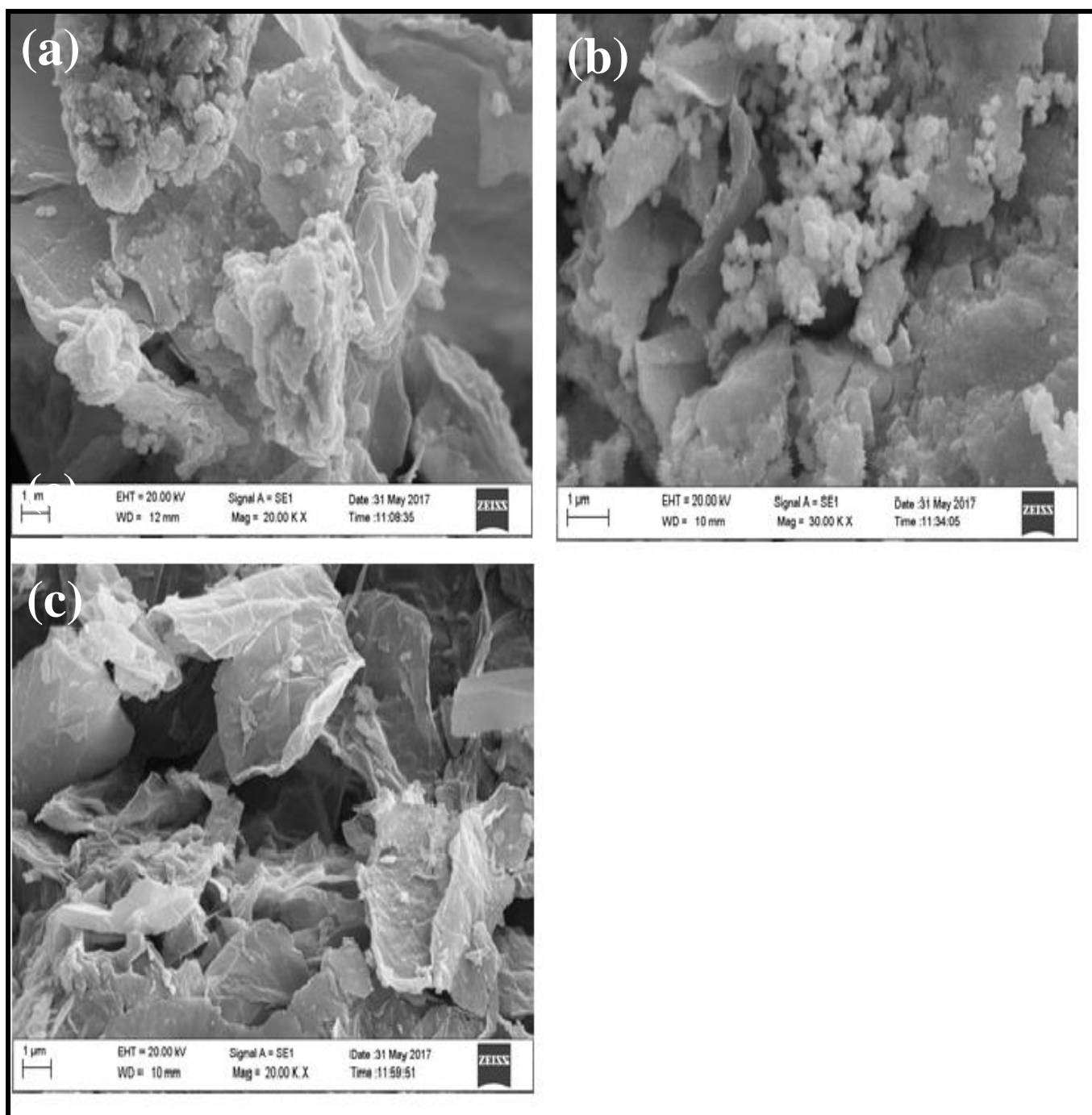
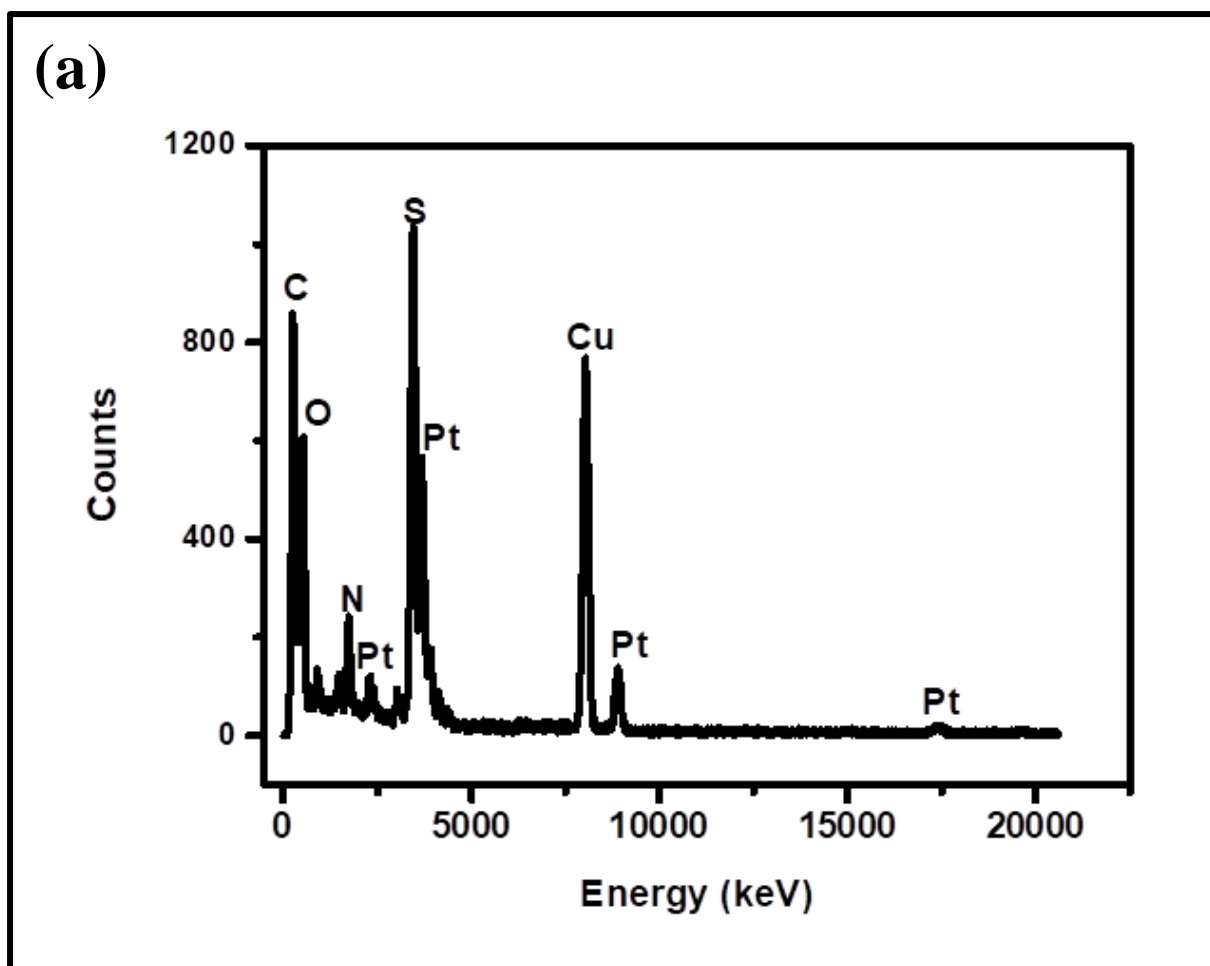


Figure 5. 2: HRSEM images of (a) GO/Pt/DBSA-PANI, (b) GO/Ag/DBSA-PANI and (c) GO/Cu/DBSA-PANI.

5.3.3 Elemental composition of (a) GO/Pt/DBSA-PANI, (b) GO/Ag/DBSA-PANI and (c) GO/Cu/DBSA-PANI

The elemental composition of the composite materials was investigated using energy dispersive X-ray (EDX) as shown in Figure 5.3 (a) - 5.3 (c). The quantitative analysis result indicates the presence of carbon, sulfur, platinum, silver and copper in the polymer composites. Also, the result confirms the formation of platinum, silver and copper nanoparticles (Yang *et al.*, 2011).



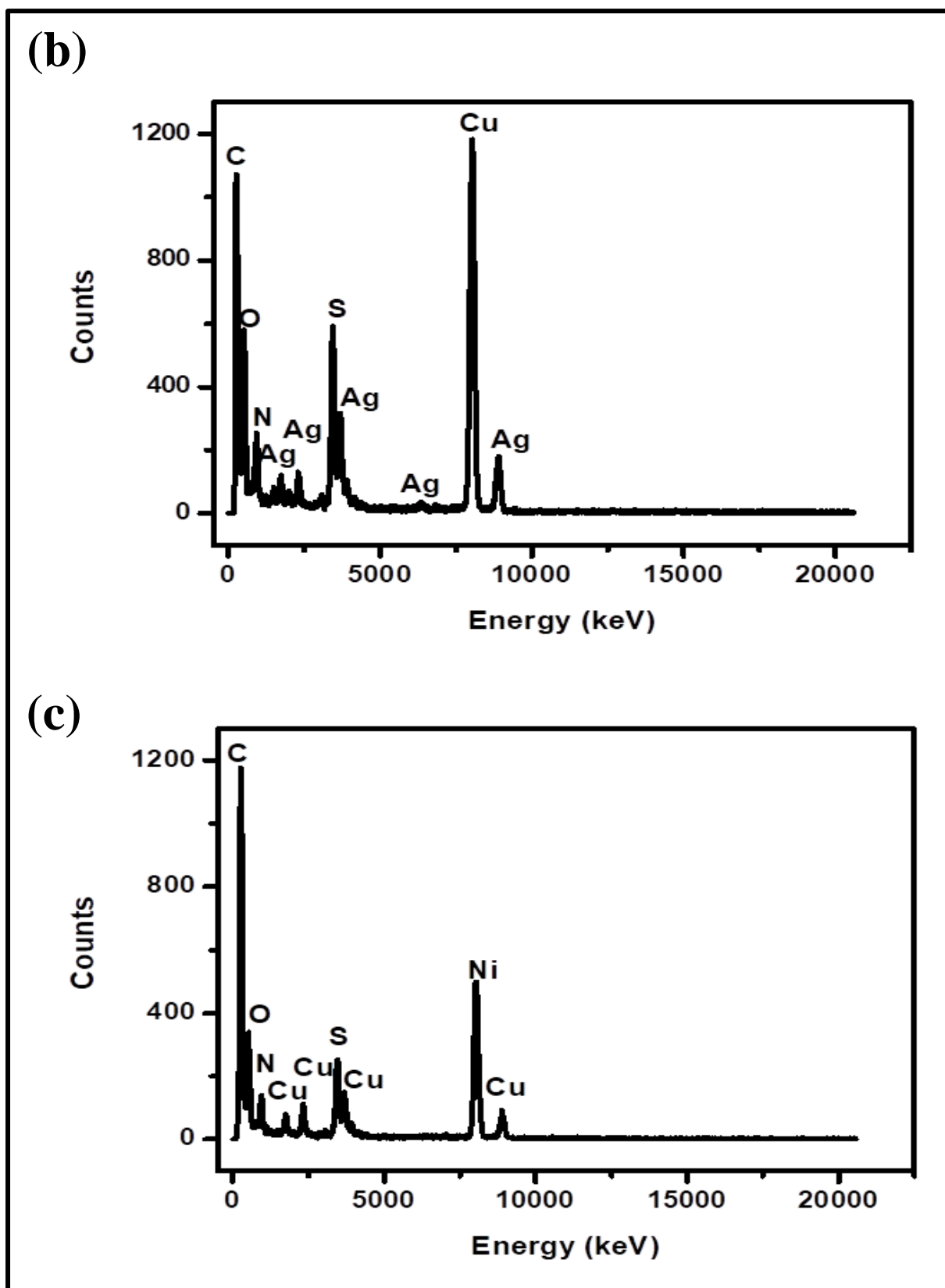
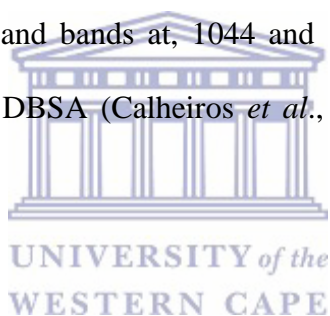


Figure 5. 3: EDX images of (a) GO/Pt/DBSA-PANI, (b) GO/Ag/DBSA-PANI and (c) GO/Cu/DBSA-PANI.

5.3.4 Structural properties of GO/Pt/DBSA-PANI, GO/Ag/DBSA-PANI and GO/Cu/DBSA-PANI.

FTIR studies of GO/Pt NPs/DBSA-PANI, GO/Ag NPs/DBSA-PANI and GO/Cu NPs/DBSA-PANI as shown in Figure 5.4 (a) to (c) were performed. The broad absorption band at around $\sim 3144\text{ cm}^{-1}$ corresponds to polyaniline N-H stretching vibrations (Bhadra, Madi, Al-Thani, & Al-Maadeed, 2014; Trchová & Stejskal, 2011). The vibrational bands centered at 1557 and 1464 cm^{-1} can be attributed to the stretching frequencies of quinoid and benzenoid rings of polyaniline, respectively. The band that is produced at 1297 cm^{-1} belongs to the C-N stretching of secondary amide group. The band at 1135 cm^{-1} is attributed to in-plane bending of the C-H bond and bands at, 1044 and 1004 cm^{-1} are due to SO_3^- group (O=S=O and S-O stretching) of DBSA (Calheiros *et al.*, 2017; Chang *et al.*, 2007; Chen, 2002).



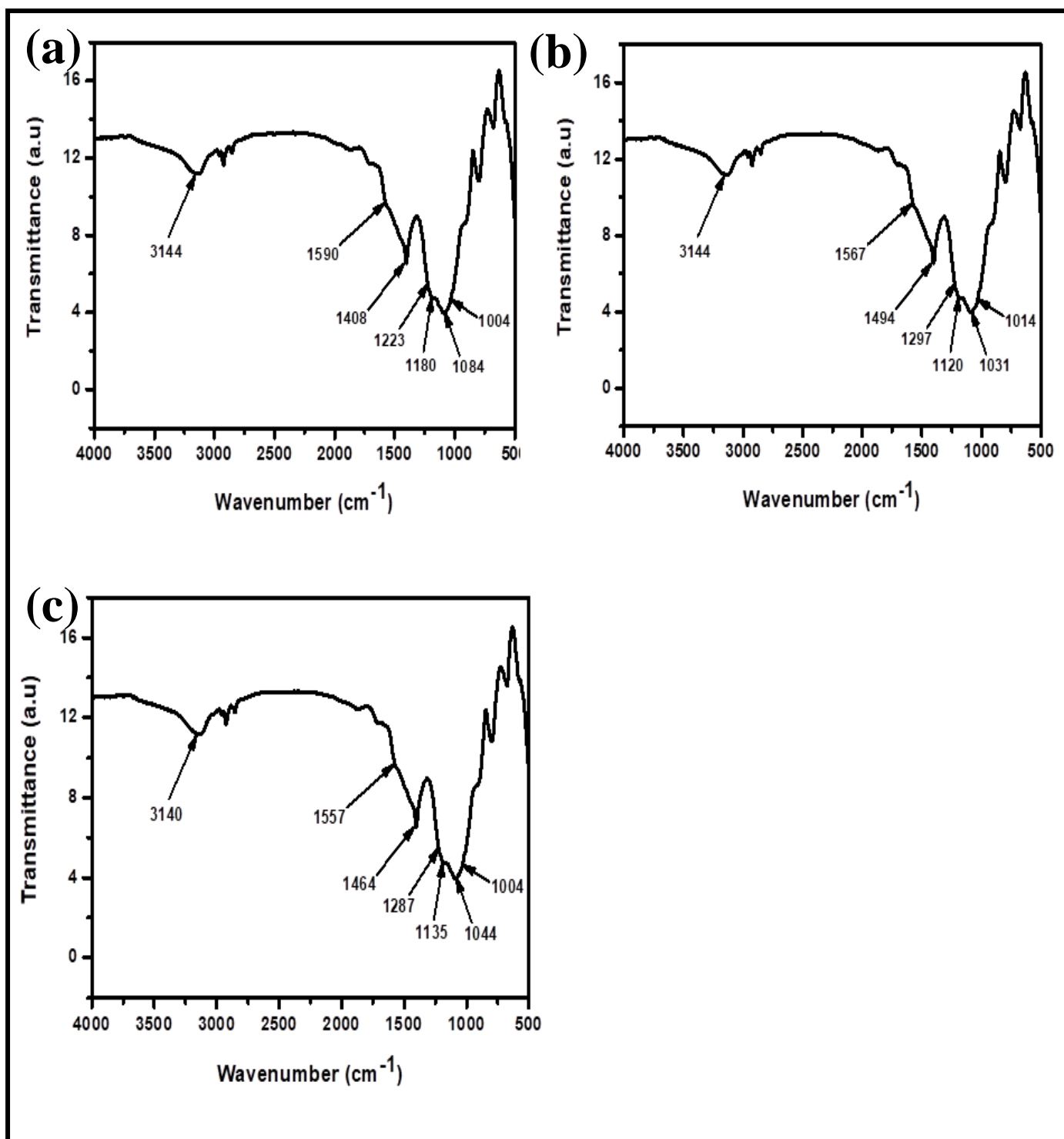


Figure 5. 4: FTIR spectra of (a) GO/Pt NPs/DBSA-PANI, (b) GO/Ag NPs/DBSA-PANI and (c) GO/Cu NPs/DBSA-PANI.

5.4 Electrochemical studies

5.4.1 Testing GO/Pt/DBSA-PANI as a supercapacitor material using Galvanostatic-charge discharge

The capacitive behaviour of GO/Pt/DBSA-PANI is shown in Figure 5.5. The voltage-time curve of GO/Pt/DBSA-PANI shows an ideal linear shape with a little deviation from the line at lower potential due to graphene oxide. GO/Pt/DBSA-PANI shows a large current density in CV curves as well as a longer charge–discharge time in V–t curves, implying a larger capacitance. The mass of the thin film of GO/Pt/DBSA-PANI was 5.2 g and the first cycle charge and discharge capacities obtained were 44.2Ah g⁻¹. The voltage range was [0 to -0.9 V] vs. Ag/AgCl. Cycling was done at a current density of 50 A g⁻¹ in an aqueous solution of 1 M H₂SO₄. The specific charge/discharge current density was found to be 56.8 A g⁻¹ (Pérez-Fernández, Martín-yerga, & Costa-garcía, 2017; F. Xu *et al.*, 2010). The specific capacitance C_{sp} can be calculated where, I , is the current density measured in Amperes per gram, t , is the time measured in seconds and, V , is the voltage.

$$C_{sp} = \frac{It}{V} \quad (1)$$

Therefore the specific capacitance, C_{sp} , is calculated as follows:

$$\begin{aligned} C_{sp} &= \frac{56.8 \times 3.6}{0.9} \\ &= 227.2 \text{ F g}^{-1} \end{aligned}$$

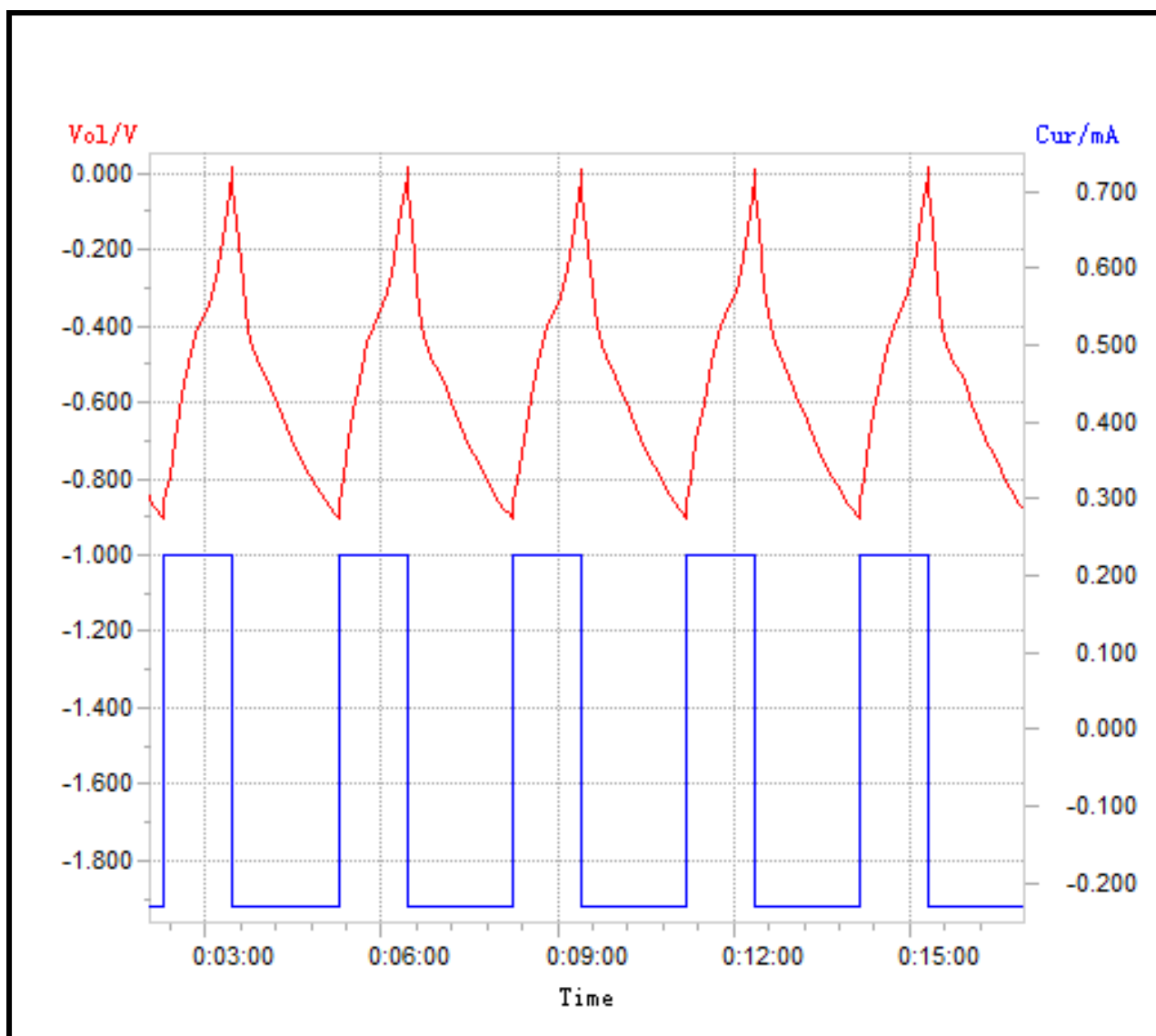
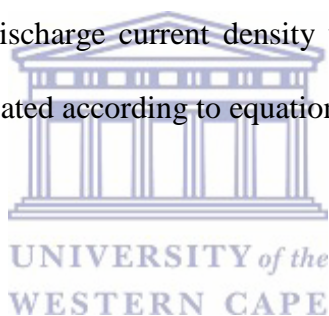


Figure 5. 5: Figure 3. 9: Voltage/time cycling plot of GO/Pt/DBSA-PANI voltage range (0 to -0.9V v Ag/AgCl) at 50 A g^{-1} in $1 \text{ M H}_2\text{SO}_4$ (aq). Specific charge/discharge current density $=56.8 \text{ A g}^{-1}$. Specific capacitance $= (56.8 \times 3.6)/0.9 = 227.2 \text{ F g}^{-1}$.

5.4.2 Testing GO/Ag/DBSA-PANI as a supercapacitor material using Galvanostatic-charge discharge

The capacitive behaviour of GO/Ag/DBSA-PANI is shown in Figure 5.6. The voltage-time curve of GO/Ag/DBSA-PANI shows an ideal linear shape with a little deviation from the line at lower potential due to graphene oxide. GO/Ag/DBSA-PANI shows a large current density in CV curves as well as a longer charge-discharge time in V-t curves, implying a larger capacitance. The mass of the thin film of GO/Ag/DBSA-PANI was 5.2 g and the first cycle charge and discharge capacities obtained were 44.2 Ah g⁻¹. The voltage range was [0 to -0.9 V] vs. Ag/AgCl. Cycling was done at a current density of 50 A g⁻¹ in an aqueous solution of 1 M H₂SO₄. The specific charge/discharge current density was found to be 51.6 A g⁻¹. The specific capacitance, C_{sp} , is calculated according to equation (1) as follows:

$$C_{sp} = \frac{51.6 \times 3.6}{0.9}$$
$$= 206.4 \text{ F g}^{-1}$$



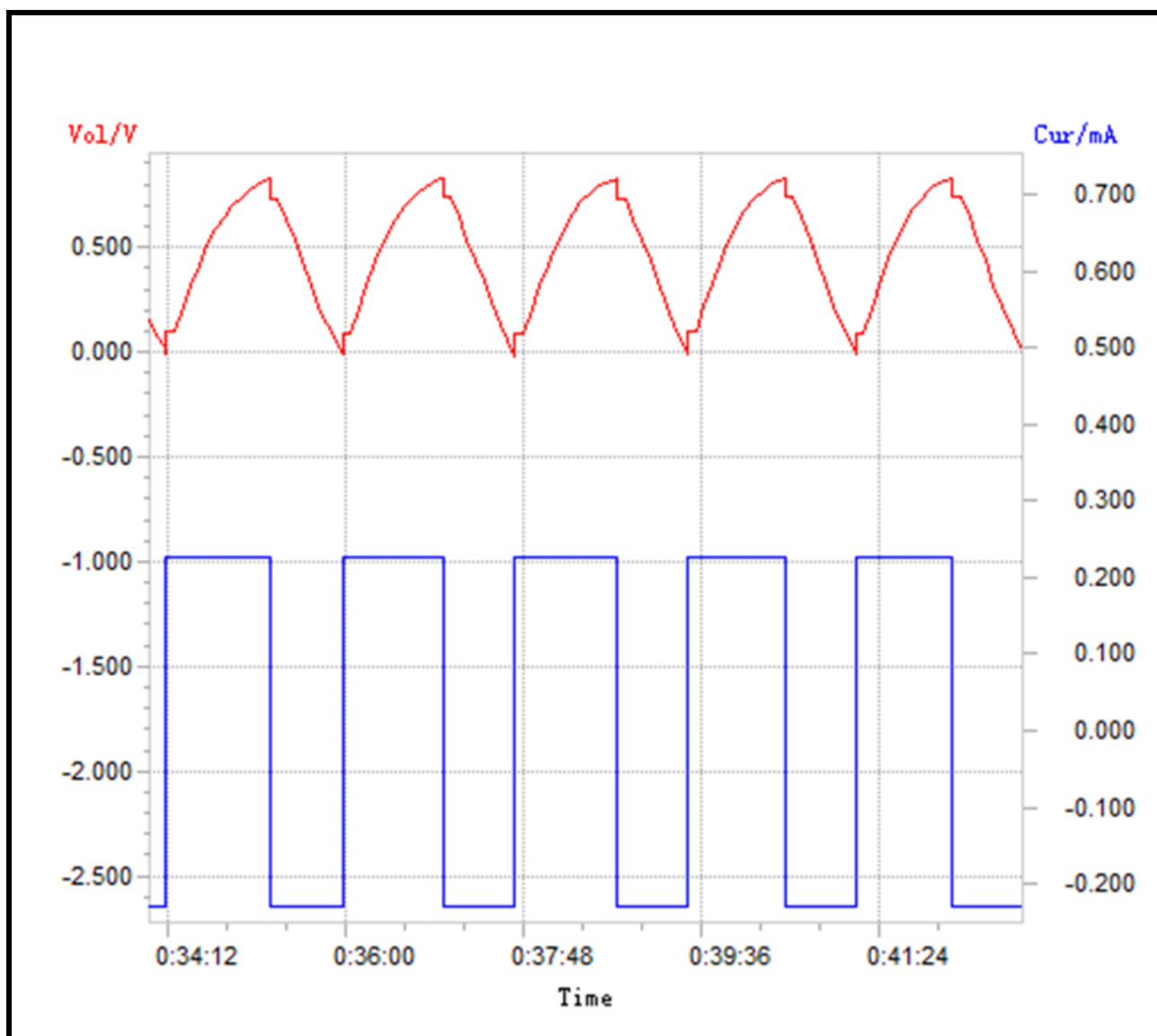


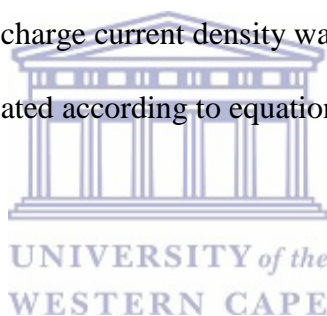
Figure 5. 6: Voltage/time cycling plot of GO/Ag/DBSA-PANI voltage range (0 to -0.9V v Ag/AgCl) at 50 mA g⁻¹ in 1M H₂SO₄ (aq). Specific charge/discharge current density =51.6 A g⁻¹. Specific capacitance = (51.6 x 3.6)/0.9 = 206.4 F g⁻¹.

5.4.3 Testing GO/Cu/DBSA-PANI as a supercapacitor material using Galvanostatic-charge discharge

The capacitive behaviour of GO/Cu/DBSA-PANI is shown in Figure 5.7. The voltage-time curve of GO/Cu/DBSA-PANI shows an ideal linear shape with a little deviation from the line at lower potential due to graphene oxide. GO/Cu/DBSA-PANI shows a large current density in CV curves as well as a longer charge-discharge time in V-t curves, implying a larger capacitance. The mass of the thin film of GO was 5.2 g and the first cycle charge and discharge capacities obtained were 44.2 Ah g⁻¹. The voltage range was [0 to -0.9 V] vs. Ag/AgCl. Cycling was performed at a current density of 50 mA g⁻¹ in a solution of aqueous 1 M H₂SO₄. The specific charge/discharge current density was determined to be 48.2 A g⁻¹. The specific capacitance, C_{sp} , is calculated according to equation (1) as follows:

$$C_{sp} = \frac{48.2 \times 3.6}{0.9}$$

$$= 192.8 \text{ F g}^{-1}$$



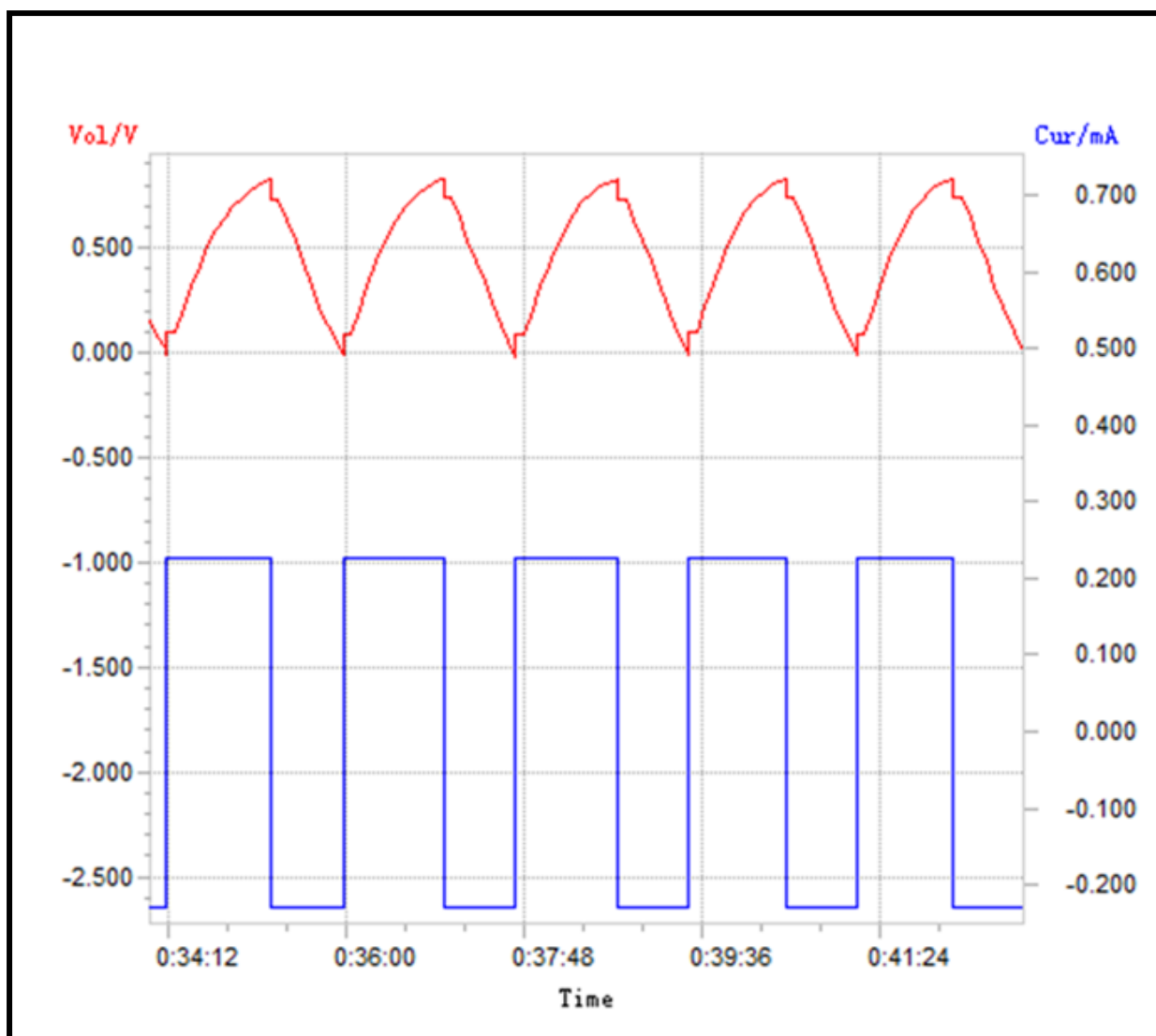


Figure 5. 7: Voltage/time cycling plot of GO/Cu/DBSA-PANI voltage range (0 to -0.9 V v Ag/AgCl) at 50 A g^{-1} in $1\text{M H}_2\text{SO}_4$ (aq). Specific charge/discharge current density = 48.2 A g^{-1} . Specific capacitance = $(48.2 \times 3.6)/0.9 = 192.8 \text{ F g}^{-1}$.

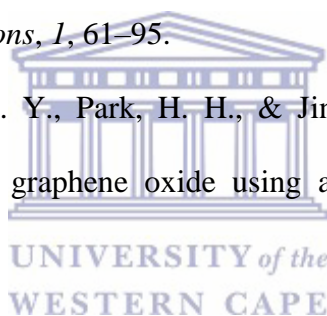
5.5 Conclusions

GO was synthesized by the modified Hummers method. It was then loaded with Pt, Ag and Cu NPs using the electrostatic self-assembly method. The resulting material was then treated with aniline and DBSA to form conducting polymer composites. HRTEM images show the structures of GO/Pt/DBSA-PANI, GO/Ag/DBSA-PANI and GO/Cu/DBSA-PANI with darker surfaces. The structures are aggregated and appear in the form of agglomerates which appear as dark regions on the HRTEM images. HRSEM images show aggregated polymer composites bounded particles and the surfaces are of glassy nature, are smooth and sharp edges. The quantitative analysis of the polymer composites indicates the presence of carbon, sulphur, platinum for the polymer composite that contains platinum. The same behaviour is apparent for the composite that contains silver and copper. FTIR studies of the polymer composites show a broad absorption band around 3144 cm^{-1} which corresponds to the stretching frequencies of quinoid and benzenoid rings of polyaniline respectively. FTIR studies also reveals a band around 1297 cm^{-1} which corresponds to C-N stretching of secondary amide group, a band around 1135 cm^{-1} attributed to the in-plane bending of the C-H group and bands that appear at 1044 and 1004 cm^{-1} due to the DBSA SO_3^- group. The specific capacitance of the polymer composites was determined from the galvanostatic charge/discharge. The specific capacitance was determined as 227.2, 206.4 and 192.8 F g^{-1} which correspond to GO/Pt/DBSA-PANI, GO/Ag/DBSA-PANI and GO/Cu/DBSA-PANI, respectively. Comparing these values with the specific capacitance of GO, which was determined as 182.8 F g^{-1} , we can conclude that the materials are good materials and therefore can be used for supercapacitor applications. Platinum is more ductile, is stable at high temperatures and has stable electrical properties when compared to both silver and copper. Hence, platinum has higher response when compared to the other metals.

References

- Afzal, A. B., & Javed Akhtar, M. (2012). Effects of silver nanoparticles on thermal properties of DBSA-doped polyaniline/PVC blends. *Iranian Polymer Journal*, 21(8), 489–496.
- Ansari, M. O., & Mohammad, F. (2012). Thermal stability and electrical properties of dodecyl-benzene-sulfonic- acid doped nanocomposites of polyaniline and multi-walled carbon nanotubes. *Composites Part B: Engineering*, 43(8), 3541–3548.
- Ashokan, S., Ponnuswamy, V., & Jayamurugan, P. (2015). Synthesis and characterization of CuO nanoparticles, DBSA doped PANI and PANI/DBSA/CuO hybrid composites for diode and solar cell device development. *Journal of Alloys and Compounds*, 646, 40–48.
- Bhadra, J., Madi, N. K., Al-Thani, N. J., & Al-Maadeed, M. A. (2014). Polyaniline/polyvinyl alcohol blends: Effect of sulfonic acid dopants on microstructural, optical, thermal and electrical properties. *Synthetic Metals*, 191, 126–134.
- Bonet, F., Delmas, V., Grugeon, S., Herrera Urbina, R., Silvert, P. Y., & Tekaia-Elhsissen, K. (1999). Synthesis of monodisperse Au, Pt, Pd, Ru and Ir nanoparticles in ethylene glycol. *Nanostructured Materials*, 11(8), 1277–1284.
- Calheiros, L. F., Soares, B. G., & Barra, G. M. O. (2017). DBSA-CTAB mixture as the surfactant system for the one step inverse emulsion polymerization of aniline: Characterization and blend with epoxy resin. *Synthetic Metals*, 226, 139–147.
- Chang, K. C., Jang, G. W., Peng, C. W., Lin, C. Y., Shieh, J. C., Yeh, J. M., & Li, W. T. (2007). Comparatively electrochemical studies at different operational temperatures for the effect of nanoclay platelets on the anticorrosion efficiency of DBSA-doped polyaniline/Na⁺-MMT clay nanocomposite coatings. *Electrochimica Acta*, 52(16), 5191–5200.

- Chen, C. H. (2002). Thermal studies of polyaniline doped with dodecyl benzene sulfonic acid directly prepared via aqueous dispersions. *Journal of Polymer Research*, 9(3), 195–200.
- Chew, T., Daik, R., & Hamid, M. (2015). Thermal conductivity and specific heat capacity of dodecylbenzenesulfonic acid-doped polyaniline particles—water based nanofluid. *Polymers*, 7(7), 1221–1231.
- Del Castillo-Castro, T., Castillo-Ortega, M. M., Villarreal, I., Brown, F., Grijalva, H., Perez-Tello, M., & Puig, J. E. (2007). Synthesis and characterization of composites of DBSA-doped polyaniline and polystyrene-based ionomers. *Composites Part A: Applied Science and Manufacturing*, 38(2), 639–645.
- Gao, W. (2015). The chemistry of graphene oxide. *Graphene Oxide: Reduction Recipes, Spectroscopy, and Applications*, 1, 61–95.
- Grinou, A., Yun, Y. S., Cho, S. Y., Park, H. H., & Jin, H. J. (2012). Dispersion of Pt nanoparticle-doped reduced graphene oxide using aniline as a stabilizer. *Materials*, 5(12), 2927–2936.
- Haba, Y., Segal, E., Narkis, M., Titelman, G. I., & Siegmann, A. (2000). Polyaniline-DBSA/polymer blends prepared via aqueous dispersions. *Synthetic Metals*, 110(3), 189–193.
- He, H., & Gao, C. (2011). Graphene nanosheets decorated with Pd, Pt, Au, and Ag nanoparticles: Synthesis, characterization, and catalysis applications. *Science China Chemistry*, 54(2), 397–404.
- Imran, S. M., Kim, Y., Shao, G. N., Hussain, M., Choa, Y. H., & Kim, H. T. (2014). Enhancement of electroconductivity of polyaniline/graphene oxide nanocomposites through in situ emulsion polymerization. *Journal of Materials Science*, 49(3), 1328–1335.



- Kumar, N. A., Choi, H.-J., Shin, Y.-R., Chang, D. W., Dai, L., & Baek, J.-B. (2012). Polyaniline-grafted reduced graphene oxide for efficient electrochemical. *American Chemical Society Nano*, 25(2), 1715–1723.
- Kumar, R., Ansari, M. O., & Barakat, M. A. (2013). DBSA doped polyaniline/multi-walled carbon nanotubes composite for high efficiency removal of Cr(VI) from aqueous solution. *Chemical Engineering Journal*, 228, 748–755.
- Li, D., & Kaner, R. B. (2008). Graphene-based materials, *Materials Science*, 320, 1170–1172.
- Li, J., Fang, K., Qiu, H., Li, S., & Mao, W. (2004). Micromorphology and electrical property of the HCl-doped and DBSA-doped polyanilines. *Synthetic Metals*, 142(1–3), 107–111.
- Long, N. V., Chien, N. D., Hayakawa, T., Hirata, H., Lakshminarayana, G., & Nogami, M. (2010). The synthesis and characterization of platinum nanoparticles: a method of controlling the size and morphology. *Nanotechnology*, 21(3), 035605.
- Mahmood, N., Zhang, C., Yin, H., & Hou, Y. (2014). Graphene-based nanocomposites for energy storage and conversion in lithium batteries, supercapacitors and fuel cells. *Journal of Materials and Chemistry A*, 2(1), 15–32.
- Njomo, N., Waryo, T., Masikini, M., Ikpo, C. O., Mailu, S., Tovide, O., & Iwuoha, E. I. (2014). Graphenated tantalum(IV) oxide and poly(4-styrene sulphonic acid)-doped polyaniline nanocomposite as cathode material in an electrochemical capacitor. *Electrochimica Acta*, 128, 226–237.
- Pérez-fernández, B., Martín-yerga, D., & Costa-garcía, A. (2017). Galvanostatic electrodeposition of copper nanoparticles on screen-printed carbon electrodes and their application for reducing sugars determination. *Talanta*, 175, 108–113.
- Snook, G. A., Kao, P., & Best, A. S. (2011). Conducting-polymer-based supercapacitor devices and electrodes. *Journal of Power Sources*, 196(1), 1–12.

- Trchová, M., & Stejskal, J. (2011). Polyaniline: The infrared spectroscopy of conducting polymer nanotubes (IUPAC Technical Report). *Pure and Applied Chemistry*, 83(10), 1803–1817.
- Wang, H., Hao, Q., Yang, X., Lu, L., & Wang, X. (2009). Graphene oxide doped polyaniline for supercapacitors. *Electrochemistry Communications*, 11(6), 1158–1161.
- Watson, V. G. (2014). Decoration of graphene oxide with silver nanoparticles and controlling the silver nanoparticle loading on graphene oxide. *The School of Engineering of the University of Dayton*.
- Xu, F., Zheng, G., Wu, D., Liang, Y., Li, Z., & Fu, R. (2010). Improving electrochemical performance of polyaniline by introducing carbon aerogel as filler. *Physical Chemistry Chemical Physics*, 12(13), 3270.
- Yang, B., Bin, D., Wang, H., Zhu, M., Yang, P., & Du, Y. (2015). High quality Pt-graphene nanocomposites for efficient electrocatalytic nitrite sensing. *Colloids and Surfaces A: Physicochemical and Engineering Aspects*, 481, 43–50.
- Yang, J., Yin, H., Jia, J., & Wei, Y. (2011). Facile synthesis of high-concentration, stable aqueous dispersions of uniform silver nanoparticles using aniline as a reductant. *Langmuir*, 27(8), 5047–5053.
- Yin, W., & Ruckenstein, E. (2000). Soluble polyaniline co-doped with dodecyl benzene sulfonic acid and hydrochloric acid. *Synthetic Metals*, 108(1), 39–46.
- Zhang, J., & Zhao, X. S. (2012). Conducting polymers directly coated on reduced graphene oxide sheets as high-performance supercapacitor electrodes. *Journal of Physical Chemistry C*, 116(9), 5420–5426.
- Zhang, W., Li, Y., Zhang, X., & Li, C. (2017). Facile synthesis of highly active reduced graphene oxide-CuI catalyst through a simple combustion method for photocatalytic reduction of CO₂ to methanol. *Journal of Solid State Chemistry*, 253, 47–51.

Zhu, Y., Murali, S., Cai, W., Li, X., Suk, J. W., Potts, J. R., & Ruoff, R. S. (2010). Graphene and graphene oxide: Synthesis, properties, and applications. *Advanced Materials*, 22(35), 3906–3924.



Chapter 6

Conclusions and Recommendations

Summary

This chapter is to confirm whether the main objectives of the study were met. It, therefore, gives a summary of all results of the study. These results have been discussed thoroughly. It also outlines the future investigations and recommendations required for further work.



6.1 Conclusions

The main objective of this work was to combine the properties of graphene oxide with those of metal nanoparticles and DBSA doped polyaniline to develop high performance supercapacitors with higher capacitances. This study reported the successful synthesis of GO by the modified Hummers method with its oxidation determined over a period of five days i.e. to ensure the degree of oxidation is high. The prepared GO was then reduced by hydrazine monohydrate. Comparison of GO and rGO by HRTEM, HRSEM and XRD studies revealed information about the crystallinity, morphology and size of the GO nanosheets which appeared to be thin, flat, bended and wrinkled and a size of 1.5 μm . GO revealed well-defined and three-dimensional interlinked graphene sheets which formed a porous network of loose sponge like structure and on comparison, rGO was composed of thinner sheets and smaller pores than GO. Also the XRD pattern of GO indicated that the AB stacking exists with larger interlayer spacing in GO. The presence of carbon and oxygen functional groups was confirmed by EDX. These results were also confirmed by FTIR, in which the characteristic bands of GO's functional groups O-H stretching vibrations, C-O (carboxylic acid and carbonyl moieties), the graphitic domains of C-C and C=C-O and the C-O and the O-H deformation of carboxylic acid groups, confirm the oxidation of graphite. When the GO was reduced, the oxygen bands were greatly reduced in intensity with a new band forming attributed to C-C bonds that are due to thermal annealing. This band is broad indicating the poorly ordered free graphene nanosheets and that a significant portion of GO was reduced. Studies by Raman spectroscopy revealed a D-band which is a second overtone of a different in-plane vibration and corresponds to defects within the sp^2 network, a G-band and a primary in-plane vibrational mode 2D-band. Reducing GO resulted in the D and G-bands shifting to lower frequencies due to incomplete defect healing. The optical studies of GO resulted in two

characteristic bands, a shoulder band corresponding to $n-\pi^*$ plasmon band and a band corresponding to $\pi-\pi^*$ plasmon band. In reduced GO the $\pi-\pi^*$ plasmon peak was shifted to a lower wavelength and the band gaps were determined to be 3.56 eV for GO and 2.89 eV for rGO, respectively. The electrochemical characteristics of GO and rGO showed that the materials were EDLC due to the slow increase of the current under the curve with increase in scan rate. The capacitance for GO was determined from area under the curve and was determined to be 180 F g^{-1} and this was confirmed by the galvanostatic charge/discharge. The specific capacitance from galvanostatic charge/discharge was determined to be 182.8 F g^{-1} and the same behaviour was observed for rGO.

Loading of GO with Pt, Ag and Cu nanoparticles (NPs) by the electrostatic self-assembly method, was successful. The functionalized GO was further treated with ethylene glycol and the respective salts that were needed to load the NPs on the surface of GO. Studies by HRTEM, HRSEM and XRD revealed information about the morphology, size and crystallinity of the prepared materials. The Pt and Ag NPs that were loaded on the surface of GO were uniformly dispersed and small with mean particle sizes of $2.3 \pm 0.2 \text{ nm}$ and $2.6 \pm 0.3 \text{ nm}$, respectively. However, the Cu NPs are observed to be larger, with mean particle sizes of $3.5 \pm 0.5 \text{ nm}$, and were not uniformly dispersed on the surface of GO due to the aggregation of the Cu NPs upon heat treatment and the weak interaction between the GO and copper atoms. Also the surface of GO was changed from smooth to rough with small particles observed on the surface of GO and the nanoparticles were observed to be spread out on the GO sheets. When GO was supported with the Pt, Ag and Cu NPs, three diffraction peaks appeared at 39.5° corresponding to (111), 46.0° corresponding to (200) and 67° corresponding to (220) diffraction planes of metallic Pt, Ag and Cu, respectively. The elemental composition was confirmed by EDS and XRF which confirm the presence of the metal nanoparticles, Pt, Ag and Cu NPs that have been loaded on the surface of GO. When

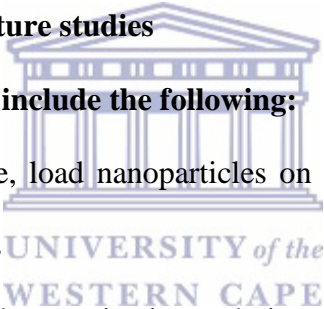
GO was loaded with metal nanoparticles, FTIR studies revealed that the intensity of peaks related to the carbonyl and epoxide functional groups are decreased indicating the partial reduction of graphene oxide, however, a small amount of carbonyl and epoxide functional groups are still retained by the rGO. Studies by Raman spectroscopy reveal that GO/Pt, GO/Ag, and GO/Cu NPs nanocomposites exhibit an increased D/G intensity ratio (1.16) compared to GO (0.95), which indicates a decrease in average size of the domain of sp^2 when GO was reduced. However, the D and G bands for the GO/Pt NPs, GO/Ag NPs and GO/Cu NPs nanocomposites were shifted towards lower frequencies. The attachment of Ag NPs to the GO surface shown in UV-Vis was confirmed primarily through the detection of a band at 406 nm, which was attributed to the silver nanoparticles plasmon resonance. Moreover, the UV-Vis spectrum of GO-Ag NPs revealed a red-shift to approximately 263 nm corresponding to the electronic transitions of C=C aromatic bonds and a shoulder disappearance. These observations suggest that GO sheets were simultaneously reduced by ethylene glycol during the formation of the Ag NPs, resulting in a partial restoration of π -conjugation.

GO that was loaded with Pt, Ag and Cu NPs was then treated with aniline and DBSA to form conducting polymer composites. Studies of GO/Pt/DBSA-PANI, GO/Ag/DBSA-PANI and GO/Cu/DBSA-PANI by HRTEM and HRSEM show the aggregated and agglomerated structures with darker surfaces. HRSEM shows that the polymer composites appear as collective and bounded particles with surfaces that are of glassy nature, smooth and have toothed edges. The quantitative analysis result of the polymer composites indicates the presence of carbon, sulphur, platinum for the polymer composite that contains platinum. The same behaviour is apparent for the composite that contains silver and copper. FTIR studies of the polymer composites show a broad absorption band around which corresponds to the stretching frequencies of quinoid and benzenoid rings of polyaniline respectively, a band which corresponds to C-N stretching of secondary amide group, a band which is attributed to

the in-plane bending of the C-H group and peaks which are due to the SO_3^- group of DBSA. The specific capacitance of the polymer composites was determined from the Galvanostatic charge/discharge. The specific capacitance was determined as 227.2, 206.4 and 192.8 F g^{-1} which correspond to GO/Pt/DBSA-PANI, GO/Ag/DBSA-PANI and GO/Cu/DBSA-PANI, respectively. Comparing these values with the specific capacitance of GO, which was determined as 182.8 F g^{-1} , we can conclude that the nanocomposites are good materials and therefore can be used for supercapacitor applications. The aims and objectives of the work were met.

6.2 Recommendations for future studies

Recommended future work will include the following:

- 
- Synthesize graphene oxide, load nanoparticles on the surface of graphene oxide by using microwave synthesis
 - Characterize using other characterization techniques such as TGA (to find the amount of functional groups and thermal stability and also observe structural transformation of the GO and loaded GO), SAXSPACE, AFM etc.
 - When assembling cells for electrochemical studies, different electrolytes will be compared since materials behave differently to every cation or anion.
 - Use different materials such as highly activated carbon (carbon nanotubes, carbon black, carbon aerogels, carbon ink etc.), other conducting polymers besides PANI, metal oxides such as ruthenium oxide, zinc oxide etc. as anodes. The synthesized material as a cathode when assembling the cells.
 - Study the exceptional conducting and mechanical properties of flexible graphene anchored polymeric electrode materials when combined with nanostructured

platinum metal nanoalloy Pt-Ag-Au in combination with different concentrations of polyvinyl alcohol gel electrolyte

References

- Afzal, A. B., & Javed Akhtar, M. (2012). Effects of silver nanoparticles on thermal properties of DBSA-doped polyaniline/PVC blends. *Iranian Polymer Journal*, 21(8), 489–496.
- Ansari, M. O., & Mohammad, F. (2012). Thermal stability and electrical properties of dodecyl-benzene-sulfonic- acid doped nanocomposites of polyaniline and multi-walled carbon nanotubes. *Composites Part B: Engineering*, 43(8), 3541–3548.
- Ashokan, S., Ponnuswamy, V., & Jayamurugan, P. (2015). Synthesis and characterization of CuO nanoparticles, DBSA doped PANI and PANI/DBSA/CuO hybrid composites for diode and solar cell device development. *Journal of Alloys and Compounds*, 646, 40–48.
- Bhadra, J., Madi, N. K., Al-Thani, N. J., & Al-Maadeed, M. A. (2014). Polyaniline/polyvinyl alcohol blends: Effect of sulfonic acid dopants on microstructural, optical, thermal and electrical properties. *Synthetic Metals*, 191, 126–134.
- Bonet, F., Delmas, V., Grugeon, S., Herrera Urbina, R., Silvert, P. Y., & Tekaiia-Elhsissen, K. (1999). Synthesis of monodisperse Au, Pt, Pd, Ru and Ir nanoparticles in ethylene glycol. *Nanostructured Materials*, 11(8), 1277–1284.
- Calheiros, L. F., Soares, B. G., & Barra, G. M. O. (2017). DBSA-CTAB mixture as the surfactant system for the one step inverse emulsion polymerization of aniline: Characterization and blend with epoxy resin. *Synthetic Metals*, 226, 139–147.

- Chang, K. C., Jang, G. W., Peng, C. W., Lin, C. Y., Shieh, J. C., Yeh, J. M., & Li, W. T. (2007). Comparatively electrochemical studies at different operational temperatures for the effect of nanoclay platelets on the anticorrosion efficiency of DBSA-doped polyaniline/Na⁺-MMT clay nanocomposite coatings. *Electrochimica Acta*, 52(16), 5191–5200.
- Chen, C. H. (2002). Thermal studies of polyaniline doped with dodecyl benzene sulfonic acid directly prepared via aqueous dispersions. *Journal of Polymer Research*, 9(3), 195–200.
- Chew, T., Daik, R., & Hamid, M. (2015). Thermal conductivity and specific heat capacity of dodecylbenzenesulfonic acid-doped polyaniline particles—water based nanofluid. *Polymers*, 7(7), 1221–1231.
- De La Fuente Salas, I. M., Sudhakar, Y. N., & Selvakumar, M. (2014). High performance of symmetrical supercapacitor based on multilayer films of graphene oxide/polypyrrole electrodes. *Applied Surface Science*, 296, 195–203.
- Del Castillo-Castro, T., Castillo-Ortega, M. M., Villarreal, I., Brown, F., Grijalva, H., Perez-Tello, M., & Puig, J. E. (2007). Synthesis and characterization of composites of DBSA-doped polyaniline and polystyrene-based ionomers. *Composites Part A: Applied Science and Manufacturing*, 38(2), 639–645.
- Gao, W. (2015). The chemistry of graphene oxide. *Graphene Oxide: Reduction Recipes, Spectroscopy, and Applications*, 1, 61–95.
- Grinou, A., Yun, Y. S., Cho, S. Y., Park, H. H., & Jin, H. J. (2012). Dispersion of Pt nanoparticle-doped reduced graphene oxide using aniline as a stabilizer. *Materials*, 5(12), 2927–2936.
- Haba, Y., Segal, E., Narkis, M., Titelman, G. I., & Siegmann, A. (2000). Polyaniline-DBSA/polymer blends prepared via aqueous dispersions. *Synthetic Metals*, 110(3), 189–193.

- He, H., & Gao, C. (2011). Graphene nanosheets decorated with Pd, Pt, Au, and Ag nanoparticles: Synthesis, characterization, and catalysis applications. *Science China Chemistry*, 54(2), 397–404.
- Imran, S. M., Kim, Y., Shao, G. N., Hussain, M., Choa, Y. H., & Kim, H. T. (2014). Enhancement of electroconductivity of polyaniline/graphene oxide nanocomposites through in situ emulsion polymerization. *Journal of Materials Science*, 49(3), 1328–1335
- Karthika, P. (2012). Functionalized Exfoliated Graphene Oxide as Supercapacitor Electrodes. *Soft Nanoscience Letters*, 2, 59–66.
- Kumar, N. A., Choi, H.-J., Shin, Y.-R., Chang, D. W., Dai, L., & Baek, J.-B. (2012). Polyaniline-grafted reduced graphene oxide for efficient electrochemical. *American Chemical Society Nano*, 25(2), 1715–1723.
- Kumar, R., Ansari, M. O., & Barakat, M. A. (2013). DBSA doped polyaniline/multi-walled carbon nanotubes composite for high efficiency removal of Cr(VI) from aqueous solution. *Chemical Engineering Journal*, 228, 748–755.
- Li, D., & Kaner, R. B. (2008). Graphene-Based Materials. *Materials Science*, 320, 1170–1172.
- Li, J., Fang, K., Qiu, H., Li, S., & Mao, W. (2004). Micromorphology and electrical property of the HCl-doped and DBSA-doped polyanilines. *Synthetic Metals*, 142(1–3), 107–111.
- Long, N. V., Chien, N. D., Hayakawa, T., Hirata, H., Lakshminarayana, G., & Nogami, M. (2010). The synthesis and characterization of platinum nanoparticles: a method of controlling the size and morphology. *Nanotechnology*, 21(3), 35605.
- Mahmood, N., Zhang, C., Yin, H., & Hou, Y. (2014). Graphene-based nanocomposites for energy storage and conversion in lithium batteries, supercapacitors and fuel cells. *Journal of Materials and Chemistry A*, 2(1), 15–32.

- Njomo, N., Waryo, T., Masikini, M., Ikpo, C. O., Mailu, S., Tovide, O., & Iwuoha, E. I. (2014). Graphenated tantalum(IV) oxide and poly(4-styrene sulphonic acid)-doped polyaniline nanocomposite as cathode material in an electrochemical capacitor. *Electrochimica Acta*, *128*, 226–237.
- Pérez-fernández, B., Martín-yerga, D., & Costa-garcía, A. (2017). Galvanostatic electrodeposition of copper nanoparticles on screen-printed carbon electrodes and their application for reducing sugars determination. *Talanta*, *175*, 108–113.
- Snook, G. A., Kao, P., & Best, A. S. (2011). Conducting-polymer-based supercapacitor devices and electrodes. *Journal of Power Sources*, *196*(1), 1–12.
- Stylianakis, M. M., Spyropoulos, G. D., Stratakis, E., & Kymakis, E. (2012). Solution-processable graphene linked to 3,5-dinitrobenzoyl as an electron acceptor in organic bulk heterojunction photovoltaic devices. *Carbon*, *50*(15), 5554–5561.
- Trchová, M., & Stejskal, J. (2011). Polyaniline: The infrared spectroscopy of conducting polymer nanotubes (IUPAC Technical Report). *Pure and Applied Chemistry*, *83*(10), 1803–1817.
- Wang, H., Hao, Q., Yang, X., Lu, L., & Wang, X. (2009). Graphene oxide doped polyaniline for supercapacitors. *Electrochemistry Communications*, *11*(6), 1158–1161.
- Watson, V. G. (2014). Decoration of Graphene Oxide With Silver Nanoparticles and Controlling the Silver Nanoparticle Loading on Graphene. *The School of Engineering of the University of Dayton*.
- Xu, F., Zheng, G., Wu, D., Liang, Y., Li, Z., & Fu, R. (2010). Improving electrochemical performance of polyaniline by introducing carbon aerogel as filler. *Physical Chemistry Chemical Physics*, *12*(13), 3270.

- Yang, B., Bin, D., Wang, H., Zhu, M., Yang, P., & Du, Y. (2015). High quality Pt-graphene nanocomposites for efficient electrocatalytic nitrite sensing. *Colloids and Surfaces A: Physicochemical and Engineering Aspects*, 481, 43–50.
- Yang, J., Yin, H., Jia, J., & Wei, Y. (2011). Facile synthesis of high-concentration, stable aqueous dispersions of uniform silver nanoparticles using aniline as a reductant. *Langmuir*, 27(8), 5047–5053.
- Yin, W., & Ruckenstein, E. (2000). Soluble polyaniline co-doped with dodecyl benzene sulfonic acid and hydrochloric acid. *Synthetic Metals*, 108(1), 39–46.
- Zhang, J., & Zhao, X. S. (2012). Conducting polymers directly coated on reduced graphene oxide sheets as high-performance supercapacitor electrodes. *Journal of Physical Chemistry C*, 116(9), 5420–5426.
- Zhang, W., Li, Y., Zhang, X., & Li, C. (2017). Facile synthesis of highly active reduced graphene oxide-CuI catalyst through a simple combustion method for photocatalytic reduction of CO₂ to methanol. *Journal of Solid State Chemistry*, 253, 47–51.
- Zhu, H., Peng, S., & Jiang, W. (2013). Electrochemical properties of PANI as single electrode of electrochemical capacitors in acid electrolytes. *The Scientific World Journal*, 2013.
- Zhu, Y., Murali, S., Cai, W., Li, X., Suk, J. W., Potts, J. R., & Ruoff, R. S. (2010). Graphene and graphene oxide: Synthesis, properties, and applications. *Advanced Materials*, 22(35), 3906–3924.